**Photoreceptor Transcriptome Analysis in Zebrafish**

A Dissertation

Presented in Partial Fulfillment of the Requirements for the

Degree of Doctor of Philosophy

with a

Major in Neuroscience

in the

College of Graduate Studies

University of Idaho

by

Chi Sun

Major Professor: Dr. Deborah Stenkamp

Committee members: Dr. Peter Fuerst, Dr. Gordon Murdoch, Dr. Michael Varnum

Department administrator: Dr. James Nagler

December 2017

**Authorization to Submit Dissertation**

This dissertation of Chi Sun, submitted for the degree of Doctor of Philosophy with a Major in Neuroscience and titled "**Photoreceptor Transcriptome Analysis in Zebrafish**," has been reviewed in final form. Permission, as indicated by the signatures and dates below, is now granted to submit final copies to the College of Graduate Studies for approval**.**

Major professor: _____ Date:_____
Dr. Deborah Stenkamp

Committee members: _____ Date:_____
Dr. Peter Fuerst

_____ Date:_____
Dr. Gordon Murdoch

_____ Date:_____
Dr. Michael Varnum

Department administrator: _____ Date:_____
Dr. James Nagler

**Abstract**

The mammalian retina does not possess the capacity of intrinsic generation of functional replacement upon the loss of retinal neurons, and functional replacement of these cells in human patients is not medically feasible at present. Identification of regulatory targets controlling retinal neurogenesis and regeneration in zebrafish can potentially provide new directions to treat retinal pathologies as well as to induce potential retinal regeneration in humans. Fortunately, next-generation sequencing (NGS) provides powerful systems-based analysis of cellular pathways, and has been used to analyze these regulatory targets in this study. The goals of this dissertation are to develop a methodology of isolating photoreceptors of different subtypes, to analyze NGS-derived photoreceptor transcriptome profiling (RNA-seq), and to study functions of selected transcripts in zebrafish photoreceptor development and maintenance.

**Acknowledgements**

Appreciation is credited to my advisor Dr. Deborah L. Stenkamp for her constant guidance throughout the course of my doctoral degree. In addition, I would also like to thank my committee members for their invaluable advice given to my research.

Various funding agencies have provided important financial resources to this research, including NIH R01 EY012346 (DLS), NIH R21 EY026814 (DLS), a Technology Access Grant (CS and DLS) available through Idaho's NIH-INBRE program (supported by NIH P20 GM103408), and the Malcolm and Carol Renfrew Faculty Fellowship (DLS).

I would like to acknowledge Dr. James Fadool for providing the *XOPS:eGFP* zebrafish, Dr. Ann Morris for the *XOPS:mCFP* zebrafish, Dr. Rachel Wong for providing *trβ2:tdTomato* transgenic line, Dr. Shoji Kawamura for the *sws1:GFP*, *rh2-2:GFP*, *lws:Pac(H)* zebrafish, and Dr. Pamela Raymond for *sws2:mCherry* zebrafish..

I am very grateful to Ms. Ruth Frey and Mr. Carlos Galicia, the scientific aides of Dr. Stenkamp's laboratory, for the technical assistance, to Ms. Ann Norton of the UI IBEST Optical Imaging Core for assistance with FACS, to Ms. Melissa Oatley for assistance with FACS at WSU CRB FACS Core, to Mr. Dan New and Dr. Sam Hunter of the UI IBEST Genomics Core for RNA-Seq experiments and assistance with bioinformatics, to Dr. Diana Mitchell for retinal lesioning experiments, to University of Utah Mutation Generation and Detection Core for assistance with CRISPR-Cas9 techniques. A research collaboration with Dr. Anand Swaroop's lab, NEI, NIH, was arranged for RNA-Seq experiments of regenerated photoreceptors and subsequent bioinformatics.

## Table of Contents

**List of Figures**

## List of Tables

**List of Abbreviations**

AGI = Audacious Goal Initiative

AMD = age-related macular degeneration

CGZ = circumferential germinal zone

CMZ = ciliary marginal zone

dpi = days post-injury

dpf = days post-fertilization

ES = embryonic stem

FACS = Fluorescence-Activated Cell Sorting

FDR = false discovery rate

GCL = ganglion cell layer

GO = gene ontology

hpf = hours post fertilization

IBEST = Institute for Bioinformatics and Evolutionary Studies

ICC = Immunocytochemistry

INL = inner nuclear layer

IPL = inner plexiform layer

iPS = induced pluripotent stem

LWS = long wavelength sensitive

MWS = medium wavelength sensitive

NGS = next-generation sequencing

NEI = National Eye Institute

ONL = outer nuclear layer

OPL = outer plexiform layer

PCR = polymerase chain reaction

qPCR = quantitative PCR

RNA-seq = RNA-sequencing

RP = retinitis pigmentosa

RPE = retinal pigmented epithelium

SWS = short wavelength sensitive

WT = wild-type

## Chapter 1. Introduction

Specific aims:

The progressive loss of rod and cone photoreceptors represent the hallmark of many inherited and age-related human retinal diseases that result in decreased visual function and blindness. Unfortunately, the mammalian retina does not possess the capacity of intrinsic generation of functional replacement upon the loss of retinal neurons, and functional replacement of these cells in human patients is not medically feasible at present.

Current medical therapies under experimental development are specifically designed for cells to acquire the properties of differentiated and fully functional rod and cone photoreceptors. However, the identification of photoreceptor type-specific transcripts is not fully realized. Another critical research challenge of growing and maintaining new photoreceptor cells requires identification and mapping of intrinsic factors regulating and maintaining photoreceptor diversity, photoreceptor differentiation, and photoreceptor survival. Fortunately, next-generation sequencing (NGS) provides powerful systems-based analysis of cellular pathways. The goals of this study are to analyze NGS-derived photoreceptor transcriptome profiling (RNA-Seq) and study selected transcripts during photoreceptor differentiation and regeneration in zebrafish.

I proposed the following three specific aims to better understand the photoreceptor-type-specific transcripts during photoreceptor differentiation and regeneration.

Specific aim I: **Identification of transcripts within rod photoreceptors of the zebrafish retina**

Specific aim II: **Isolation of photoreceptors from mature, developing, and regenerating zebrafish retinae and microglia from regenerating zebrafish retinae for gene expression analysis**

Specific aim III: **Zebrafish rxrγa mutants: generation, validation, and preliminary characterization of opsin expression phenotype**

Significance:

Photoreceptors constitute more than 70% of the cells in the vertebrate retina and convert light into electrical signals. Normal and healthy photoreceptors are controlled by a multitude of interacting factors that determine the precise developmental organization and life-long maintenance of interconnected neurons for optimal visual function. Disruption of the intercellular interactions and these complex interacting factors during development or in the mature retina can give rise to cellular pathology, mainly manifesting as loss of vision.

Knowledge of distinct features of the transcriptomes of mature, differentiating, and regenerated rod and cone photoreceptors is currently incomplete however critical in identifying regulatory genes that may be involved in photoreceptor development, degenerations, and regeneration, and in understanding regulation of morphological maturation of these two cell populations. So far, characterization of several regulatory genes that are essential for the photoreceptor development in vertebrate, such as cone-rod homeobox (CRX) and neural retina leucine zipper (NRL), has been documented [1, 2].

However, research has not been fully extended to elucidate the underlying gene regulatory network for photoreceptor differentiation. Insights from such proposed study can identify therapeutic targets and cultivate the development of better protocols for the derivation of photoreceptors from mammalian embryonic stem (ES) cells and induced pluripotent stem (iPS) cells [3].

According to the broadcasted message by the National Eye Institute (NEI), the Audacious Goal Initiative (AGI) aims to foster the research field that helps to enable the restoration of vision through regeneration of the retina (nei.nih.gov). The central goal is to

replace cells of the retina that have been damaged by disease or injury and to restore their connections to the visual centers of the brain. The targeted cell types include photoreceptors and ganglion cells. In this proposal, regulatory transcripts involved in the regeneration of rods will be particularly studied.

Zebrafish retina and zebrafish as a model:

Zebrafish (*Danio rerio*), a tropical freshwater vertebrate fish, is originally found in South Asia. It usually becomes sexually mature within 3-4 months after fertilization. An adult zebrafish is 2-3 inches long on average, and life span is about 3 years. Importantly, zebrafish is now become a leading model for the analysis of the vertebrate visual system [4, 5].

The vertebrate retina develops from the neural tube ectoderm. As the neural tube closes, the optic vesicle is derived from the anterior part of the grooves. After the evagination of the optic vesicles, an optic cup is formed [6]. Neural retina and nonpigmented layer of optic cup develops from inner optic cup layer and retinal pigmented epithelium (RPE) develops from outer optic cup layer [6]. Although both tissues are derived from optic cup layer and the same region of the neural tube, the retina is a multilayered tissue containing the photoreceptors and other neurons responsible for vision, while the RPE forms a single-layer pigment cells adjacent to the photoreceptor layer.

As the morphogenesis of cells at the optic cup comes to completion, the first wave of post-mitotic retinal neurons differentiates. Classification of the major retinal cells is conventionally according to the morphological characteristics of these cells and is well conserved in all vertebrates. There are five major classes of retinal cells differentiated during neurogenesis: ganglion, amacrine, bipolar, horizontal, and photoreceptor cells. Müller glia are also generated in the same window of retinal neurogenesis. Birth-dating studies in mammalian models have shown that retinal ganglion cell is the first to be generated, followed

by the onset of cone photoreceptor and horizontal cell genesis shortly thereafter. The appearance of amacrine cell occurs slightly later, with rod photoreceptor cells, bipolar cells and Müller glia being the latest born cell types [7, 8].

In the zebrafish, ganglion cell precursors are the first to become postmitotic around 27 hpf (hours post fertilization), and ganglion cell differentiation is conserved in many vertebrate animals [8, 9]. Formation of the distinctive ganglion cell layer is confirmed in histological sections by 36 hpf [9]. Cells forming the INL also become postmitotic about 10 hours after the first ganglion cells precursors exit the cell cycle. These precursors of INL cells and ganglion cells are located at a small patch of the ventral retina [9]. At around 34 hpf, it is observable that terminal divisions of retinal progenitor cells can generate pairs of ganglion and photoreceptor cells, which shows these cells are probably born in overlapping windows of time [10]. By 60 hpf, more than 90% of cells in the central region of retina become postmitotic. At this period, most cells of different layers become postmitotic in non-overlapping manner [9]. In contrast to mammals, zebrafish retina undergoes neurogenesis throughout the lifespan [11].

The spatial arrangement of zebrafish photoreceptors presents regular neuronal mosaics. The wavelength sensitivity of a photoreceptor subtype is determined by the photopigment that is responsible for the light transduction, and is composed of an opsin and a chromophore. Zebrafish express 10 different opsins, each encoded by a separate gene [12-14]. There are two, tandemly-duplicated Lws-opsin (*lws-1* and *-2*) and four, tandemly-quadruplicated Mws-opsin genes (*rh2-1*, *rh2-2*, *rh2-3*, and *rh2-4*), in contrast to Sws1- and Sws2-opsins, which are each encoded by a single gene (*sws-1* and *-2*, respectively). The opsin of rods is coded by *rh1* gene, and *rhol* (*rhodopsin-like*) is also expressed in rods. The expression of these opsins at given developmental stages may follow a spatiotemporal pattern, at which some opsins are expressed at specific locations of the retina [15, 16].

Unlike the case that other retinal cells are generated at cilia marginal zone (CMZ), neurogenesis of rod photoreceptors happen in the outer nuclear layer throughout the zebrafish lifespan [11].

For photoreceptor cells, cones usually exit from the mitotic cycle and commit to the photoreceptor lineage earlier than rods. In zebrafish, cone progenitors are produced by the asymmetric division, giving rise to a cone and another retinal cell type before the dedicated precursors are generated [17, 18]. Cone photoreceptors of the same type are produced by symmetric division of dedicated precursors. At the early stage of development, newly generated rods and cones remain morphologically indistinct, which has hindered direct studies of the events that generate photoreceptor diversity. By 48-50 hfp, the photoreceptor cell layer can be identified in histological sections. Rods express opsin around 50 hpf, shortly followed by red and blue cones. Opsin expression triggers photoreceptor outer segment differentiation, and outer segments of rods and cones appear at a small patch of the ventral retina around 60 hpf [19]. At 4 dpf (days post fertilization), photoreceptor subtypes already become morphologically distinct [20, 21].

In an adult retina, the outermost layer of neurons is termed the outer nuclear layer (ONL) consisting of rod and cone photoreceptors. Rods are highly sensitive in low-light situations, whereas cones are involved more in photopic vision and help to discriminate color and provide high acuity vision. The outer plexiform layer (OPL) consists of synapses of rod and cone photoreceptors interacting with the dendrites of bipolar and horizontal cells. The inner nuclear layer (INL) contains bipolar, horizontal and amacrine perikarya. Dendrites of horizontal cells only project within OPL, while dendrites of bipolar cells and amacrine cells form synaptic connections with dendrites of the ganglion cells at inner plexiform layer (IPL). Synaptic activities of amacrine cells are limited to the INL. The innermost layer of the retina proximal to the lens comprises ganglion cells and displaced amacrine cells. Vision signals

from these retinal neurons are transmitted through the optic nerve and then lateral geniculate nucleus in the thalamus to the visual cortex of cerebral cortex.

Ganglion cells can be divided into two classes. When light signals reach the center of the receptive field, ON-center ganglion cells become excited while OFF-center ganglion cells become inhibited. Cone photoreceptors interact with bipolar cells to activate in either an ON or OFF pathway. ON-bipolar cells become depolarized by light signals, and OFF-bipolar cells become hyperpolarized. Bipolar cells connect to the downstream ganglion cells, in the manner that, depolarization of ON-bipolar cells further depolarizes the connecting ON-center ganglion cells. Ganglion cell activity can also be mediated by amacrine cells [22].

Müller glia, astrocytes and microglia are the major non-neuronal cells present in vertebrate retina. In adult zebrafish, cell bodies of Müller glia are located in the INL, but their end-feet can reach the inner and outer limiting membranes of retina tissue [23, 24]. This cellular morphology enables Müller glia to span for the entire tissue and provide structural support for the retina. Also, this morphological relationship between neurons and Müller glia is manifested by a series of functional interactions, including the maintenance of the homeostasis of the retinal extracellular milieu, the regulation of blood flow in the retina, and the roles in neuroprotection [23, 25, 26]. Moreover, in adult zebrafish, Müller glia re-enter into the cell cycle upon a lesion injury to retinas, which enables neuronal regeneration [27, 28].

Astrocytes are the major component of the optic stalk and involved in the development of the retinal vasculature. Reciprocal interaction between astrocytes and endothelial cells controls angiogenesis and astrocyte maturation. Functions of astrocytes in developing zebrafish retina are not yet fully understood [29, 30].

Microglia are the main resident immune cells in the retina, can be found distributed throughout the inner mouse retina in a laminated pattern [31]. Also, microglia are involved in retinal responses to injury and disease [32, 33]. Microglia-Müller communications in retinal

inflammation signals the overall injury response [34]. However, the roles of microglia in zebrafish retina development and neuroprotection, as well as in neuronal regeneration, are not clearly discovered.

For all the experiments introduced in this dissertation, zebrafish was used as the primary animal model. The main reason is that a large variety of molecular, genetic, and cellular research techniques and approaches is available to analyze zebrafish visual system development and functions. In addition, imaging availability continues to be a strength of the zebrafish model. Together with a large assortment of transgenic lines expressing fluorescent proteins in different types of neurons and tissues, developmental and physiological processes in zebrafish retina can be directly visualized. Moreover, it is possible to create and maintain transparent embryos to observe different cellular events like angiogenesis and cell migration.

High fertility rate provides zebrafish the power of large sample size for significant statistical analysis in a given experiment. With all these advantages, the zebrafish is also used for high-throughput screening of small molecules, which helps to discover potential therapeutic compounds. In recent years, gene-editing techniques such as CRISPR are frequently applied to the zebrafish model, and loss-of-function studies of various genes are thus achieved [35].

The neuronal morphology of the vertebrate retina has been conserved in evolution. Early studies by Cajal and others noted retinae of animals from vertebrate phyla share similar tissue organization. In specific, human and zebrafish retinae display the same layered pattern and the same neuronal classification, i.e. photoreceptors occupying the outermost layer and the ganglion cells forming the innermost neuronal layer. Gross histological features of mammalian and teleost retinae show very few differences, where photoreceptors, bipolar, horizontal, amacrine, and ganglion cells of a zebrafish have respectively similar structures to

their counterparts in human. During early retinal development, expressions of factors that influence retinal progenitors display similar patterns in zebrafish and mammals, for example, *vsx2* expression in zebrafish and *Chx10* (orthologue to *vsx2* in zebrafish) expression in mice are similar at certain windows of time. Also, related phenotypes in humans and zebrafish are resulted from the same genetic loci [36-38]. Unlike mice, zebrafish rely primarily on cone photoreceptors for vision, same as humans. Humans have 3 spectral types of cones, while there are 4 morphological subtypes of cones in zebrafish retina [39].

In this dissertation, various experimental approaches are practiced to study genetic-morphological transformations, morphological features, and factors controlling cell differentiation that ultimately contribute to the functional vertebrate visual system.

## Retinal regeneration in zebrafish:

Unlike mammals, Müller glia in zebrafish retina can generate multipotent progenitors to differentiate into the damaged and lost neurons following retinal injury. This regeneration process has been illustrated at the cellular level, and visual function is gradually restored after recovery [40, 41]. Interestingly, studies on gene expression profiling of Müller glia in mammalian retinas show a good extent of similarities to retinal progenitors [42, 43]. The main question is why the regenerative response in mammalian vertebrates is so minimal as compared with the functional regenerative response in fish [44, 45]. Lineage analysis of Müller-derived progenitors has been documented, however, factors governing the asymmetric division of these multipotent cells have not been evaluated [46, 47]. Furthermore, the capacity of the number of mitotic divisions by activated Müller glia in zebrafish is still unknown [48]. In other words, it is unclear if activated Müller glia undergo multiple divisions to regenerate neurons.

Dedifferentiation of Müller glia is not sufficient to trigger re-entry into the cell cycle. Previous studies have suggested that neuronal regeneration in teleost fish retina will not be triggered unless a minimum level of retinal cell loss is reached [49]. Ablation of a small patch of rod photoreceptors does not induce Müller glia-derived regeneration in zebrafish [50].

Neuronal connectivity during retinal regeneration is required for the recovery of visual functions including vision acuity, motion perception and color vision. Synaptic specializations with minor morphological misallocations of synaptic patterning are formed at plexiform layers upon recovery from injury [41, 51]. Though promising and enlightening, it is still unclear if the regenerative mechanisms in zebrafish retina are correctly and broadly understood and if could be applicable to therapeutic practices in humans.

Still, zebrafish serves as an excellent animal model to understand the pathogenesis of retinal diseases, and the regenerative mechanisms provide a basis for future treatments. Progression of age-related macular degeneration (AMD) results in photoreceptor loss, causing vision loss that often leads to blindness [52]. Other diseases such as retinitis pigmentosa (RP) and glaucoma could also lead to blindness due to loss of retinal cells and degeneration of retinal tissue. All these diseases could be cured by targeting regeneration for the loss of cells and integrating regenerated neurons into the functional retina. However, the application of regeneration into clinical treatments is made more complicated that, even if neurogenesis and regeneration can be induced, functional metabolism, circuitry and synaptic connections have to be restored and correctly facilitated.

Müller glia in humans function similarly as those in zebrafish, involved in structural support, recycling of neurotransmitters, ion buffering, and processing free radicals. However, Müller glia respond to injuries by gliosis but have no regenerative capability [24]. With a good assortment of homologous genes and proteins found in two types of Müller glia in humans and zebrafish, it is possible to induce human Müller glia to re-enter cell cycle for

neurogenesis, if expressions of genes that are responsible for regenerative functions can be altered.

Studies demonstrated that the regenerated retinal cells reforms circuits that allow for color vision [53]. The neural tracing methods were used to gain insights into the visual pathway during regeneration [53]. In summary, retinal regeneration in zebrafish not only restores the overall anatomy [40, 41] but the visual function as well. However, biochemical mechanisms and molecular signatures involved in the regeneration are yet clearly understood.

## Factors involved in vertebrate retinal neurogenesis:

The neural retina and RPE arise from a common pool of progenitors during optic vesicle development [54]. In fish, these progenitors express the same transcription factor-encoding genes, such as *lhx2*, *pax6*, *six3*, *vsx2*, and 3 members of *rx* genes (*zrx1/2/3*), and signaling from surrounding tissues subsequently program the differentiation of the optic vesicle into different domains, in which cells can still be transdifferentiated [55]. Multiple signaling pathways, including Fgf, Notch, Wnt, Bmp, Shh, and TGFβ, also control the expression of transcription factors that function in the differentiation and fate choice of the neural retina and RPE domains [55, 56].

In specific, expression of *pax6* is essential for the maintenance of progenitor cell multipotency [57, 58]. In the absence of *pax6* expression, the expressions of two downstream targets, neurogenin 2 (*neurog2*) and atonal homolog 7 (*atoh7/ath5*) are missing [59-61], as a result, formation of ganglion cell layer is compromised [62]. In zebrafish, *atoh7* expression defines a cell lineage which undergoes asymmetric divisions to a daughter with ganglion cell fate and the other daughter with a different fate of photoreceptor, amacrine, or horizontal cell [10]. *Vsx1* expression primarily regulates the development of bipolar cells,

while *vsx2* influences the development of Müller glia and a subset of bipolar cells that is distinct from cells expressing *vsx1* [36]. Together with *pax6*, sex-determining region Y-box containing gene 2 (*sox2*) regulates progenitor cell multipotency, but their expressions are inversely correlated at different regions of eyecup, in the sense, *sox2* expression is higher than that of pax6 at the central eyecup but lower in the peripheral [63]. Thus, a precise ratio of *sox2* and *pax6* expression levels is required for the maintenance of progenitor cell identity and multipotency potential. *Pax6* expression is restricted to ganglion and amacrine cells [64]. Neurogenic differentiation 1 (*neurod1*), another basic helix-loop-helix (bHLH) transcription factor, plays important roles in retinal cell genesis and neuronal development [65, 66]. It regulates terminal photoreceptor differentiation and controls survival of rod photoreceptors, in absence of NeuroD1, the progressive photoreceptor degeneration is resulted [67]. NeuroD1 also determines cone photoreceptor patterning through its association with thyroid hormone receptor β2 expression during retinal development [68].

Some factors involved in subtype specification may have regulatory roles at earlier time points. For example, LIM-homeodomain 1 (Lsl1) is involved in the development of amacrine, bipolar and ganglion cells [69, 70]. Bhlhb5, a member of the Olig subfamily of bHLH transcription factors, is associated with with the generation of selective GABAergic amacrine and Type 2 OFF-cone bipolar subtypes [71]. More factors have specific roles in cell fate determinations. Notably, Nrl directs photoreceptor progenitors to the rod fate [1] [72]. Rx1 in zebrafish is required for the neurogenesis of retinal progenitor cells and important for photoreceptor differentiation [73]. Rx2 is expressed in the early neural retina, and regulates cone photoreceptor differentiation [73, 74]. Crx, a homeodomain containing transcription factor, may be involved in patterning the early optic primordium and in promoting the differentiation of retinal progenitors [75].

A knowledge gap remains: how are early regulatory activities in progenitors integrated with downstream transcriptional programs to determine cell specification and diversity? Also, the presence of any upstream genes governing these cell-fate factors is unclear.

RNA-Seq experiments:

Deep sequencing of RNA with NGS (RNA-Seq) allows a comprehensive evaluation and quantification of all subtypes of RNA molecules expressed in a cell or tissue [76]. RNA-Seq technology can detect transcripts expressed at low levels and permit the identification of unannotated transcripts and new spliced isoforms [77-79]. With a steady reduction in the costs of NGS, RNA-Seq is now emerging as a method of choice for comprehensive transcriptome profiling, and also allows comprehensive evaluation of alternative transcripts and coding polymorphisms. In addition, simultaneous evaluation of multiple genes that respond to an extrinsic micro-environment or intrinsic biological stimuli is now achievable by NGS. Such studies are also critical for delineating gene networks that can be targeted for treating specific diseases. With these recent advances in NGS, it is possible to assay genome-wide differences in gene expression between relatively small cell populations, which is useful and necessary in understanding the molecular mechanisms that drive rod and cone photoreceptor diversifications and disease models.

Since specific patterns of gene expression define the morphology and function of distinct cell types and tissues, changes in gene expression are associated with complex biologic processes, including cellular development, aging, maintenance, and disease pathogenesis. RNA-Seq and differential expression analysis on the enriched photoreceptor populations can help to identify these differentially expressed genes that may underlie functions specific to photoreceptor subtypes.

References


1. Mears AJ, Kondo M, Swain PK, Takada Y, Bush RA, Saunders TL, Sieving PA, Swaroop A: **Nrl is required for rod photoreceptor development**. *Nat Genet* 2001, **29**.
2. Xie BB, Zhang XM, Hashimoto T, Tien AH, Chen A, Ge J, Yang XJ: **Differentiation of retinal ganglion cells and photoreceptor precursors from mouse induced pluripotent stem cells carrying an Atoh7/Math5 lineage reporter**. *PloS one* 2014, **9**(11):e112175.
3. Chen S, Wang QL, Nie Z, Sun H, Lennon G, Copeland NG, Gilbert DJ, Jenkins NA, Zack DJ: **Crx, a novel Otx-like paired-homeodomain protein, binds to and transactivates photoreceptor cell-specific genes**. *Neuron* 1997, **19**(5):1017-1030.
4. Link BA, Collery RF: **Zebrafish Models of Retinal Disease**. *Annual Review of Vision Science* 2015, **1**(1):125-153.
5. Gestri G, Link BA, Neuhauss SCF: **The Visual System of Zebrafish and its Use to Model Human Ocular Diseases**. *Developmental neurobiology* 2012, **72**(3):302-327.
6. Chow RL, Lang RA: **Early Eye Development in Vertebrates**. *Annual Review of Cell and Developmental Biology* 2001, **17**(1):255-296.
7. Young RW: **Cell differentiation in the retina of the mouse**. *The Anatomical record* 1985, **212**(2):199-205.
8. Cepko CL, Austin CP, Yang X, Alexiades M, Ezzeddine D: **Cell fate determination in the vertebrate retina**. *Proceedings of the National Academy of Sciences of the United States of America* 1996, **93**(2):589-595.
9. Hu M, Easter SS: **Retinal neurogenesis: the formation of the initial central patch of postmitotic cells**. *Developmental biology* 1999, **207**(2):309-321.
10. Poggi L, Vitorino M, Masai I, Harris WA: **Influences on neural lineage and mode of division in the zebrafish retina in vivo**. *The Journal of Cell Biology* 2005, **171**(6):991-999.
11. Marcus RC, Delaney CL, Easter SS, Jr.: **Neurogenesis in the visual system of embryonic and adult zebrafish (Danio rerio). off**. *Visual neuroscience* 1999, **16**(3):417-424.
12. Allison WT, Barthel LK, Skebo KM, Takechi M, Kawamura S, Raymond PA: **Ontogeny of cone photoreceptor mosaics in zebrafish**. *The Journal of comparative neurology* 2010, **518**(20):4182-4195.
13. Hamaoka T, Takechi M, Chinen A, Nishiwaki Y, Kawamura S: **Visualization of rod photoreceptor development using GFP-transgenic zebrafish**. *Genesis (New York, NY : 2000)* 2002, **34**(3):215-220.
14. Vihtelic TS, Doro CJ, Hyde DR: **Cloning and characterization of six zebrafish photoreceptor opsin cDNAs and immunolocalization of their corresponding proteins**. *Visual neuroscience* 1999, **16**(3):571-585.
15. Chinen A, Hamaoka T, Yamada Y, Kawamura S: **Gene duplication and spectral diversification of cone visual pigments of zebrafish**. *Genetics* 2003, **163**(2):663-675.
16. Takechi M, Kawamura S: **Temporal and spatial changes in the expression pattern of multiple red and green subtype opsin genes during zebrafish development**. *The Journal of experimental biology* 2005, **208**(Pt 7):1337-1345.
17. Hafler BP, Surzenko N, Beier KT, Punzo C, Trimarchi JM, Kong JH, Cepko CL: **Transcription factor Olig2 defines subpopulations of retinal progenitor cells biased toward specific cell fates**. *Proc Natl Acad Sci U S A* 2012, **109**(20):7882-7887.
18. He J, Zhang G, Almeida Alexandra D, Cayouette M, Simons Benjamin D, Harris William A: **How Variable Clones Build an Invariant Retina**. *Neuron* 2012, **75**(5):786-798.
19. Schmitt EA, Dowling JE: **Early retinal development in the zebrafish, Danio rerio: Light and electron microscopic analyses**. *The Journal of comparative neurology* 1999, **404**(4):515-536.
20. Branchek T, Bremiller R: **The development of photoreceptors in the zebrafish, Brachydanio rerio. I. Structure**. *The Journal of comparative neurology* 1984, **224**(1):107-115.
21. Branchek T: **The development of photoreceptors in the zebrafish, brachydanio rerio. II. Function**. *The Journal of comparative neurology* 1984, **224**(1):116-122.
22. Masland RH: **The tasks of amacrine cells**. *Visual neuroscience* 2012, **29**(1):3-9.

23. Hippert C, Graca AB, Barber AC, West EL, Smith AJ, Ali RR, Pearson RA: **Muller glia activation in response to inherited retinal degeneration is highly varied and disease-specific**. *PloS one* 2015, **10**(3):e0120415.
24. Bringmann A, Pannicke T, Grosche J, Francke M, Wiedemann P, Skatchkov SN, Osborne NN, Reichenbach A: **Muller cells in the healthy and diseased retina**. *Progress in retinal and eye research* 2006, **25**(4):397-424.
25. Newman E, Reichenbach A: **The Muller cell: a functional element of the retina**. *Trends in neurosciences* 1996, **19**(8):307-312.
26. Reichenbach A, Bringmann A: **New functions of Muller cells**. *Glia* 2013, **61**(5):651-678.
27. Yurco P, Cameron DA: **Responses of Müller glia to retinal injury in adult zebrafish**. *Vision Research* 2005, **45**(8):991-1002.
28. Goldman D: **Müller glia cell reprogramming and retina regeneration**. *Nature reviews Neuroscience* 2014, **15**(7):431-442.
29. Tao C, Zhang X: **Development of astrocytes in the vertebrate eye**. *Developmental dynamics : an official publication of the American Association of Anatomists* 2014, **243**(12):1501-1510.
30. Fruttiger M: **Development of the retinal vasculature**. *Angiogenesis* 2007, **10**(2):77-88.
31. Santos AM, Calvente R, Tassi M, Carrasco MC, Martin-Oliva D, Marin-Teva JL, Navascues J, Cuadros MA: **Embryonic and postnatal development of microglial cells in the mouse retina**. *The Journal of comparative neurology* 2008, **506**(2):224-239.
32. Karlstetter M, Ebert S, Langmann T: **Microglia in the healthy and degenerating retina: insights from novel mouse models**. *Immunobiology* 2010, **215**(9-10):685-691.
33. Gomes-Leal W: **Microglial physiopathology: how to explain the dual role of microglia after acute neural disorders?** *Brain and Behavior* 2012, **2**(3):345-356.
34. Wang M, Wong WT: **Microglia-Müller Cell Interactions in the Retina**. *Advances in experimental medicine and biology* 2014, **801**:333-338.
35. Liu J, Zhou Y, Qi X, Chen J, Chen W, Qiu G, Wu Z, Wu N: **CRISPR/Cas9 in zebrafish: an efficient combination for human genetic diseases modeling**. *Human Genetics* 2017, **136**(1):1-12.
36. Vitorino M, Jusuf PR, Maurus D, Kimura Y, Higashijima S, Harris WA: **Vsx2 in the zebrafish retina: restricted lineages through derepression**. *Neural development* 2009, **4**:14.
37. Liu IS, Chen JD, Ploder L, Vidgen D, van der Kooy D, Kalnins VI, McInnes RR: **Developmental expression of a novel murine homeobox gene (Chx10): evidence for roles in determination of the neuroretina and inner nuclear layer**. *Neuron* 1994, **13**(2):377-393.
38. Clark AM, Yun S, Veien ES, Wu YY, Chow RL, Dorsky RI, Levine EM: **Negative regulation of Vsx1 by its paralog Chx10/Vsx2 is conserved in the vertebrate retina**. *Brain research* 2008, **1192**:99-113.
39. Endeman D, Klaassen LJ, Kamermans M: **Action Spectra of Zebrafish Cone Photoreceptors**. *PloS one* 2013, **8**(7):e68540.
40. Sherpa T, Fimbel SM, Mallory DE, Maaswinkel H, Spritzer SD, Sand JA, Li L, Hyde DR, Stenkamp DL: **Ganglion Cell Regeneration Following Whole-Retina Destruction in Zebrafish**. *Developmental neurobiology* 2008, **68**(2):166-181.
41. Sherpa T, Lankford T, McGinn TE, Hunter SS, Frey RA, Sun C, Ryan M, Robison BD, Stenkamp DL: **Retinal regeneration is facilitated by the presence of surviving neurons**. *Developmental neurobiology* 2014, **74**(9):851-876.
42. Roesch K, Jadhav AP, Trimarchi JM, Stadler MB, Roska B, Sun BB, Cepko CL: **The transcriptome of retinal Muller glial cells**. *The Journal of comparative neurology* 2008, **509**(2):225-238.
43. Jadhav AP, Roesch K, Cepko CL: **Development and neurogenic potential of Muller glial cells in the vertebrate retina**. *Progress in retinal and eye research* 2009, **28**(4):249-262.
44. Fischer AJ, Bongini R: **Turning Muller glia into neural progenitors in the retina**. *Molecular neurobiology* 2010, **42**(3):199-209.
45. Karl MO, Reh TA: **Regenerative medicine for retinal diseases: activating endogenous repair mechanisms**. *Trends in molecular medicine* 2010, **16**(4):193-202.

46. Fausett BV, Goldman D: **A role for alpha1 tubulin-expressing Muller glia in regeneration of the injured zebrafish retina**. *The Journal of neuroscience : the official journal of the Society for Neuroscience* 2006, **26**(23):6303-6313.
47. Ramachandran R, Reifler A, Parent JM, Goldman D: **Conditional gene expression and lineage tracing of tuba1a expressing cells during zebrafish development and retina regeneration**. *The Journal of comparative neurology* 2010, **518**(20):4196-4212.
48. Fischer AJ, Reh TA: **Potential of Muller glia to become neurogenic retinal progenitor cells**. *Glia* 2003, **43**(1):70-76.
49. Braisted JE, Raymond PA: **Regeneration of dopaminergic neurons in goldfish retina**. *Development (Cambridge, England)* 1992, **114**(4):913-919.
50. Montgomery JE, Parsons MJ, Hyde DR: **A novel model of retinal ablation demonstrates that the extent of rod cell death regulates the origin of the regenerated zebrafish rod photoreceptors**. *The Journal of comparative neurology* 2010, **518**(6):800-814.
51. D'Orazi FD, Zhao X-F, Wong RO, Yoshimatsu T: **Mismatch of Synaptic Patterns between Neurons Produced in Regeneration and during Development of the Vertebrate Retina**. *Current biology : CB* 2016, **26**(17):2268-2279.
52. Curcio CA, Medeiros NE, Millican CL: **Photoreceptor loss in age-related macular degeneration**. *Investigative ophthalmology & visual science* 1996, **37**(7):1236-1249.
53. McGinn TE, Mitchell DM, Meighan PC, Partington N, Leoni DC, Jenkins CE, Varnum MD, Stenkamp DL: **Restoration of Dendritic Complexity, Functional Connectivity, and Diversity of Regenerated Retinal Bipolar Neurons in Adult Zebrafish**. *The Journal of Neuroscience* 2017.
54. Heermann S, Schutz L, Lemke S, Krieglstein K, Wittbrodt J: **Eye morphogenesis driven by epithelial flow into the optic cup facilitated by modulation of bone morphogenetic protein**. *eLife* 2015, **4**.
55. Fuhrmann S, Zou C, Levine EM: **Retinal pigment epithelium development, plasticity, and tissue homeostasis**. *Experimental eye research* 2014, **123**:141-150.
56. Sinn R, Wittbrodt J: **An eye on eye development**. *Mechanisms of development* 2013, **130**(6-8):347-358.
57. Marquardt T, Ashery-Padan R, Andrejewski N, Scardigli R, Guillemot F, Gruss P: **Pax6 is required for the multipotent state of retinal progenitor cells**. *Cell* 2001, **105**(1):43-55.
58. Farhy C, Elgart M, Shapira Z, Oron-Karni V, Yaron O, Menuchin Y, Rechavi G, Ashery-Padan R: **Pax6 Is Required for Normal Cell-Cycle Exit and the Differentiation Kinetics of Retinal Progenitor Cells**. *PloS one* 2013, **8**(9):e76489.
59. Riesenberg AN, Le TT, Willardsen MI, Blackburn DC, Vetter ML, Brown NL: **Pax6 regulation of Math5 during mouse retinal neurogenesis**. *Genesis (New York, NY : 2000)* 2009, **47**(3):175-187.
60. Skowronska-Krawczyk D, Chiodini F, Ebeling M, Alliod C, Kundzewicz A, Castro D, Ballivet M, Guillemot F, Matter-Sadzinski L, Matter JM: **Conserved regulatory sequences in Atoh7 mediate non-conserved regulatory responses in retina ontogenesis**. *Development (Cambridge, England)* 2009, **136**(22):3767-3777.
61. Willardsen MI, Suli A, Pan Y, Marsh-Armstrong N, Chien C-B, El-Hodiri H, Brown NL, Moore KB, Vetter ML: **Temporal regulation of Ath5 gene expression during eye development**. *Developmental biology* 2009, **326**(2):471-481.
62. Wang SW, Kim BS, Ding K, Wang H, Sun D, Johnson RL, Klein WH, Gan L: **Requirement for math5 in the development of retinal ganglion cells**. *Genes & development* 2001, **15**(1):24-29.
63. Matsushima D, Heavner W, Pevny LH: **Combinatorial regulation of optic cup progenitor cell fate by SOX2 and PAX6**. *Development (Cambridge, England)* 2011, **138**(3):443-454.
64. Nishina S, Kohsaka S, Yamaguchi Y, Handa H, Kawakami A, Fujisawa H, Azuma N: **PAX6 expression in the developing human eye**. *The British Journal of Ophthalmology* 1999, **83**(6):723-727.
65. Ochocinska MJ, Hitchcock PF: **NeuroD regulates proliferation of photoreceptor progenitors in the retina of the zebrafish**. *Mechanisms of development* 2009, **126**(3-4):128-141.

66. Cherry TJ, Wang S, Bormuth I, Schwab M, Olson J, Cepko CL: **NeuroD factors regulate cell fate and neurite stratification in the developing retina**. *The Journal of neuroscience : the official journal of the Society for Neuroscience* 2011, **31**(20):7365-7379.
67. Pennesi ME, Cho J-H, Yang Z, Wu SH, Zhang J, Wu SM, Tsai M-J: **BETA2/NeuroD1 Null Mice: A New Model for Transcription Factor-Dependent Photoreceptor Degeneration**. *The Journal of Neuroscience* 2003, **23**(2):453-461.
68. Liu H, Etter P, Hayes S, Jones I, Nelson B, Hartman B, Forrest D, Reh TA: **NeuroD1 regulates expression of thyroid hormone receptor 2 and cone opsins in the developing mouse retina**. *The Journal of neuroscience : the official journal of the Society for Neuroscience* 2008, **28**(3):749-756.
69. Elshatory Y, Everhart D, Deng M, Xie X, Barlow RB, Gan L: **Islet-1 controls the differentiation of retinal bipolar and cholinergic amacrine cells**. *The Journal of neuroscience : the official journal of the Society for Neuroscience* 2007, **27**(46):12707-12720.
70. Zhuang S, Zhang Q, Zhuang T, Evans SM, Liang X, Sun Y: **Expression of Isl1 during mouse development**. *Gene expression patterns : GEP* 2013, **13**(8):407-412.
71. Feng L, Xie X, Joshi PS, Yang Z, Shibasaki K, Chow RL, Gan L: **Requirement for Bhlhb5 in the specification of amacrine and cone bipolar subtypes in mouse retina**. *Development (Cambridge, England)* 2006, **133**(24):4815-4825.
72. Oh EC, Khan N, Novelli E, Khanna H, Strettoi E, Swaroop A: **Transformation of cone precursors to functional rod photoreceptors by bZIP transcription factor NRL**. *Proc Natl Acad Sci U S A* 2007, **104**(5):1679-1684.
73. Nelson SM, Park L, Stenkamp DL: **Retinal homeobox 1 is required for retinal neurogenesis and photoreceptor differentiation in embryonic zebrafish**. *Developmental biology* 2009, **328**(1):24-39.
74. Chuang JC, Raymond PA: **Zebrafish genes rx1 and rx2 help define the region of forebrain that gives rise to retina**. *Developmental biology* 2001, **231**(1):13-30.
75. Shen YC, Raymond PA: **Zebrafish cone-rod (crx) homeobox gene promotes retinogenesis**. *Developmental biology* 2004, **269**(1):237-251.
76. Mortazavi A, Williams BA, McCue K, Schaeffer L, Wold B: **Mapping and quantifying mammalian transcriptomes by RNA-Seq**. *Nature methods* 2008, **5**(7):621-628.
77. Wilhelm BT, Marguerat S, Watt S, Schubert F, Wood V, Goodhead I, Penkett CJ, Rogers J, Bahler J: **Dynamic repertoire of a eukaryotic transcriptome surveyed at single-nucleotide resolution**. *Nature* 2008, **453**(7199):1239-1243.
78. Trapnell C, Williams BA, Pertea G, Mortazavi A, Kwan G, van Baren MJ, Salzberg SL, Wold BJ, Pachter L: **Transcript assembly and quantification by RNA-Seq reveals unannotated transcripts and isoform switching during cell differentiation**. *Nature biotechnology* 2010, **28**(5):511-515.
79. Bradford JR, Hey Y, Yates T, Li Y, Pepper SD, Miller CJ: **A comparison of massively parallel nucleotide sequencing with oligonucleotide microarrays for global transcription profiling**. *BMC genomics* 2010, **11**:282.

**Chapter 2: Transcripts within rod photoreceptors of the zebrafish retina**

Chi Sun, Carlos Galicia, and Deborah L. Stenkamp

Publications status: under revision for BMC Genomics

Abstract

Background: The purpose of this study was to identify transcripts of retinal rod photoreceptors of the zebrafish. The zebrafish is an important animal model for vision science due to rapid and tractable development, persistent neurogenesis of rods throughout the lifespan, and capacity for functional retinal regeneration.

Results: Zebrafish rods, and non-rod retinal cells of the *XOPS:eGFP* transgenic line, were separated by cell dissociation and fluorescence-activated cell sorting (FACS), followed by RNA-seq. At a false discovery rate of <0.01, 597 transcripts were upregulated ("enriched") in rods vs. non-rod retinal cells, and 1032 were downregulated ("depleted"). 13,324 total transcripts were detected in rods, including many not previously known to be expressed by rods. 45 transcripts were validated by qPCR in FACS-sorted rods. Transcripts enriched in rods from adult retinas were also enriched in rods from larval and juvenile retinas, and were also enriched in rods sorted from retinas subjected to a neurotoxic lesion and allowed to regenerate. Many transcripts enriched in rods were upregulated in retinas of wildtype retinas vs. those of a zebrafish model for rod degeneration.

Conclusions: We report the generation and validation of an RNA-seq dataset describing the rod transcriptome of the zebrafish, which is now available as a resource for further studies of rod photoreceptor biology and comparative transcriptomics.

Background

Within the vertebrate neural retina, photoreceptor cells are the sensory neurons that detect photons and convert this physical information into electrochemical signals. Rod photoreceptors contain the visual pigment rhodopsin, are highly sensitive to light, and provide predominantly convergent information to downstream neurons to maximize light detectability in low-light situations. Cone photoreceptors contain cone visual pigments (cone opsins) with distinct peak spectral sensitivities, and provide convergent and divergent information to downstream neurons, which process differential input to discriminate color and provide high acuity vision. Photoreceptors display distinctive morphologies with specialized apical projections, the outer segments, which are highly modified nonmotile cilia [1]. Outer segments include membranous disks to increase surface area for containing opsins and other phototransduction proteins, and photoreceptors maintain these outer segments with a high rate of protein synthesis, together with mechanisms for selective protein targeting and trafficking [2]. Rod photoreceptors in humans are particularly sensitive to genetic changes in structural and functional components; such defects cause hereditary retinal degenerations, which typically involve rod cell death, followed by cone cell death and loss of vision [3]. There is therefore great interest in increasing our depth of understanding of rod photoreceptor biology, health, the factors leading to cell death, and the discovery of strategies for promoting rod survival and/or rod replacement.

The zebrafish, an important animal model in vision research, is an example of a vertebrate with the endogenous capacity for rod replacement [4]. The zebrafish retina grows throughout its lifespan through the addition of new neurons at the retinal periphery, called the circumferential germinal zone (CGZ) or ciliary marginal zone (CMZ) [5-7]. In addition, Müller glia throughout the growing retina divide at a slow rate, generating a transiently-amplifying population of rod progenitors that migrate to the photoreceptor layer, and divide to generate

rod photoreceptors [8]. The zebrafish retina therefore accumulates rods over its lifespan from these dedicated rod lineages. In zebrafish models of rod degeneration, either the most immediate precursors within the photoreceptor layer accelerate the production of new rods [9, 10], or the progenitor lineage is stimulated to increase rod neurogenesis to replace rods lost to damage [10]. In response to more widespread retinal damage due to chemical trauma, the progenitors generated by cell division of Müller glia gain the capacity to regenerate other types of retinal neurons [11-14], ultimately resulting in restoring visual function [11, 15]. The existence of the rod lineage is well-documented in zebrafish [8, 16, 17], and in other teleosts [18-20], and holds promise to inform the development of rod replacement strategies to treat human retinal disease. However, our knowledge of rods, and the rod lineage, within the zebrafish remains limited to a small number of rod-specific markers (primarily phototransduction components) [21], and a network of transcription factors important for rod determination and differentiation [5, 16, 22-25]. A single, distinctive marker for cells of the dedicated lineage that generates new rods, other than incorporation of S-phase markers, remains surprisingly elusive.

In the present study, we begin to fill this knowledge gap through RNA-sequencing (RNA-seq) analysis of the transcriptome of isolated rod photoreceptors, in comparison with non-rod retinal cells. In the transgenic line *XOPS:eGFP*, rod photoreceptors exclusively express high levels of GFP [26], permitting isolation of rods from other retinal cells by fluorescence-activated cell sorting (FACS). This approach revealed transcripts that were upregulated in rods vs. non-rods, those that were present in rods but not differentially expressed, and those that were downregulated in rods vs. non-rods. Quantitative PCR (qPCR) studies suggested that this transcriptome is remarkably stable over the zebrafish lifespan from larval to adult ages, and appeared similar in rods that had regenerated following a chemical lesion. The zebrafish rod transcriptome is now a resource that can be

mined for the identification of novel structural and functional components of rods, and possibly their progenitors, and for future comparative analyses with transcriptomes of rods and/or cones from key model organisms.

## Methods

### *Animals and tissue preparation*

All procedures involving animals were carried out in compliance with protocols approved by the University of Idaho Animal Care and Use Committee. Zebrafish (*Danio rerio*) were maintained on a 14:10 light:dark cycle in recirculating, monitored system water, housed and propagated according to [27]. For this study we used the *XOPS:eGFP* transgenic line, in which the *Xenopus* rod opsin promoter drives expression of eGFP exclusively in rod photoreceptors [26], the gift of James Fadool, and a wild-type strain originally obtained from Scientific Hatcheries (now Aquatica Tropicals). In addition we used the *XOPS:mCFP* transgenic line, the gift of Ann Morris. In this line, the presence of mCFP in retinal rods leads to rapid rod degeneration, and a proliferative response to this degeneration by the rod precursor population [9].

To obtain retinal tissues for fluorescence-activated cell sorting (FACS), *XOPS:eGFP* fish were dark-adapted for 10-12 hours, anaesthetized with MS-222, and eyes enucleated with fine forceps. Corneas and lenses were removed, and retinas were peeled free from the RPE and whole eyecup in saline. In some cases, as indicated in Results, we used whole adult (1.5 yrs), juvenile (1 month), or larval (14 days post-fertilization; dpf) retinas for FACS and quantitative RT-PCR (qPCR). In all cases, RNA isolation was performed immediately following tissue collection or FACS.

Tissues for *in situ* hybridization were fixed in phosphate-buffered, 4% paraformaldehyde containing 5% sucrose for 1 hr at room temperature, and washed in

phosphate-buffered 5% sucrose, and then a graded series ending in 20% sucrose for overnight cyroprotection at 4°C. Tissues were embedded in a 1:2 solution of OCT embedding medium (Sakura Finetek) and phosphate-buffered, 20% sucrose, and frozen in isobutane supercooled with liquid $N_2$. After freezing solid, tissues were sectioned at 5 µm on a Leica CM3050 cryostat [15, 28].

*Cell dissociation and FACS*

Whole retinas were dissociated into cell suspensions by incubating with 0.225% trypsin (Fisher ThermoScientific) and 0.001% papain (Worthington Biochemical) for 10 minutes at 37°C. Dissociation was stopped by the addition of fetal bovine serum (10% v/v final concentration). Suspended cells were pelleted and incubated with DNAseI at room temperature for 15 min. Cells were pelleted and resuspended in 100 µL phosphate-buffered (pH 6.5) saline (PBS) and immediately FACS-sorted.

GFP+ vs. GFP- retinal cells were sorted using a BD FACSAria flow cytometer, using the 488 nm laser and FITC fluorescence filter, and the 70 µm nozzle. Some cells were collected for fluorescence microscopy, or for post-sort FACS analysis. For RNA-seq or qPCR, GFP+ and GFP- cells were collected separately in the FACS sheath fluid, and RNA was immediately extracted.

*RNA isolation and quantitative real-time PCR (qPCR)*

RNA was extracted from tissue samples using the NucleoSpin® RNA kit (Macherey-Nagel) using the manufacturer's protocol, quantified and quality-checked on a Nanodrop spectrophotometer, and cDNA was synthesized using the SuperScript® kit (New England Biotech) using random hexamer primers. Gene-specific primers used for qPCR were designed using AlleleID7/84 (Premier Biosoft), and are provided in Table 2.1. Amplification

was carried out using a model 7900HT Fast Real-Time PCR System and SYBR-Green PCRMaster Mix (Applied Biosystems, Inc.), using 18S as the reference transcript [29].

*Library construction, RNA-seq, and bioinformatics*

Both quantity and quality of RNA were assessed by using an Agilent 2100 Bioanalyzer. All samples used for RNA-seq had an RNA integrity number (RIN) > 8.0, and the experimental design retained pairing information between GFP+ cells and GFP- cells derived from both retinas of a single fish, allowing us to analyze them as paired samples. At least 5 ng of RNA was available per sample, and provided to the University of Idaho's Institute for Bioinformatics and Evolutionary Studies (IBEST) Genomics Core for RNA amplification, the generation of cDNA, sequencing, and bioinformatics. Quality and quantity of cDNA libraries were verified by Bioanalyzer. All sample preparation was achieved with Ovation® RNA-Seq System V2 (NuGEN), and sequencing performed on an Illumina (San Diego, CA) MiSeq with MiSeq Reagent Kit v3, 600 cycle kit. Four replicates (from four different fish) were sequenced (Fig. 2.1A). Reads were quality-trimmed with Sickle (https://github.com/najoshi/sickle), and paired reads were overlapped with FLASH [30]. Overlapped reads were aligned against Zv9.75 using the Burrows-Wheeler aligner [31]. BAM files were sorted with using SAMtools [32], and reads were counted by feature using HTSeq-count [33]. Counts were analyzed and differentially expressed genes were identified with R [34] and edgeR [35]. Descriptive plots were generated, and gene ontology (GO) analysis and hierarchical clustering were performed, with R and GOstats [36]. Comparison with a publicly available microarray dataset [37] was done using paralogue and probe identifier information available via Ensembl's BioMart (http://www.ensembl.org/biomart/martview/95190a55c419b703e7582fb25e0470be).

*Probe preparation and in situ hybridization*

Zebrafish *rho* (*rhodopsin*) cDNA, in pBK-CMV phagemid, was the gift of T. Vihtelic. Other cDNAs were generated as follows. Total RNA was extracted from homogenized adult zebrafish retina, and cDNA was generated using random hexamers and oligo(dT) primers. Gene-specific primers (Table 2.2) corresponding to *rhol*, *dscamb*, *rxrga*, and *rxrgb* predicted mRNAs were designed using Primer-BLAST (https://www.ncbi.nlm.nih.gov/tools/primer-blast/), were used for PCR amplifications, and the resulting amplicons were gel-purified and ligated using TA-ligation into the pGEM-T-Easy vector (Promega), which contains T7 and SP6 promoters. cDNAs were sequence-verified (*ElimBio;* St. Hayward, CA), with sequencing results compared to original genomic sequence using nucleotide Blast software and viewed in *Sequencher* (GeneCodes). Digoxigenin (dig) –labeled cRNA probes were prepared using T7 or SP6 RNA polymerase (Roche) according to the manufacturer's instructions. *In situ* hybridization was carried out according to Nelson et al. [16]. In brief, sections were rehydrated, permeabilized with proteinase K, dehydrated and incubated with probe in a solution containing 50% formamide, with hybridization temperatures optimized for each probe using PolyPro [38]. Hybridized tissues were treated with RNAse A, and the presence of dig was detected with anti-dig antibodies conjugated to alkaline phosphatase, followed by an NBT-BCIP (Roche) or BM-purple (Sigma) color reaction carried out according to the manufacturer's instructions. *In situs* were imaged on a Leica DM2500 upright microscope with a Leica DFC700T camera using DIC optics. In addition to antisense probes, sense probes were also prepared and confirmed not to generate detectable signal.

*Retinal damage and regeneration*

The retinas of adult *XOPS:eGFP* fish (1 yr) were chemically lesioned to destroy all retinal neurons while sparing Müller glia [13]. Briefly, fish were anaesthetized by tricaine and

an incision was made across the cornea with a sapphire blade. Using a Hamilton syringe, 0.4 µL - 0.6 µL of 200 µM ouabain was injected into the vitreal chamber of the right eye, resulting in an estimated intraocular concentration of 10 µM. Loss of GFP+ photoreceptors was verified in sectioned retinas obtained from parallel experiments at three days post-injury (3 dpi), and by viewing retinas of live, anaesthetized fish with epifluorescence stereomicroscopy (Leica M165 FC), also at 3 dpi. Lesioned zebrafish were allowed to recover, and regenerate their retinas [11] until 14 dpi or 30 dpi, and were humanely sacrificed to collect retinas for cell dissociation, FACS, and qPCR.

## Results

### *Transcripts of rods of adult zebrafish retina*

We isolated highly pure rod and non-rod retinal cell populations by FACS-sorting cell suspensions from adult *XOPS:eGFP* zebrafish retinas (Fig. 2.1A). GFP+ cells (P1 in Fig. 2.1B) made up 10-20% of all collected retinal cells and constituted a distinctive cell population as compared with the GFP- population (P2 in Fig. 2.1B). To verify purity of our sorted populations, a separate sample from one fish was used to collect GFP+ cells using the same FACS-sorting parameters as those used for RNA-seq, and we subsequently examined the sorted population by fluorescence microscopy and by post-sort analysis (Fig. 2.1C). These results indicated that P1 population was highly enriched for GFP+ cells (Fig. 2.1C), and therefore suitable for transcriptome analysis.

We performed RNA-seq on both the rod (GFP+; P1) and the non-rod (GFP-; P2) populations, in order to identify transcripts enriched, present, or depleted in the rod population as compared with other retinal cells (similar to the approach of [39]). The resulting dataset is publicly available via the Gene Expression Omnibus (GEO; accession #

GSE100062). Sequencing depth ranged from 2,781,516 to 3,480,515 reads per sample, and mapping percentages ranged from 97.0% to 97.4% per sample. Multidimensional scaling showed good separation of GFP+ vs. GFP- samples along the first dimension and separation by sample along the second dimension. The plot of estimated Biological Coefficient of Variation (BCV) indicated a trend in dispersion associated with expression, leading us to fit a trended model within edgeR before doing differential expression analysis. Differentially expressed transcripts were identified as those significantly upregulated or downregulated in the GFP+ population vs. the GFP- population. Those identified with a false discovery rate (FDR) of < 0.01 consisted of 1629 distinct entries (597 upregulated, 1032 downregulated); those identified with an FDR of <0.05 consisted of 2439 entries. The top 50 upregulated and top 50 downregulated transcripts within the GFP+ vs. GFP- populations, based upon FDR, are provided as Tables 2.3 and 2.4, respectively. Numerous transcripts known to be expressed exclusively by rods were significantly upregulated (enriched) in the GFP+ cell population, including *rho*, *pde6g*, *rom1b*, and *gnat1* (Table 2.3). Numerous transcripts known to be primarily expressed by other retinal cell types were significantly downregulated (depleted) in the GFP+ cell population, including cone transcripts *opn1lw2* (long wavelength-sensitive cone opsin 2), *opn1mw3* (cone opsin *rh2-3*), and *cnga3a*, and the macrophage/microglial marker *mpeg1* [40] (Table 2.4). These outcomes further confirmed the rod (GFP+) vs. non-rod (GFP-) identities of our sample cell populations.

To provide broad classification of rod-enriched transcripts, we used gene ontology (GO) analysis. GO molecular function categories significantly overrepresented in GFP+ samples included those related to cyclic nucleotide metabolism, intermediary metabolism, and ion transport (Fig. 2.2A), and GO biological processes that were overrepresented included intracellular transport processes, photoreceptor cell development, and the kit and notch signaling pathways (Fig. 2.2B). GO cellular component categories significantly

overrepresented in the GFP+ samples included those related to cytoskeletal components and those related to cilia (Fig. 2.2C). These categories reflect the underlying structure, function, and very likely the ongoing developmental programs engaged for maintaining rod structure and function. It is surprising, however, that some of these categories were overrepresented considering the large number of cones in the GFP- retinal cell population that were also expected to demonstrate similar molecular functions, biological processes, and cellular components. Hierarchical clustering of the rod-enriched transcripts returned only three, highly similar clusters (Fig. 2.2D), suggesting very little sample heterogeneity within the GFP+ samples and within the GFP- samples. Our experimental design included sex as a potential biological variable, such that we could analyze a sex X rod interaction. This analysis returned only five entries with an FDR < 0.05 (Table 2.5).

The analyses described above focused upon transcripts that were differentially expressed in GFP+ vs. GFP- cells, therefore identifying enriched transcripts in either population. To identify additional transcripts present in rods, but not necessarily enriched in comparison with other retinal cells, we generated a list of transcripts for which all GFP+ samples returned a non-zero value. This list of transcripts present in rods amounted to 13,324 distinct entries (not shown), approximately 23% of the total number of predicted transcripts (58,549; Ensembl GRCz10) encoded by the zebrafish genome. This list included numerous photoreceptor (but not rod-specific) genes such as *irbp*, *neurod*, *crx*, and *rx1*, and some genes not previously known to be expressed in rod photoreceptors, such as *opsin 4.1*, a zebrafish *melanopsin* [41], and several nuclear hormone receptors including *rxrγa*. The latter is noteworthy because the mouse orthologue (*RXRγ*) was reported to be cone-specific [42].

Forty-five transcripts were selected for validation analysis by qPCR in independently sorted GFP+ vs. GFP- cells from adult *XOPS:eGFP* zebrafish. Selected transcripts that were

detected by RNA-seq as significantly enriched in rods, were all likewise determined to be significantly enriched in rods by qPCR, at similar relative magnitudes (Fig. 2.3A). Selected transcripts that were detected by RNA-seq as present, though not enriched in rods, were all detectable by qPCR (see first five genes in Fig. 2.3B). Transcripts detected by RNA-seq as significantly depleted but still present in rods, were nearly all determined to be significantly depleted in rods by qPCR, with the exception of *mef2cb*, where qPCR did not detect a significant difference (see last six genes in Fig. 2.3B). These qPCR results provide strong validation that the RNA-seq dataset generated in this study will serve as a reliable resource for many future applications.

*Rod photoreceptor transcripts over the lifespan and in a genetic model for rod degeneration*

As zebrafish grow, they continue to generate new rods throughout the retina from a dedicated rod lineage [4, 16], the apex of which (stem cell for rod lineage) has been identified as the Müller glial cell [8]. Therefore we wished to determine whether the rod transcriptome remained consistent over the zebrafish lifespan, or if the rod population of larval zebrafish would be distinct from the accumulated (and generally older) rod population of adult zebrafish. A subset of the selected transcripts that were qPCR validated in adult zebrafish, were therefore evaluated further by qPCR in GFP+ vs. GFP- retinal cell populations obtained from larval zebrafish sacrificed at 14 dpf (days post-fertilization), and juvenile zebrafish sacrificed at 30 dpf. In general, the relative expression levels of selected rod-enriched transcripts within the GFP+ vs. GFP- cell populations were remarkably stable from larval through adult stages (Fig. 2.4A). However, *rho* transcripts appeared more highly enriched in rods of adult zebrafish than in rods of larval or juvenile zebrafish, suggesting that rods of adults may accumulate transcript at higher levels than rods of younger fish. *Rhol* (rhodopsin-like) transcripts showed the opposite trend (Fig. 2.4A), consistent with the recent findings of

[43], who detected limited expression of *rhol* in adult retina. Other transcripts more highly enriched in the rods of younger fish were *gngt1*, *ngf*, and *aipl1*. Transcripts present, or present but significantly depleted in adult rods, were less consistent over the lifespan; notable were *rxrga* and *mef2ca*, which were not differentially expressed in GFP+ vs. GFP- cells of larvae or juveniles, but were significantly downregulated (depleted) in rods of older zebrafish (Fig. 2.4B). Rod-specific functions for the encoded nuclear hormone receptor may be distinctive for rods of younger vs. older zebrafish.

We next measured expression (by qPCR) of selected transcripts in whole retinas obtained from WT zebrafish and from *XOPS:mCFP* zebrafish, which show a chronic rod degeneration that stimulates proliferation of a rod precursor population [37]. We anticipated that transcripts identified in the present study as rod-enriched, would be upregulated in WT retinas (containing mature rods) vs. *XOPS:mCFP* retinas (not containing mature rods). This was true for *rho*, *rhol*, *dscamb*, and *ngf*, but not true for *esrrd*, *nrl*, and *nr2f1b*, which were not differentially expressed in WT vs. *XOPS:mCFP* retinas (Fig. 2.5A). It is possible that the latter genes may have other retinal functions in the response to the chronic loss of rods. We also tested two transcripts present (but not enriched) in rods, *rxrgb* and *Lplastin*, and these were both significantly differentially downregulated in WT vs. *XOPS:mCFP* retinas (Fig. 2.5B), again suggestive of roles in response to chronic loss of rods. Two transcripts depleted in rods, and known to be expressed in cones in zebrafish or other model organisms, *rxrga* and *thrb* [42, 44-46], were not differentially expressed in WT vs. *XOPS:mCFP* retinas, consistent with their likely predominant localization to cones, which are unaffected in the *XOPS:mCFP* zebrafish [9]. Differentially expressed genes in WT vs. *XOPS:mCFP* retinas have previously been identified using microarray (GEO Acc # GSE22221) [37], allowing a deeper comparison of the two datasets. Using a cutoff of $p<0.01$ for both datasets returned 94 shared entries (Fig. 2.5C), including known photoreceptor genes *aanat1*, *pde6a*, *rom1a*, and *rom1b*. We

believe the number shared by the datasets is limited to 94 transcripts is in part due to the incomplete representation of zebrafish transcripts on the Agilent chip used for the microarray study.

Selected transcripts were further examined by *in situ* hybridization to visualize spatial expression patterns. For these studies we selected *rhol* and *dscamb* as rod-enriched transcripts, and *rxrga* and *rxrgb* as transcripts present in rods (Fig. 2.6). The expression pattern of *rho* is shown for reference as an example of a rod-exclusive hybridization pattern (Fig. 2.6A). *Rhol* (*rh1-2*) was previously detected as a second *rho* gene in zebrafish [47] and other teleost fish [43], with demonstrated phototransduction functions and expression in the photoreceptor layer [43]. In the present study we have confirmed that *rhol* is expressed (and enriched) in rods, based upon RNA-seq and qPCR of purified rods (Fig. 2.6B). In tissues sampled at 14 dpf, *rhol* was expressed in the photoreceptor layer, in a subset of cells matching the distribution of rods, but restricted primarily to the peripheral retina. This predominantly peripheral pattern was evident in retinas sampled at 1 month, and in adult retina, where only very weak expression was detected in central retina (Fig. 2.6B). In retinas of the *XOPS:mCFP* line that displays rod degeneration, *rhol* was not detected by *in situ* hybridization, even though some developing/dying *rho*-expressing cells are present (Fig. 2.6B). In rods that express *rhol*, the timing of expression may be delayed as compared with *rho* (*rho* is first expressed embryonically, while *rhol* is first expressed in larvae [47]), and rods of *XOPS:mCFP* zebrafish may simply not survive long enough to express *rhol*.

*Dscamb* is one of two zebrafish orthologues of mammalian *Dscam*. Mammalian Dscam encodes a homophilic cell adhesion molecule with numerous roles in retinal cell patterning and refinement of circuitry [48, 49], but is not expressed in mouse rods [50] (although *dscamlike1* is expressed in mouse rods; [51]. In larval and juvenile zebrafish retinas, *dscamb* was expressed in some cells of the outer nuclear layer (photoreceptor layer;

ONL), in a pattern consistent with identities of rods and possibly a subset of cones, and was also seen in the inner nuclear layer (INL) and ganglion cell layer (GCL) in a pattern suggestive of amacrine cells (Fig. 2.6C). Expression of *dscamb* in adult zebrafish retinas showed similar patterns (Fig. 2.6C). The *XOPS:mCFP* retinas showed apparently greatly reduced expression in the photoreceptor layer, consistent with *dscamb* localization to rods (Fig. 2.6C).

In larval and juvenile zebrafish, *rxrga* and *rxrgb* were both diffusely expressed in all retinal cellular layers, and more strongly localized to the far peripheral photoreceptor layer and the stem/progenitor cell-containing CMZ (Fig. 2.6D,E). The former pattern suggests transient higher expression in newly-generated photoreceptors, consistent with our previous report of expression of transient expression of *rxrga* in photoreceptors of zebrafish embryos [52]. Juvenile and adult zebrafish WT retinas, and those of *XOPS:mCFP* fish, both showed a diffuse pattern throughout all cellular layers, although the juvenile samples showed more pronounced expression of *rxrga* within the GCL and inner INL (Fig. 2.6D,E). These findings are consistent with the lack of significant enrichment of these transcripts in rods of adult zebrafish as detected by RNA-seq and qPCR (Fig. 2.3).

*Rod photoreceptor transcripts in regenerated retina*

The zebrafish regenerates a functional retina following widespread damage due to intravitreal injection of the neurotoxin ouabain [11]. However, regenerated fish retinas display histological errors [14, 15] and disruptions of two-dimensional patterning [53, 54]. Although microarray and other analyses have revealed transcriptional changes in response to damage and accompanying the proliferative response of Müller glia [55-57], the molecular signatures of identified, regenerated retinal neurons have never been compared with those of native, undamaged retinal neurons. We sampled regenerated retinas at 14 dpi, a time when all

retinal layers are known to be re-established, but with some histological errors and very thin plexiform layers [11]. Another set of regenerated retinas was sampled at 30 dpi, when plexiform layers have expanded, but histological errors remain [15]. Regenerated *XOPS:eGFP* retinas were dissociated, FACS-sorted, and subjected to qPCR of selected transcripts. Transcripts that were detected as significantly rod-enriched in undamaged retinas were also significantly rod-enriched in regenerated retinas at 14 and 30 dpi (Fig. 2.7A), providing an initial indication that regenerated rods are similar at the transcript level as the undamaged rods. Both *rho* and *rhol* were more highly enriched in the regenerating rods, and *nrl* was more highly enriched at 14 dpi (Fig. 2.7A). *Rxrgb* was detected, but not differentially expressed, in all samples, while *rxrga* was significantly depleted in rods of undamaged retina and at 14 dpi, but not 30 dpi (Fig. 2.7B). *Thrb*, important for determination of red-sensitive cones [46] was detected, but highly significantly depleted in all samples (Fig. 2.7B). Together these findings suggest that the rod transcriptome in regenerated retina possibly carries a molecular signature similar to that of undamaged rods.

## Discussion

We report for the first time, transcripts enriched, present, and depleted in purified rod photoreceptors of the adult zebrafish retina, now available as a resource for other investigators with interests in rod health, structure, function, and neurogenesis. The dataset was validated by qPCR of 45 transcripts, and many transcripts present in rods were not previously recognized as rod-enriched. Analysis of FACS-sorted fluorescent rods from transgenic zebrafish appears to be an excellent approach for expanding our knowledge of rod biology, and in the future may be applied to other photoreceptor subpopulations [58],

since there are numerous transgenic tools available that selectively fluorescently label specific cone subtypes [59, 60].

The rod transcriptome appears to be remarkably stable over the zebrafish lifespan, at least for the rod-enriched transcripts studied in this manner, and at the sampling times used. The rod population of adult zebrafish, which includes the rods generated larvally – these rods are nearly as old as the zebrafish themselves – as well as the many rods that accumulated through adulthood, likely carries a molecular signature similar to that of the newly-generated rods of larval retina. The potential exceptions are the transcripts encoding the visual pigment proteins themselves, *rho* and *rhol*. *Rho* is more abundant in the rods from older fish, where the rod population includes many older rods. However, *rhol* is more abundant in those of younger fish. Interestingly, the peak spectral sensitivity of *rhol* is shifted 5 nm shorter than that of *rho* [43], although it is not known whether this difference is meaningful in the visual environment of zebrafish when rods are utilized. It is possible that the higher levels of *rhol* in rods of younger zebrafish are important for a visually-mediated behavior such as a prey capture strategy, that is different in larval/juvenile vs. adult zebrafish [61]. Extending the unbiased RNA-seq approach for the study of rod transcripts over the zebrafish lifespan may reveal other functional changes.

We used two approaches to evaluate rod transcripts in situations where the zebrafish retina responds to rod damage. In the first approach, we analyzed selected rod-enriched, and rod-depleted genes in WT retinas vs. those with chronic loss and attempted replacement of rods (*XOPS:mCFP*) [9]. Some of these rod-enriched transcripts were upregulated in WT retinas vs. *XOPS:mCFP*, consistent with the lack of mature rods in the *XOPS:mCFP* retinas. However, some were not, pointing to alternative roles for these transcripts in some aspect of the response to chronic damage, for example in the environment of high levels of cell death, or in upregulation of rod precursor proliferation. The second approach was to analyze

selected rod-enriched, and rod-depleted genes following widespread retinal damage and a regeneration period. We found that transcripts enriched in undamaged, native rods, also were enriched in regenerated rods. Again the extension of the unbiased RNA-seq approach is likely to be even more illuminating, but this initial result suggests that regenerated rods do not differ in expression of a set of selected transcripts in comparison with undamaged, native rods. This finding implies that regenerated retinal neurons may not carry with them alternative molecular signatures, and likely recover their distinctive functions.

## Conclusions

We report the generation and validation of an RNA-seq dataset describing the rod transcriptome of the zebrafish. This transcriptome appears stable across the zebrafish lifespan, and similar in regenerated rods as compared with undamaged rods. Future applications of this study include comparative photoreceptor transcriptomics (rods vs. each cone subtype), and comparative analysis with transcriptome information available from other model organisms including mouse [62], as well as from stem cell-derived human retinal organoids [63]. Such studies have potential to reveal further distinctions of cones vs. rods, and distinctions among vertebrates that may resolve questions of vertebrate photoreceptor evolution [25, 64-66].

References


1. May-Simera H, Nagel-Wolfrum K, Wolfrum U: **Cilia - The sensory antennae in the eye**. *Progress in retinal and eye research* 2017.
2. Nemet I, Ropelewski P, Imanishi Y: **Rhodopsin Trafficking and Mistrafficking: Signals, Molecular Components, and Mechanisms**. *Prog Mol Biol Transl Sci* 2015, **132**:39-71.
3. Nash BM, Wright DC, Grigg JR, Bennetts B, Jamieson RV: **Retinal dystrophies, genomic applications in diagnosis and prospects for therapy**. *Transl Pediatr* 2015, **4**(2):139-163.
4. Stenkamp DL: **The rod photoreceptor lineage of teleost fish**. *Progress in retinal and eye research* 2011, **30**(6):395-404.
5. Stenkamp DL: **Neurogenesis in the fish retina**. *International review of cytology* 2007, **259**:173-224.
6. Marcus RC, Delaney CL, Easter SS, Jr.: **Neurogenesis in the visual system of embryonic and adult zebrafish (Danio rerio). off**. *Visual neuroscience* 1999, **16**(3):417-424.
7. Raymond PA, Barthel LK, Bernardos RL, Perkowski JJ: **Molecular characterization of retinal stem cells and their niches in adult zebrafish**. *BMC developmental biology* 2006, **6**:36.
8. Bernardos RL, Barthel LK, Meyers JR, Raymond PA: **Late-stage neuronal progenitors in the retina are radial Muller glia that function as retinal stem cells**. *The Journal of neuroscience : the official journal of the Society for Neuroscience* 2007, **27**(26):7028-7040.
9. Morris AC, Schroeter EH, Bilotta J, Wong RO, Fadool JM: **Cone survival despite rod degeneration in XOPS-mCFP transgenic zebrafish**. *Investigative ophthalmology & visual science* 2005, **46**(12):4762-4771.
10. Montgomery JE, Parsons MJ, Hyde DR: **A novel model of retinal ablation demonstrates that the extent of rod cell death regulates the origin of the regenerated zebrafish rod photoreceptors**. *The Journal of comparative neurology* 2011, **518**(6):800-814.
11. Sherpa T, Fimbel SM, Mallory DE, Maaswinkel H, Spritzer SD, Sand JA, Li L, Hyde DR, Stenkamp DL: **Ganglion cell regeneration following whole-retina destruction in zebrafish**. *Developmental neurobiology* 2008, **68**(2):166-181.
12. Fimbel SM, Montgomery JE, Burket CT, Hyde DR: **Regeneration of inner retinal neurons after intravitreal injection of ouabain in zebrafish**. *The Journal of neuroscience : the official journal of the Society for Neuroscience* 2007, **27**(7):1712-1724.
13. Nagashima M, Barthel LK, Raymond PA: **A self-renewing division of zebrafish Muller glial cells generates neuronal progenitors that require N-cadherin to regenerate retinal neurons**. *Development (Cambridge, England)* 2013, **140**(22):4510-4521.
14. Powell C, Cornblath E, Elsaeidi F, Wan J, Goldman D: **Zebrafish Muller glia-derived progenitors are multipotent, exhibit proliferative biases and regenerate excess neurons**. *Sci Rep* 2016, **6**:24851.
15. Sherpa T, Lankford T, McGinn TE, Hunter SS, Frey RA, Sun C, Ryan M, Robison BD, Stenkamp DL: **Retinal regeneration is facilitated by the presence of surviving neurons**. *Developmental neurobiology* 2014.
16. Nelson SM, Frey RA, Wardwell SL, Stenkamp DL: **The developmental sequence of gene expression within the rod photoreceptor lineage in embryonic zebrafish**. *Developmental dynamics : an official publication of the American Association of Anatomists* 2008, **237**(10):2903-2917.
17. Morris AC, Scholz T, Fadool JM: **Rod progenitor cells in the mature zebrafish retina**. *Adv Exp Med Biol* 2008, **613**:361-368.
18. Otteson DC, D'Costa AR, Hitchcock PF: **Putative stem cells and the lineage of rod photoreceptors in the mature retina of the goldfish**. *Developmental biology* 2001, **232**(1):62-76.
19. Julian D, Ennis K, Korenbrot JI: **Birth and fate of proliferative cells in the inner nuclear layer of the mature fish retina**. *The Journal of comparative neurology* 1998, **394**(3):271-282.
20. Mack AF, Papanikolaou D, Lillo C: **Investigation of the migration path for new rod photoreceptors in the adult cichlid fish retina**. *Experimental neurology* 2003, **184**(1):90-96.

21. Morris AC, Fadool JM: **Studying rod photoreceptor development in zebrafish**. *Physiology & behavior* 2005, **86**(3):306-313.
22. Hitchcock P, Kakuk-Atkins L: **The basic helix-loop-helix transcription factor neuroD is expressed in the rod lineage of the teleost retina**. *The Journal of comparative neurology* 2004, **477**(1):108-117.
23. Nelson SM, Park L, Stenkamp DL: **Retinal homeobox 1 is required for retinal neurogenesis and photoreceptor differentiation in embryonic zebrafish**. *Developmental biology* 2009, **328**(1):24-39.
24. Wilson SG, Wen W, Pillai-Kastoori L, Morris AC: **Tracking the fate of her4 expressing cells in the regenerating retina using her4:Kaede zebrafish**. *Experimental eye research* 2016, **145**:75-87.
25. Sotolongo-Lopez M, Alvarez-Delfin K, Saade CJ, Vera DL, Fadool JM: **Genetic Dissection of Dual Roles for the Transcription Factor six7 in Photoreceptor Development and Patterning in Zebrafish**. *PLoS Genet* 2016, **12**(4):e1005968.
26. Fadool JM: **Development of a rod photoreceptor mosaic revealed in transgenic zebrafish**. *Developmental biology* 2003, **258**(2):277-290.
27. Westerfield M: **The Zebrafish Book; A guide for the laboratory use of zebrafish (Danio rerio)**, vol. 5th edition. Eugene, OR: University of Oregon Press; 2007.
28. Barthel LK, Raymond PA: **Improved method for obtaining 3-microns cryosections for immunocytochemistry**. *The journal of histochemistry and cytochemistry : official journal of the Histochemistry Society* 1990, **38**(9):1383-1388.
29. Mitchell DM, Stevens CB, Frey RA, Hunter SS, Ashino R, Kawamura S, Stenkamp DL: **Retinoic Acid Signaling Regulates Differential Expression of the Tandemly-Duplicated Long Wavelength-Sensitive Cone Opsin Genes in Zebrafish**. *PLoS Genet* 2015, **11**(8):e1005483.
30. Magoc T, Salzberg SL: **FLASH: fast length adjustment of short reads to improve genome assemblies**. *Bioinformatics* 2011, **27**(21):2957-2963.
31. Li H, Durbin R: **Fast and accurate short read alignment with Burrows-Wheeler transform**. *Bioinformatics* 2009, **25**(14):1754-1760.
32. Li H, Handsaker B, Wysoker A, Fennell T, Ruan J, Homer N, Marth G, Abecasis G, Durbin R, Genome Project Data Processing S: **The Sequence Alignment/Map format and SAMtools**. *Bioinformatics* 2009, **25**(16):2078-2079.
33. Anders S, Pyl PT, Huber W: **HTSeq--a Python framework to work with high-throughput sequencing data**. *Bioinformatics* 2015, **31**(2):166-169.
34. Team RC: **R: A language and environment for statistical computing.** In.; 2014.
35. Robinson MD, McCarthy DJ, Smyth GK: **edgeR: a Bioconductor package for differential expression analysis of digital gene expression data**. *Bioinformatics* 2010, **26**(1):139-140.
36. Falcon S, Gentleman R: **Using GOstats to test gene lists for GO term association**. *Bioinformatics* 2007, **23**(2):257-258.
37. Morris AC, Forbes-Osborne MA, Pillai LS, Fadool JM: **Microarray Analysis of XOPS-mCFP Zebrafish Retina Identifies Genes Associated with Rod Photoreceptor Degeneration and Regeneration**. *Investigative ophthalmology & visual science* 2011.
38. Moraru C, Moraru G, Fuchs BM, Amann R: **Concepts and software for a rational design of polynucleotide probes**. *Environ Microbiol Rep* 2011, **3**(1):69-78.
39. Gao Z, Mao CA, Pan P, Mu X, Klein WH: **Transcriptome of Atoh7 retinal progenitor cells identifies new Atoh7-dependent regulatory genes for retinal ganglion cell formation**. *Developmental neurobiology* 2014, **74**(11):1123-1140.
40. Svahn AJ, Graeber MB, Ellett F, Lieschke GJ, Rinkwitz S, Bennett MR, Becker TS: **Development of ramified microglia from early macrophages in the zebrafish optic tectum**. *Developmental neurobiology* 2013, **73**(1):60-71.
41. Bellingham J, Chaurasia SS, Melyan Z, Liu C, Cameron MA, Tarttelin EE, Iuvone PM, Hankins MW, Tosini G, Lucas RJ: **Evolution of melanopsin photoreceptors: discovery and characterization of a new melanopsin in nonmammalian vertebrates**. *PLoS biology* 2006, **4**(8):e254.

42. Roberts MR, Hendrickson A, McGuire CR, Reh TA: **Retinoid X receptor (gamma) is necessary to establish the S-opsin gradient in cone photoreceptors of the developing mouse retina**. *Investigative ophthalmology & visual science* 2005, **46**(8):2897-2904.
43. Morrow JM, Lazic S, Dixon Fox M, Kuo C, Schott RK, de AGE, Santini F, Tropepe V, Chang BS: **A second visual rhodopsin gene, rh1-2, is expressed in zebrafish photoreceptors and found in other ray-finned fishes**. *The Journal of experimental biology* 2017, **220**(Pt 2):294-303.
44. Roberts MR, Srinivas M, Forrest D, Morreale de Escobar G, Reh TA: **Making the gradient: thyroid hormone regulates cone opsin expression in the developing mouse retina**. *Proc Natl Acad Sci U S A* 2006, **103**(16):6218-6223.
45. Applebury ML, Farhangfar F, Glosmann M, Hashimoto K, Kage K, Robbins JT, Shibusawa N, Wondisford FE, Zhang H: **Transient expression of thyroid hormone nuclear receptor TRbeta2 sets S opsin patterning during cone photoreceptor genesis**. *Developmental dynamics : an official publication of the American Association of Anatomists* 2007, **236**(5):1203-1212.
46. Suzuki SC, Bleckert A, Williams PR, Takechi M, Kawamura S, Wong RO: **Cone photoreceptor types in zebrafish are generated by symmetric terminal divisions of dedicated precursors**. *Proc Natl Acad Sci U S A* 2013, **110**(37):15109-15114.
47. Morrow JM, Lazic S, Chang BS: **A novel rhodopsin-like gene expressed in zebrafish retina**. *Visual neuroscience* 2011, **28**(4):325-335.
48. Fuerst PG, Koizumi A, Masland RH, Burgess RW: **Neurite arborization and mosaic spacing in the mouse retina require DSCAM**. *Nature* 2008, **451**(7177):470-474.
49. Li S, Sukeena JM, Simmons AB, Hansen EJ, Nuhn RE, Samuels IS, Fuerst PG: **DSCAM promotes refinement in the mouse retina through cell death and restriction of exploring dendrites**. *The Journal of neuroscience : the official journal of the Society for Neuroscience* 2015, **35**(14):5640-5654.
50. de Andrade GB, Long SS, Fleming H, Li W, Fuerst PG: **DSCAM localization and function at the mouse cone synapse**. *The Journal of comparative neurology* 2014, **522**(11):2609-2633.
51. Fuerst PG, Bruce F, Tian M, Wei W, Elstrott J, Feller MB, Erskine L, Singer JH, Burgess RW: **DSCAM and DSCAML1 function in self-avoidance in multiple cell types in the developing mouse retina**. *Neuron* 2009, **64**(4):484-497.
52. Stevens CB, Cameron DA, Stenkamp DL: **Plasticity of photoreceptor-generating retinal progenitors revealed by prolonged retinoic acid exposure**. *BMC developmental biology* 2011, **11**:51.
53. Stenkamp DL, Cameron DA: **Cellular pattern formation in the retina: retinal regeneration as a model system**. *Molecular Vision* 2002, **8**:280-293.
54. Stenkamp DL, Powers MK, Carney LH, Cameron DA: **Evidence for two distinct mechanisms of neurogenesis and cellular pattern formation in regenerated goldfish retinas**. *The Journal of comparative neurology* 2001, **431**(4):363-381.
55. Craig SE, Calinescu AA, Hitchcock PF: **Identification of the molecular signatures integral to regenerating photoreceptors in the retina of the zebra fish**. *Journal of ocular biology, diseases, and informatics* 2008, **1**(2-4):73-84.
56. Sifuentes CJ, Kim JW, Swaroop A, Raymond PA: **Rapid, Dynamic Activation of Muller Glial Stem Cell Responses in Zebrafish**. *Investigative ophthalmology & visual science* 2016, **57**(13):5148-5160.
57. Qin Z, Barthel LK, Raymond PA: **Genetic evidence for shared mechanisms of epimorphic regeneration in zebrafish**. *Proc Natl Acad Sci U S A* 2009, **106**(23):9310-9315.
58. Glaviano A, Smith AJ, Blanco A, McLoughlin S, Cederlund ML, Heffernan T, Sapetto-Rebow B, Alvarez Y, Yin J, Kennedy BN: **A method for isolation of cone photoreceptors from adult zebrafish retinae**. *BMC neuroscience* 2016, **17**(1):71.
59. Allison WT, Barthel LK, Skebo KM, Takechi M, Kawamura S, Raymond PA: **Ontogeny of cone photoreceptor mosaics in zebrafish**. *The Journal of comparative neurology* 2011, **518**(20):4182-4195.

60. Tsujimura T, Hosoya T, Kawamura S: **A single enhancer regulating the differential expression of duplicated red-sensitive opsin genes in zebrafish**. *PLoS genetics* 2010, **6**(12):e1001245.
61. Westphal RE, O'Malley DM: **Fusion of locomotor maneuvers, and improving sensory capabilities, give rise to the flexible homing strikes of juvenile zebrafish**. *Front Neural Circuits* 2013, **7**:108.
62. Kim JW, Yang HJ, Brooks MJ, Zelinger L, Karakulah G, Gotoh N, Boleda A, Gieser L, Giuste F, Whitaker DT *et al*: **NRL-Regulated Transcriptome Dynamics of Developing Rod Photoreceptors**. *Cell Rep* 2016, **17**(9):2460-2473.
63. Kaewkhaw R, Kaya KD, Brooks M, Homma K, Zou J, Chaitankar V, Rao M, Swaroop A: **Transcriptome Dynamics of Developing Photoreceptors in Three-Dimensional Retina Cultures Recapitulates Temporal Sequence of Human Cone and Rod Differentiation Revealing Cell Surface Markers and Gene Networks**. *Stem cells (Dayton, Ohio)* 2015, **33**(12):3504-3518.
64. Ogawa Y, Shiraki T, Kojima D, Fukada Y: **Homeobox transcription factor Six7 governs expression of green opsin genes in zebrafish**. *Proc Biol Sci* 2015, **282**(1812):20150659.
65. Adler R, Raymond PA: **Have we achieved a unified model of photoreceptor cell fate specification in vertebrates?** *Brain research* 2008, **1192**:134-150.
66. Kim JW, Yang HJ, Oel AP, Brooks MJ, Jia L, Plachetzki DC, Li W, Allison WT, Swaroop A: **Recruitment of Rod Photoreceptors from Short-Wavelength-Sensitive Cones during the Evolution of Nocturnal Vision in Mammals**. *Dev Cell* 2016, **37**(6):520-532.

**Figures and Tables**

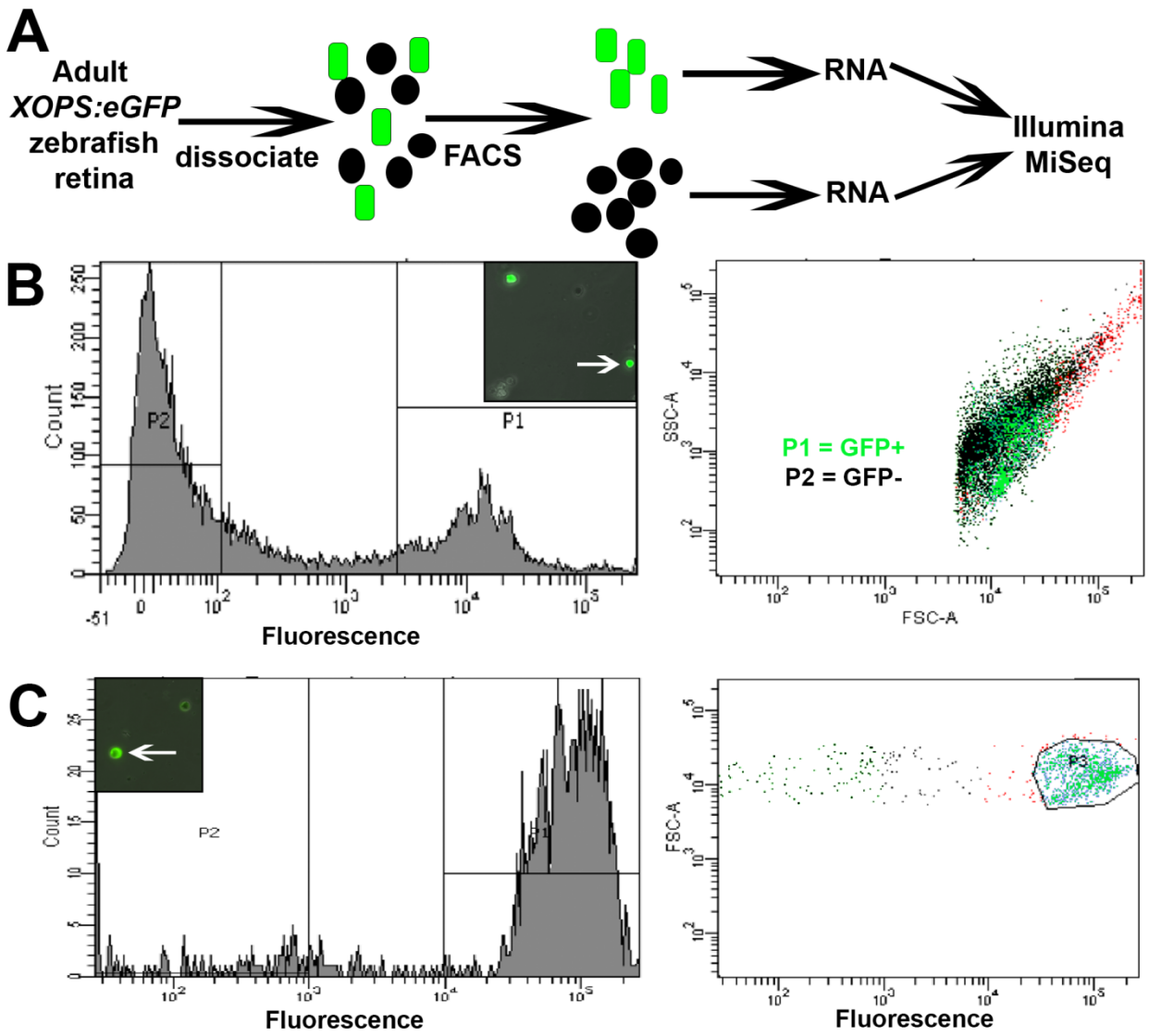


***Figure 2.1.*** Dissociation, FACS purification, and RNA-seq analysis of GFP+ rod photoreceptors and GFP- retinal cells. A. Experimental procedure. B. Representative FACS results showing dissociated cells (inset; arrow indicates GFP+ cell), GFP+ population collected in P1, GFP- population collected in P2. Cells not in P1 or P2 are in red in the second panel. C. Post-sort analysis of a sorted GFP+ population by fluorescence microscopy (inset; arrow indicates GFP+ cell) and FACS. SSC, side scatter (reflecting object complexity); FSC, forward scatter (reflecting object size).

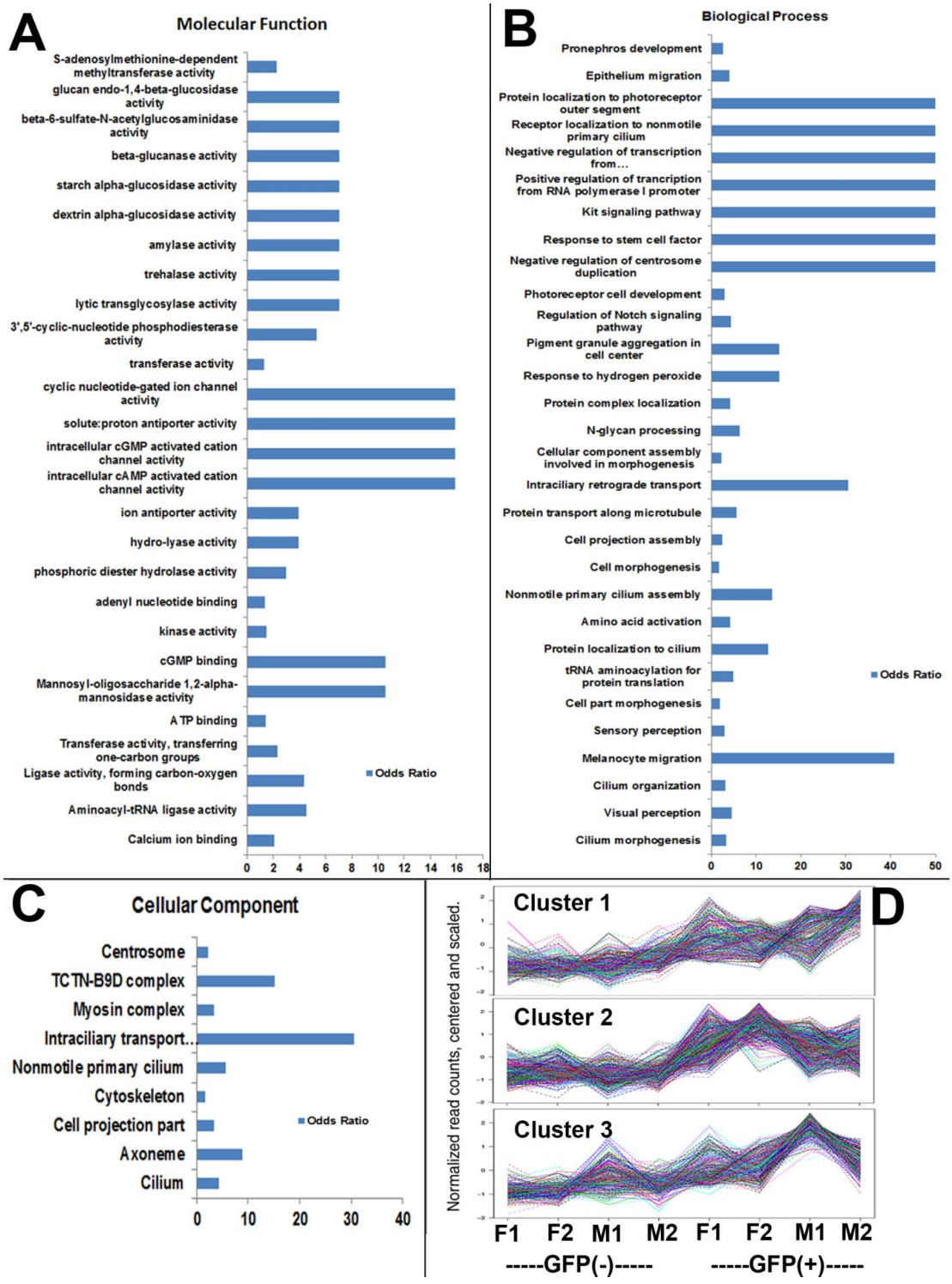


***Figure 2.2.*** Gene ontology (GO) and hierarchical cluster analysis. A-C. Molecular functions (A), biological processes (B), and cellular components (C) overrepresented in the GFP+ (rod photoreceptor) cell population. D. Hierarchical clustering of rod-enriched transcripts reveals only three, highly similar clusters. F, female; M, male.

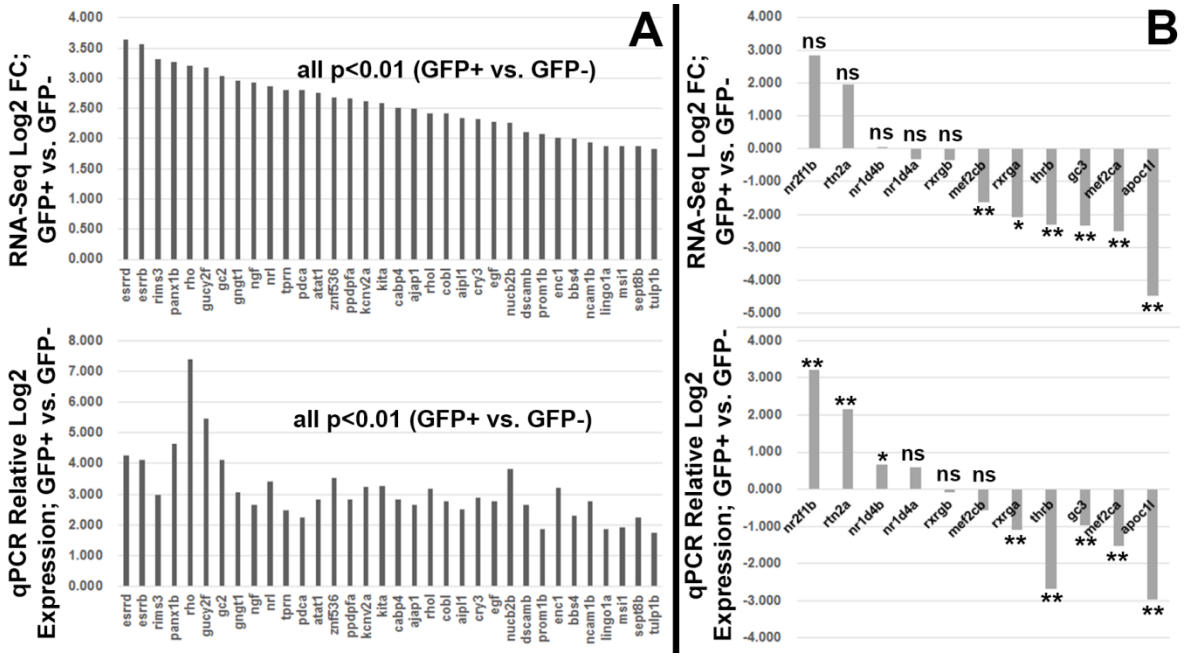


***Figure 2.3.*** Quantitative PCR (qPCR) validation of transcripts enriched in GFP+ (rod photoreceptor) cells (A), and present or depleted in GFP+ cells (B). Top panel in each shows RNA-Seq results; bottom panel shows qPCR. **, p<0.01; *, p<0.05; ns, not significantly differentially expressed, for GFP+ vs. GFP- (three biological replicates).

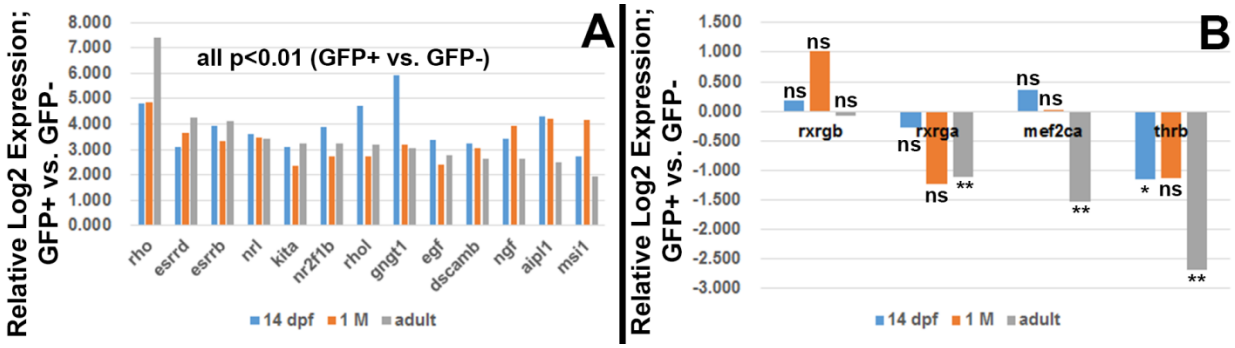


***Figure 2.4.*** A. qPCR of selected transcripts enriched (A), or present (and not differentially expressed) or present (and depleted) in GFP+ (rod photoreceptor) cells (B), in larval retinas (14 dpf), juvenile retinas (1M), and adult retinas. **, p<0.01; *, p<0.05; ns, not significantly differentially expressed, for GFP+ vs. GFP- (three biological replicates).

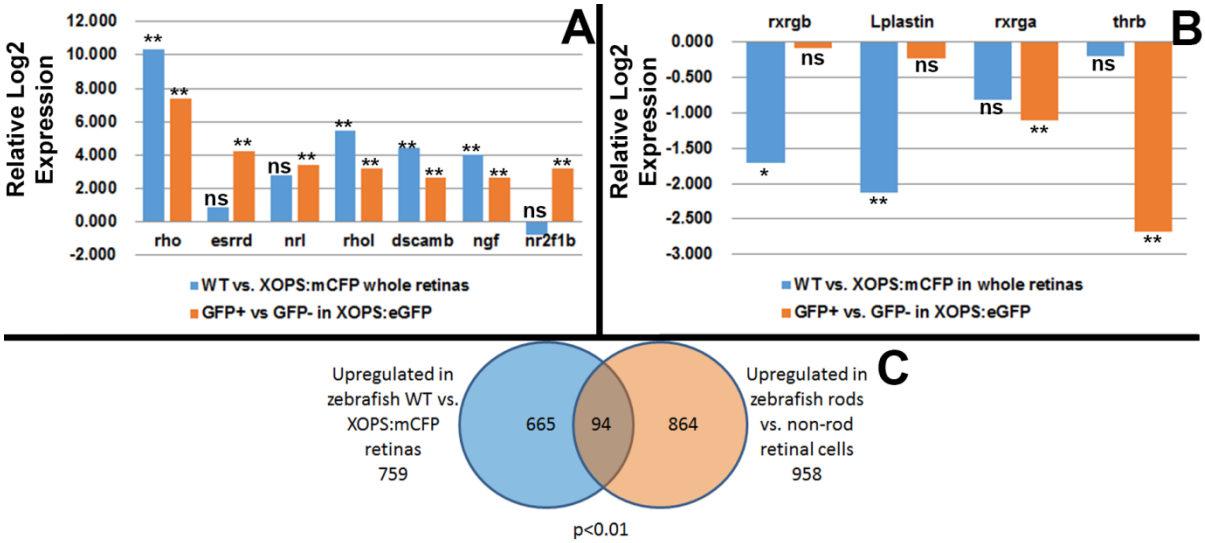


***Figure 2.5.*** qPCR of selected transcripts enriched (A), or present (and not differentially expressed) or present (and depleted) in GFP+ (rod photoreceptor) cells (B), and relative expression in WT vs. *XOPS:mCFP* retinas. **, p<0.01; *, p<0.05; ns, not significantly differentially expressed for GFP+ vs. GFP- cells, or for WT vs. *XOPS:mCFP* retinas (three biological replicates). C. Numbers of unique transcripts upregulated in GFP+ vs. GFP- retinal cells (present study), those upregulated in WT vs. *XOPS:mCFP* retinas [37], at p<0.01, and those shared by both sets.

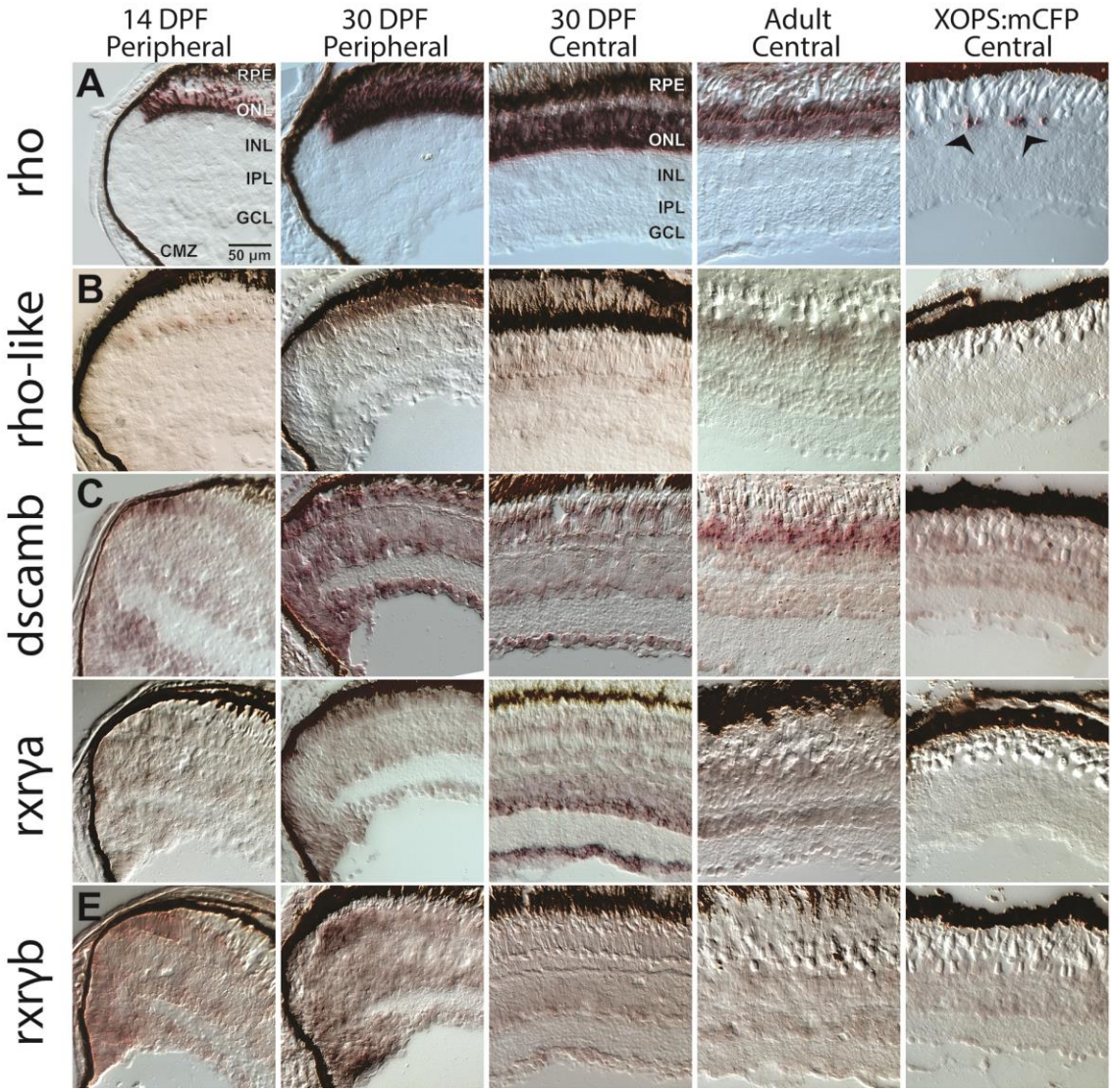


***Figure 2.6.*** *In situ* hybridization for transcripts enriched (*rho, rhol, dscamb*) or present (*rxrga, rxrgb*) in rods of adult zebrafish, using tissues sampled from larvae (14 days post-fertilization; 14 DPF), juveniles (30 DPF), and adult WT fish, and from *XOPS:mCFP* transgenics, which show a chronic rod degeneration[9]. A. Expression patterns for *rho*. Arrows in last panel show degenerating rods in *XOPS:mCFP* retina. B. Expression patterns for *rhol*. C. Expression patterns for *dscamb*. D. Expression patterns for *rxrga*. E. Expression patterns for *rxrgb*. DPF, days post-fertilization; CMZ, ciliary marginal zone; RPE, retinal pigmented epithelium; ONL, outer nuclear layer (photoreceptor layer); INL, inner nuclear layer; IPL, inner plexiform layer; GCL, ganglion cell layer. Scale bar (applies to all) = 50 µm.

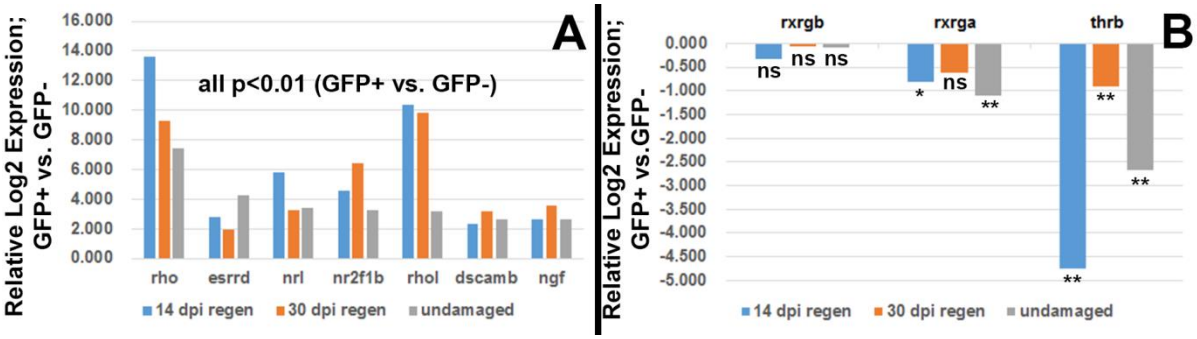


***Figure 2.7.*** qPCR of selected transcripts enriched (A), or present (and not differentially expressed) or present (and depleted) in GFP+ (rod photoreceptor) cells (B), in regenerated retinas at 14 days post-injury (dpi), 30 dpi, and in undamaged retinas. **, p<0.01; *, p<0.05; ns, not significantly differentially expressed, for GFP+ vs. GFP- (three biological replicates).

**Table 2.1. Primers used for qPCR.**

| Gene | Sense Primer 5' -> 3' | Anti-sense Primer 5'-> 3' |
|---|---|---|
| aipl1 | TCCAGTCAGTCTTTACAC | CCTTAGTTCCAGTCACAA |
| ajap1 | GGAGTAAGGTGTCTAACT | TTCCTGATATTCGTCCAT |
| apoc1l | CCCAATTACCTTGTGTTT | ACAGTGTGACTTTGTATTG |
| atat1 | CTAATGTGAATCTGCTATA | ACTCAAGTTACTATCCAA |
| bbs4 | ACCACATTAGGACTGCTG | TCATAGGTCAGAGCGTTTC |
| cabp4 | AGTTCGTTATGATGTTGTCTCT | CTATGATGATCCGCCACTG |
| cobl | TCTAACCATACAGCAGAATCCA | GTCCAGGCGACAACATTG |
| cry3 | TTACTCTTCTGGATTTCC | ATATAAACACACCGTACA |
| dscamb | AAGAAGATGGTCTGACTC | CAAGGGAAAGCAAGTATT |
| egf | TAAGTGAGTGGACAATGTT | GTCTTCGTGTTCCATCTA |
| enc1 | ACGAGTCAGTATATTTCT | GTAAGTAACGAGCCTATA |
| esrrb | CGTCTCCTCATACTTCAG | TCCTCCACTCTATTAGCA |
| esrrd | CATGACCTTATGTGACCTT | CAGAAACCTGGTATGTGT |
| gc2 | CTGTGTTAATTGGTGGAA | AGAGTATCGTAGGACATAA |
| gc3 | CTCTATTCACTGCCATAT | CATGGTTACTGTTAAGAC |
| gngt1 | AATCCATTCATTCAACACAACAT | ACTTCCATCTTCGCCTTATC |
| gucy2f | TAGCATTACACTATGGATT | GCCTATGATTCCTACTTT |
| kcnv2a | GCAGGAGTTAAGTAAGGATAT | TAGGAGTGGAGAACAGTC |
| kita | AATAAGCTTGCCGCCACCATGGAATATCACTG CGTTCT | CAAATATTTGTAGGTGAGCACAATCAGGATGA GAAC |
| lingo1a | TGCTTGTACGGATTGAAT | ATGTTGAGGAAACGAAGA |
| Lplastin | GCAGTGGGTGAACGAAACAC | TCGAGATCGCATACTTGGCG |
| mef2ca | TGTAATCATTCAGCGTAGTG | TCTAAGGTGTGCCGTTAT |
| mef2cb | CCCGTGAATAACCAGATC | GTGACATGCTGTTTCTTT |
| mpeg1.1 | CGGGTTCAAGTCCGTAACCA | TGGCGTCAGCGATTTCTTCT |
| msi1 | CGAGCCCAGCCTAAGTTG | ATCTTCAATAGTCGTGTTCACTGA |
| ncam1b | AGTTTGATAAAGATGTTCGTTTC | TTAATGCTGCGGAAGTCA |
| ngf | GAGAAGACTACAAGCGAAT | CGACAACAATAAGGAGGAT |
| nr1d4a | AATCATCTTATCGCACAAC | ATAGTAGTAGGTAGTAGGAGTA |
| nr1d4b | AACGGTCACTATAACTTC | GAATAGCTGTTGTGTTTAG |

| | | |
|---|---|---|
| nr2f1b | TGAGAAGAACACAGAGTAA | AGGATTGCTGACTATAACA |
| nrl | GATGGTCAGAGGAGAATG | GGTTGTAACGAGTGCTTA |
| nucb2b | ATGATATGGTGGAGATGGA | CTTGTTCGTGGCAGTAAT |
| panx1b | GCAGAGTGATTCTAAGTA | GAGTGAGATGAGTAACAA |
| pdca | TGCCGATGTGGAATAATCAGA | ACAGCGTCATTACTCATTCTATCT |
| ppdpfa | TAGCGTTTACCCGACCAA | TTTCCCCGTCCTCTAAAG |
| prom1b | CAGTTGGAGTGACAGTTG | TCAGGTCTCTTATGTTGGT |
| rtn2a | GGACACATAGACACAGACAA | CCTTCCAGTAGACCAGGT |
| rho | ACTTCCGTTTCGGGGAGAAC | GAAGGACTCGTTGTTGACAC |
| rhol | GCTGTGAGATGCTGGATT | GTTGTTGTTGTTGTTGTTGTC |
| rims3 | AGAGGAGGTCAGTTAGAG | TATATGTTGCTGGAATGTTC |
| rxrga | TTCACACTGGTCATTCAA | AAGGCATTATAGAGCGATT |
| rxrgb | ACATAATACAGACAGAGACT | TAATAGCACAAGACAGAATC |
| thrb | TCTGGTCTGATGAGTCTA | GTATTAGCCTGGTGATGA |
| tprn | CAAACAACAAACATATAATCAAGT | TCTGAATGGTCGTGAATG |
| tulp1b | CAAGGAATCAACAGAGAAG | CATCATCATCATCGTCATC |
| sept8b | CTATCGTGGACTACATTGA | ATGAAGTACAGGCAGATG |
| znf536 | CAATGGACAGAATTTAGGAATCA | CACAAAGAGGACAGGGATAT |
| 18S | GAACGCCACTTGTCCCTCTA | GTTGGTGGAGCGATTTGTCT |

**Table 2.2. Primers used for generation of *in situ* probes.**

| Primer name | Primer sequence 5'-> 3' | Probe length |
|---|---|---|
| rhol_probe_F | CGAAGTGACCCGAATGGTGA | 764b |
| rhol_probe_R | GCGGAATGAACCGCCTTAAC | |
| dscamb_probe_F | TCTGGATCCCCGGAGACAAT | 757b |
| dscamb_probe_R | TCTGGATCCCCGGAGACAAT | |
| rxrga_probe_F | GGAGAAGATCCTGGACGCTG | 734b |
| rxrga_probe_R | AGTGTGCGCTGGGGTTTATT | |
| rxrgb_probe_F | CGCGGAATGGATACTCACGA | 807b |
| rxrgb_probe_R | TCCGCTGCATGGCAGATATT | |

**Table 2.3. Top 50 transcripts significantly upregulated (enriched) in GFP+ (rods) vs GFP- retinal cell populations.**

| Name | Description | logFC | FDR |
|---|---|---|---|
| gc2 | guanylyl cyclase 2 [Source:ZFIN;Acc:ZDB-GENE-011128-8] | 3.032892 | 5.22E-22 |
| esrrd | estrogen-related receptor delta [Source:ZFIN;Acc:ZDB-GENE-040616-3] | 3.642435 | 8.52E-17 |
| zgc:112334 | zgc:112334 [Source:ZFIN;Acc:ZDB-GENE-050809-120] | 3.829432 | 3.64E-16 |
| gngt1 | guanine nucleotide binding protein (G protein), gamma transducing activity polypeptide 1 [Source:ZFIN;Acc:ZDB-GENE-030131-7596] | 2.959265 | 4.60E-16 |
| arhgap29a | Rho GTPase activating protein 29a [Source:ZFIN;Acc:ZDB-GENE-030131-9510] | 2.653423 | 8.20E-16 |
| kitb | kit receptor b [Source:ZFIN;Acc:ZDB-GENE-050916-2] | 2.782837 | 1.06E-15 |
| si:dkey-204f11.59 | si:dkey-204f11.59 [Source:ZFIN;Acc:ZDB-GENE-040724-220] | 3.212857 | 2.27E-15 |
| ajap1 | adherens junctions associated protein 1 [Source:ZFIN;Acc:ZDB-GENE-041210-353] | 2.499397 | 7.05E-15 |
| OSBPL1A (2 of 2) | oxysterol binding protein-like 1A [Source:HGNC Symbol;Acc:16398] | 2.427894 | 7.09E-15 |
| pde6g | phosphodiesterase 6G, cGMP-specific, rod, gamma [Source:ZFIN;Acc:ZDB-GENE-030904-1] | 3.045885 | 9.01E-15 |
| UBAP1L (1 of 2) | ubiquitin associated protein 1-like [Source:HGNC Symbol;Acc:40028] | 2.868683 | 9.01E-15 |
| rcvrna | recoverin a [Source:ZFIN;Acc:ZDB-GENE-050913-106] | 2.719941 | 5.43E-14 |
| rom1b | retinal outer segment membrane protein 1b [Source:ZFIN;Acc:ZDB-GENE-040426-1073] | 2.85896 | 5.78E-14 |
| rorb | RAR-related orphan receptor B [Source:ZFIN;Acc:ZDB-GENE-061204-2] | 2.48207 | 6.19E-14 |
| tmtops2a | teleost multiple tissue opsin 2a [Source:ZFIN;Acc:ZDB-GENE-130129-3] | 2.265541 | 1.05E-13 |
| cerkl | ceramide kinase-like [Source:ZFIN;Acc:ZDB-GENE-070410-38] | 2.181324 | 1.11E-13 |
| cobl | cordon-bleu homolog (mouse) [Source:ZFIN;Acc:ZDB-GENE-091020-11] | 2.417617 | 1.19E-13 |
| hcn3 | hyperpolarization activated cyclic nucleotide-gated potassium channel 3 [Source:ZFIN;Acc:ZDB-GENE-060503-193] | 3.197947 | 1.51E-13 |
| zgc:162144 | zgc:162144 [Source:ZFIN;Acc:ZDB-GENE-030131-7630] | 2.775518 | 1.70E-13 |
| gnb1b | guanine nucleotide binding protein (G protein), beta polypeptide 1b [Source:ZFIN;Acc:ZDB-GENE-040426-2855] | 2.767042 | 1.70E-13 |
| unc119.2 | unc-119 homolog 2 [Source:ZFIN;Acc:ZDB-GENE-030131-7635] | 2.116224 | 1.79E-13 |
| PTPDC1 (1 of 3) | protein tyrosine phosphatase domain containing 1 [Source:HGNC Symbol;Acc:30184] | 3.253732 | 2.91E-13 |
| pdca | phosducin a [Source:ZFIN;Acc:ZDB-GENE-031023-1] | 2.797727 | 3.06E-13 |

| | | | |
|---|---|---|---|
| rom1a | retinal outer segment membrane protein 1a [Source:ZFIN;Acc:ZDB-GENE-040426-1765] | 3.176656 | 3.68E-13 |
| kcnv2a | potassium channel, subfamily V, member 2a [Source:ZFIN;Acc:ZDB-GENE-091117-27] | 2.625431 | 4.38E-13 |
| rho | rhodopsin [Source:ZFIN;Acc:ZDB-GENE-990415-271] | 3.214731 | 4.63E-13 |
| cplx4c | complexin 4c [Source:ZFIN;Acc:ZDB-GENE-101018-1] | 2.863052 | 7.98E-13 |
| samd11 | sterile alpha motif domain containing 11 [Source:ZFIN;Acc:ZDB-GENE-060428-2] | 2.708617 | 9.40E-13 |
| BX248120.1 | Uncharacterized protein [Source:UniProtKB/TrEMBL;Acc:E7F7S5] | 2.586515 | 1.34E-12 |
| saga | S-antigen; retina and pineal gland (arrestin) a [Source:ZFIN;Acc:ZDB-GENE-040426-1538] | 3.089512 | 1.44E-12 |
| arhgef10lb | Rho guanine nucleotide exchange factor (GEF) 10-like b [Source:ZFIN;Acc:ZDB-GENE-090313-222] | 2.476543 | 1.60E-12 |
| guca1a | guanylate cyclase activator 1A [Source:ZFIN;Acc:ZDB-GENE-011128-5] | 2.765826 | 1.68E-12 |
| si:dkeyp-41f9.3 | si:dkeyp-41f9.3 [Source:ZFIN;Acc:ZDB-GENE-091118-56] | 2.849587 | 1.72E-12 |
| TDRD7B | Tudor domain-containing protein 7B [Source:UniProtKB/Swiss-Prot;Acc:E7FDW8] | 2.840789 | 2.06E-12 |
| PLCH2 (1 of 2) | phospholipase C, eta 2 [Source:HGNC Symbol;Acc:29037] | 2.020111 | 2.30E-12 |
| cabp4 | calcium binding protein 4 [Source:ZFIN;Acc:ZDB-GENE-081104-291] | 2.513244 | 2.77E-12 |
| guca1b | guanylate cyclase activator 1B [Source:ZFIN;Acc:ZDB-GENE-011128-6] | 2.703103 | 2.78E-12 |
| grk1a | G protein-coupled receptor kinase 1 a [Source:ZFIN;Acc:ZDB-GENE-050823-1] | 2.930581 | 1.10E-11 |
| gnb1a | guanine nucleotide binding protein (G protein), beta polypeptide 1a [Source:ZFIN;Acc:ZDB-GENE-030131-823] | 2.886447 | 1.19E-11 |
| slc6a15 | solute carrier family 6 (neutral amino acid transporter), member 15 [Source:ZFIN;Acc:ZDB-GENE-050420-93] | 2.779643 | 1.45E-11 |
| ppdpfa | pancreatic progenitor cell differentiation and proliferation factor a [Source:ZFIN;Acc:ZDB-GENE-030219-204] | 2.669857 | 1.71E-11 |
| pde6b | phosphodiesterase 6B, cGMP-specific, rod, beta [Source:ZFIN;Acc:ZDB-GENE-090421-2] | 3.049742 | 2.01E-11 |
| znf536 | zinc finger protein 536 [Source:ZFIN;Acc:ZDB-GENE-030616-624] | 2.683055 | 2.19E-11 |
| SUSD3 | sushi domain containing 3 [Source:HGNC Symbol;Acc:28391] | 2.124055 | 2.28E-11 |
| gnat1 | guanine nucleotide binding protein (G protein), alpha transducing activity polypeptide 1 [Source:ZFIN;Acc:ZDB-GENE-011128-11] | 2.967409 | 3.45E-11 |
| sagb | S-antigen; retina and pineal gland (arrestin) b [Source:ZFIN;Acc:ZDB-GENE-050913-98] | 3.155676 | 3.69E-11 |
| asmt | acetylserotonin O-methyltransferase [Source:ZFIN;Acc:ZDB-GENE- | 1.844975 | 4.41E-11 |

| | | | |
|---|---|---|---|
| | 080220-43] | | |
| pfkfb4l | 6-phosphofructo-2-kinase/fructose-2,6-biphosphatase 4, like [Source:ZFIN;Acc:ZDB-GENE-031031-4] | 1.93027 | 4.63E-11 |
| alpl | alkaline phosphatase, liver/bone/kidney [Source:ZFIN;Acc:ZDB-GENE-040420-1] | 2.701265 | 5.22E-11 |
| slc24a1 | solute carrier family 24 (sodium/potassium/calcium exchanger), member 1 [Source:ZFIN;Acc:ZDB-GENE-060503-191] | 2.88482 | 7.45E-11 |

**Table 2.4. Top 50 transcripts significantly downregulated (depleted) in GFP+ (rods) vs GFP- retinal cell populations.**

| Name | Description | logFC | FDR |
|---|---|---|---|
| si:dkey-27i16.2 | si:dkey-27i16.2 [Source:ZFIN;Acc:ZDB-GENE-030131-9667] | -6.03866537 | 1.88E-38 |
| ptprc | protein tyrosine phosphatase, receptor type, C [Source:ZFIN;Acc:ZDB-GENE-050208-585] | -6.06476722 | 3.46E-31 |
| apoc1l | apolipoprotein C-I like [Source:ZFIN;Acc:ZDB-GENE-030131-1074] | -4.46320866 | 2.75E-30 |
| cd74a | CD74 molecule, major histocompatibility complex, class II invariant chain a [Source:ZFIN;Acc:ZDB-GENE-000901-1] | -4.67633439 | 1.65E-28 |
| bzw1b | basic leucine zipper and W2 domains 1b [Source:ZFIN;Acc:ZDB-GENE-040426-2881] | -3.66358803 | 9.06E-28 |
| si:dkey-25o1.6 | si:dkey-25o1.6 [Source:ZFIN;Acc:ZDB-GENE-091204-276] | -5.26240739 | 3.27E-27 |
| si:ch211-260d11.1 | si:ch211-260d11.1 [Source:ZFIN;Acc:ZDB-GENE-091204-40] | -6.02459793 | 1.05E-26 |
| lgals3bpb | lectin, galactoside-binding, soluble, 3 binding protein b [Source:ZFIN;Acc:ZDB-GENE-040426-2262] | -5.09075533 | 1.25E-26 |
| coro1a | coronin, actin binding protein, 1A [Source:ZFIN;Acc:ZDB-GENE-030131-9512] | -7.62303025 | 1.06E-25 |
| hbaa1 | hemoglobin alpha adult-1 [Source:ZFIN;Acc:ZDB-GENE-980526-79] | -9.74873113 | 1.70E-25 |
| si:dkey-25o1.5 | si:dkey-25o1.5 [Source:ZFIN;Acc:ZDB-GENE-091204-344] | -9.53659867 | 7.14E-23 |
| sla2 | Src-like-adaptor 2 [Source:ZFIN;Acc:ZDB-GENE-080204-98] | -9.56172956 | 2.35E-22 |
| inpp5d | inositol polyphosphate-5-phosphatase D [Source:ZFIN;Acc:ZDB-GENE-100922-30] | -4.44994274 | 1.17E-21 |
| mpeg1 | macrophage expressed 1 [Source:ZFIN;Acc:ZDB-GENE-030131-7347] | -9.35334321 | 2.15E-21 |
| ZFP36 | ZFP36 ring finger protein [Source:HGNC Symbol;Acc:12862] | -5.4525006 | 1.53E-20 |
| ankrd33ab | ankyrin repeat domain 33Ab [Source:ZFIN;Acc:ZDB-GENE-100729-1] | -3.13603996 | 1.97E-20 |
| pfn1 | profilin 1 [Source:ZFIN;Acc:ZDB-GENE-031002-33] | -4.86406116 | 2.72E-20 |
| grk7a | G-protein-coupled receptor kinase 7a [Source:ZFIN;Acc:ZDB-GENE-050824-1] | -2.77617205 | 5.07E-20 |
| rcv1 | recoverin [Source:ZFIN;Acc:ZDB-GENE-030131-7590] | -2.80718642 | 2.57E-19 |
| tagapa | T-cell activation RhoGTPase activating protein a [Source:ZFIN;Acc:ZDB-GENE-040426-1877] | -6.39333701 | 1.05E-18 |
| si:dkey-126g1.9 | si:dkey-126g1.9 [Source:ZFIN;Acc:ZDB-GENE-030131-9862] | -2.79689496 | 1.53E-18 |
| havcr1 | hepatitis A virus cellular receptor 1 [Source:ZFIN;Acc:ZDB-GENE-040718-131] | -7.67482315 | 1.91E-18 |

| | | | |
|---|---|---|---|
| slc1a8b | solute carrier family 1 (glutamate transporter), member 8b [Source:ZFIN;Acc:ZDB-GENE-070912-552] | -2.5380374 | 3.55E-18 |
| csf1ra | colony stimulating factor 1 receptor, a [Source:ZFIN;Acc:ZDB-GENE-001205-1] | -4.24059459 | 1.94E-17 |
| si:ch211-250g4.3 | si:ch211-250g4.3 [Source:ZFIN;Acc:ZDB-GENE-060503-506] | -7.55964405 | 3.53E-17 |
| arpc1b | actin related protein 2/3 complex, subunit 1B [Source:ZFIN;Acc:ZDB-GENE-030131-7414] | -4.66326368 | 6.41E-17 |
| CT826376.1 | Uncharacterized protein [Source:UniProtKB/TrEMBL;Acc:E7F690] | -2.34407255 | 7.14E-17 |
| pdcb | phosducin b [Source:ZFIN;Acc:ZDB-GENE-031023-2] | -2.4532108 | 9.01E-17 |
| opn1lw2 | opsin 1 (cone pigments), long-wave-sensitive, 2 [Source:ZFIN;Acc:ZDB-GENE-040718-141] | -2.76413479 | 5.15E-16 |
| ba1 | ba1 globin [Source:ZFIN;Acc:ZDB-GENE-990415-18] | -6.23069882 | 6.15E-16 |
| opn1mw3 | opsin 1 (cone pigments), medium-wave-sensitive, 3 [Source:ZFIN;Acc:ZDB-GENE-030728-6] | -2.56365947 | 9.40E-16 |
| hbaa1 | hemoglobin alpha adult-1 [Source:ZFIN;Acc:ZDB-GENE-980526-79] | -6.44638081 | 2.14E-15 |
| zgc:195245 | zgc:195245 [Source:ZFIN;Acc:ZDB-GENE-081022-200] | -2.62839443 | 2.47E-15 |
| arr3a | arrestin 3a, retinal (X-arrestin) [Source:ZFIN;Acc:ZDB-GENE-040718-102] | -3.02133496 | 2.47E-15 |
| zgc:100919 | zgc:100919 [Source:ZFIN;Acc:ZDB-GENE-040718-248] | -4.70079878 | 3.07E-15 |
| gc3 | guanylyl cyclase 3 [Source:ZFIN;Acc:ZDB-GENE-011128-9] | -2.32749631 | 4.00E-15 |
| ppp1r18 | protein phosphatase 1, regulatory subunit 18 [Source:ZFIN;Acc:ZDB-GENE-060503-350] | -2.29809174 | 5.42E-15 |
| CD68 | CD68 molecule [Source:HGNC Symbol;Acc:1693] | -3.83135448 | 5.42E-15 |
| il1b | interleukin 1, beta [Source:ZFIN;Acc:ZDB-GENE-040702-2] | -4.3585252 | 5.67E-15 |
| cplx4a | complexin 4a [Source:ZFIN;Acc:ZDB-GENE-060526-116] | -2.12559816 | 7.51E-15 |
| cnga3a | cyclic nucleotide gated channel alpha 3a [Source:ZFIN;Acc:ZDB-GENE-090611-2] | -2.2388126 | 1.69E-14 |
| ccr9a | chemokine (C-C motif) receptor 9a [Source:ZFIN;Acc:ZDB-GENE-060130-125] | -4.13641441 | 1.75E-14 |
| opn1lw1 | opsin 1 (cone pigments), long-wave-sensitive, 1 [Source:ZFIN;Acc:ZDB-GENE-990604-41] | -2.8443546 | 1.89E-14 |
| KEL | Kell blood group, metallo-endopeptidase [Source:HGNC Symbol;Acc:6308] | -8.54223593 | 2.27E-14 |
| si:ch1073-403i13.1 | si:ch1073-403i13.1 [Source:ZFIN;Acc:ZDB-GENE-100921-25] | -4.50874649 | 2.31E-14 |
| wasb | Wiskott-Aldrich syndrome (eczema-thrombocytopenia) b [Source:ZFIN;Acc:ZDB-GENE-030131-7098] | -5.26157912 | 2.52E-14 |

| | | | |
|---|---|---|---|
| SLC24A2 (1 of 2) | solute carrier family 24 (sodium/potassium/calcium exchanger), member 2 [Source:HGNC Symbol;Acc:10976] | -2.22076034 | 2.67E-14 |
| pbxip1b | pre-B-cell leukemia homeobox interacting protein 1b [Source:ZFIN;Acc:ZDB-GENE-070112-2032] | -2.27917445 | 3.27E-14 |
| CD53 | CD53 molecule [Source:HGNC Symbol;Acc:1686] | -5.72855472 | 3.28E-14 |
| slc25a25a | solute carrier family 25 (mitochondrial carrier; phosphate carrier), member 25a [Source:ZFIN;Acc:ZDB-GENE-040426-2396] | -2.50025348 | 3.72E-14 |

**Table 2.5. Sex X rod interaction.**

| Name | Description | logFC | FDR | Comment |
|---|---|---|---|---|
| pmela | premelanosome protein a [Source:ZFIN;Acc:ZDB-GENE-030131-9818] | 15.0198 | 6.05E-06 | Absent in female rods; Present in male rods |
| slc6a6b | solute carrier family 6 (neurotransmitter transporter, taurine), member 6b [Source:ZFIN;Acc:ZDB-GENE-030131-3077] | -4.06708 | 3.31E-05 | Enriched in female rods; depleted in male rods |
| naa35 | N(alpha)-acetyltransferase 35, NatC auxiliary subunit [Source:ZFIN;Acc:ZDB-GENE-030131-306] | -5.25565 | 0.025774 | Enriched in female rods; depleted in male rods |
| si:ch211-89f7.1 | si:ch211-89f7.1 [Source:ZFIN;Acc:ZDB-GENE-060526-180] | -2.75147 | 0.025774 | Enriched in female rods; less enriched in male rods |
| ush2a | Usher syndrome 2A (autosomal recessive, mild) [Source:ZFIN;Acc:ZDB-GENE-060503-794] | -2.65862 | 0.025941 | Enriched in female rods; not enriched in male rods |

**Chapter 3: Isolation of photoreceptors from mature, developing, and regenerating zebrafish retinae and microglia from regenerating zebrafish retinae for gene expression analysis**

Chi Sun, Deborah L. Stenkamp

Publication status: In preparation for Exp Eye Research

Abstract

Background: This work describes experimental procedures for the dissociation of retina of the zebrafish (*Danio rerio*) to produce a suspension of single cells, and for subsequent fluorescence-activated cell sorting (FACS). Establishing this methodology to purify photoreceptors and retinal microglia is useful for the identification of key molecular signatures that underlie photoreceptor development, survival and regeneration, as well as functions of microglia during retinal regeneration.

Results: Methods for dissociation of zebrafish retinae, FACS, and RNA isolation were optimized. This methodology has been applied to isolate pure sorted samples of rods and long wavelength-sensitive (LWS) cones from developing retinae at 14 and 30 days post-fertilization (dpf); rods and LWS cones from 2-3 regenerating retinae at 14 and 30 days post-injury (dpi); rods, LWS cones, medium wavelength-sensitive (MWS; Rh2-2) cones, short wavelength-sensitive (SWS2) cones, and UV-sensitive cones from 2-4 adult mature retinae. We also successfully separated *lws1*-expressing LWS cones from *lws2*-expressing LWS cones from 4 fish of a transgenic line in which *lws1* is reported with green fluorescence protein (GFP) and *lws2* is reported with red fluorescence protein (RFP). On average, 9000 activated microglia were sorted from 8 regenerating (7 dpi) retinae of a transgenic line in which microglia express GFP. Electropherograms verified downstream isolation of high-

quality RNA from sorted samples. Examples of post-sorting analysis, as well as results of qRT-PCR studies validated the good sorting purity. For example, RNA samples derived from isolated Rh2-2 cones contained detectable *rh2-2* opsin mRNA, but no other types of opsin mRNA.

Conclusion: We successfully isolated specific photoreceptor subtypes from developing, regenerating, and mature retinae, and microglia from regenerating retinae. Highly pure sorted samples can subsequently be used for gene expression analysis, such as qRT-PCR and RNA-seq, which may reveal molecular signatures of photoreceptors and microglia for comparative transcriptomics studies.

## Introduction

Zebrafish (*Danio rerio*) is a useful vertebrate model system for studies of development, disease, and regeneration. Presently this animal is also the major vertebrate model system that primarily relies on vision for predator avoidance and foraging, and the genome is known and genetically modifiable, making the zebrafish an excellent model for vision science [1, 2]. Zebrafish photoreceptor diversity includes one type of rod, and four morphological types of cones. The spectral photoreceptor subtypes overlap with morphological subtypes: two members of double cones include those that are long wavelength-sensitive and medium wavelength-sensitive (LWS and MWS cones, respectively), long-single cones that are short wavelength-sensitive (SWS2 cones), short-single cones that are ultraviolet-sensitive (UV cones, a.k.a. SWS1 cones), and rods [3]. With the four cone photoreceptor subtypes in zebrafish, this animal's vision is considered tetrachromatic [4]. The spatial arrangement of these photoreceptors presents a regular and stereotyped neuronal mosaic [5, 6]. LWS/MWS double cones form alternating rows with SWS2 and UV cones [5],

and rods typically form a regular array in association with the UV cones [6]. The wavelength sensitivity of a photoreceptor subtype is determined by the photopigment that is responsible for the light transduction [5] and this pigment is composed of an opsin and a chromophore. Zebrafish express 10 different photoreceptor opsins, each encoded by a separate gene [7, 8]. There are two, tandemly-duplicated *lws* opsin (*lws1* and *lws2*) and four, tandemly-quadruplicated *mws* opsin genes (*rh2-1*, *rh2-2*, *rh2-3*, and *rh2-4*), in contrast to UV (Sws1 and Sws2 opsins), which are each encoded by a single gene (*sws1* and *sws2*, respectively) [7]. The opsins of rods, rhodopsin, are encoded by the *rh1* gene and a second gene, *rh1-2*, also known as *rhodopsin-like* [8]. The expression of the replicated cone opsins at given developmental stages show spatiotemporal patterns, such that specific opsins are expressed at specific locations of the retina [7, 9]. Knowledge of distinct features of the transcriptomes of developing, mature, and regenerating rod and cone photoreceptors has not been fully unveiled, and especially the identification of photoreceptor subtype-specific transcripts is yet to be realized [10-12].

During the development of the zebrafish retina, electrophysiological responses of rods are not evident until 15 to 21 days post-fertilization (dpf). One the other hand, UV cone function becomes distinct at 5 dpf, SWS2 cone function at 7 to 8 dpf, and the double cones are functional at 10 to12 dpf. By the end of the first two weeks post-fertilization, zebrafish larvae have fully functional cones [13, 14]. At 30 dpf, zebrafish juveniles have not become sexually mature and all photoreceptor subtypes are functional [15, 16]. Also, gene expression analysis of rods from 30 dpf zebrafish retinae shows results similar to that of rods from adult retinae (See Chapter 2).

Zebrafish have the capacity to regenerated damaged retinal neurons. Following damage, Müller glia cells re-enter the cell cycle, and multipotent neuronal progenitors differentiate to regenerate all retinal cell types, with appropriate bipolar neuron morphologies

and connectivities [15, 17-22]. Furthermore, there is behavioral and electrophysiological evidence of functional recovery of vision [21-23]. Beyond these measures, however, the structural and functional characteristics of regenerated retinal neurons, particularly photoreceptors, are not well-documented. Our previous report of the rod transcriptome of the zebrafish suggested at least some similarity in gene expression in regenerated vs. native rods (Sun et al., in revision).

Microglia are a specialized subpopulation of macrophages resident in brain and retina, which respond to neuronal damage and to infection [24]. Microglia have been investigated in the models of retinal degenerative diseases [24-27]. However, the functions of microglia in the context of a retinal regenerative response in zebrafish remain largely unknown.

Studies of retinal development, retinal disease, and retinal regeneration in the zebrafish would be considerably advanced by the development of methods for the isolation of specific photoreceptor subtypes, and of microglia, for cell-selective analysis of gene expression. Presently a reliable and efficient practice is to use a flow cytometry cell sorting methodology to purify photoreceptors [28, 29]. As of this writing, adult mouse photoreceptors [30], mouse embryonic retinal precursors [31, 32], retinal progenitor cells derived from human induced-pluripotent stem cells [33], zebrafish rod photoreceptors (Sun et al., in revision), and zebrafish cone photoreceptors (all cone types together) [34] have been successfully isolated. Zebrafish Müller glia have been successfully isolated from damaged retina for gene expression analysis by microarray [35] and RNA-seq [36]. In contrast, a systematic method for the isolation of each zebrafish photoreceptor type, at different developmental stages and in regenerating retina, has not been fully established. In addition, a method for the isolation of activated microglia during retinal regeneration in zebrafish has not been developed.

In this paper, we introduce a technique that allows the isolation of photoreceptors of any given subtype from the subtype-specific transgenic reporter lines at adult and developmental stages, as well as during retinal regeneration. Another, similar technique is also described for the isolation of microglia from regenerating retina. The goals of these techniques are to: (1) rapidly dissociate the retina tissue for flow cytometry; (2) establish a reproducible workflow to purify specific cone subtypes, rods, and microglia; (3) extract high-quality RNA for specific downstream applications including RNA-Seq; (4) optimize procedures to reduce the numbers of larval, juvenile, and adult fish needed for specific downstream applications such as transcriptomic analysis; and (5) improve dissociation efficiencies to allow photoreceptor isolation inform different biological conditions, such as larval retina and regenerated retina.

## Materials and Supplies

### *Animals*

Zebrafish were maintained in recirculating, filtered, and monitored system water at 28.5°C, on a 14:10 light/dark cycle, according to [37]. All procedures involving animals were approved by the University of Idaho Animal Care and Use Committee. Rods were isolated from the line referred to as *XOPS:eGFP*, in which rods express green fluorescent protein (GFP) under control of a *Xenopus* rod opsin promoter [6]. LWS cones were isolated from *trβ2:tdTomato* transgenic zebrafish in which LWS cones express tdTomato fluorescent protein under control of the *thyroid receptor beta 2* promoter [38]. A subset of MWS cones were isolated from *rh2-2:GFP* transgenic zebrafish, in which Rh2 subtype Rh2-2 cones express GFP under control of GFP-reporter constructed adjacent to upstream regions of Rh2-2 [39]. UV cones were isolated from *sws1:GFP* transgenic zebrafish, in which UV cones

express GFP under control of the UV opsin promoter [40]. SWS2 cones were isolated from *sws2:mcherry* transgenic zebrafish, in which SWS2 cones express mCherry fluorescent protein under control of the *sws2* promoter [41]. *LWS:PAC(H)* transgenic zebrafish harbor a P1-artificial chromosome (PAC) clone that encompasses the *lws* locus. The PAC clone was modified such that GFP-polyA sequence is inserted after the *lws1* promoter, reporting expression of *lws1*, and RFP-polyA sequence is inserted after the *lws2* promoter, reporting *lws2* [42]. Expression of *lws1*, and hence GFP, is most abundant in the ventral-nasal region of the adult retina, whereas expression of *lws2*, and hence RFP, is confined to the central and dorsal-temporal region of the adult retina [42]. Microglia in regenerating retina were isolated from *mpeg1:eGFP* (a.k.a *gl22:eGFP*), in which the *macrophage expressed gene 1* (*mpeg1*) promoter drives expression of eGFP [43]. The transgenic lines were the kind gifts of Jim Fadool (*XOPS:eGFP*), Rachel Wong (*TRβ2:tdTomato*), Shoji Kawamura and the RIKEN international resource facility (*rh2-2:GFP* and *sws1:GFP*), and Pamela Raymond (*sws2:mCherry*). The *gl22:eGFP* transgenic line was obtained from the Zebrafish International Resource Center (ZIRC).

*Chemicals*

Chemicals in the dissociation medium included trypsin (0.05% trypsin) (TrypLE™ Express Enzyme (1X), no phenol red, Gibco), neutral protease (Dispase) (Lyophilized, Worthington Biochemical), papain (Lyophilized, Worthington Biochemical), Catalase (Worthington Biochemical), and superoxide dismutase (Worthington Biochemical). HI-FBS (Heat-Inactivated Fetal Bovine Serum, Gibco) was used as the reaction quencher.

The following chemicals were used for different purposes. Fish were anaesthetized with MS-222 (Sigma-Aldrich) before dissection. Chemical lesion to retina was caused by the injection of ouabain (ouabain octahydrate, Sigma-Aldrich). We used rDNase set (Macherey-

Nagel) for DNAseI reaction. For RNA extractions, we used NucleoSpin® RNA kit (Macherey-Nagel) and TRIzol LS Reagent (Ambion). We made RNAse-free PBS in the lab and adjusted pH to the required values.

*Supplies*

Dissection tools were purchased from Fine Science Tools. The flow cytometer used in this experiment was SONY Cell Sorter SH800. RNA quality was assessed by 2100 Bioanalyzer (Agilent Genomics) or Fragment Analyzer (Advanced Analytical). Quantitative real-time PCR (qPCR) experiments were performed with a 7900HT Fast Real-Time PCR System and SYBR-Green PCRMaster Mix (Applied Biosystems, Inc.).

## Detailed Methods

*Retinal damage*

The retinae of adult zebrafish of transgenic lines *XOPS:eGFP* and *trβ2:tdTomato* (1.5 yrs) were subjected to chemical lesion by intraocular ouabain (ouabain octahydrate, Sigma-Aldrich), a lesion which destroys all retinal cells but spares Müller glia [21, 23]. The retinae of adult zebrafish of transgenic line *mpeg1:eGFP* (8 mos) were subjected to chemical lesion by 40 µM ouabain, which destroys inner retinal neurons but spares photoreceptors and Müller glia [17, 19, 21, 22]. The working stocks of ouabain were prepared in 0.65% sterile saline solution. Fish were anaesthetized by tricaine and an incision was made across the cornea with a sapphire blade. 0.4-0.6 µL of ouabain solution containing 200 µM (for extensive lesions in *XOPS:eGFP* and *trβ2:tdTomato* fish; final intraocular concentration estimated at 10 µM) or 40 µM (for inner retina-selective lesions of *mpeg1:eGFP* fish; final intraocular concentration estimated at 2 µM) was injected into the vitreal chamber of the right eye using

a Hamilton syringe. Loss of fluorescence-positive photoreceptors (in transgenic lines *XOPS:eGFP* and *trβ2:tdTomato*) was verified by viewing retinae of anaesthetized fish with epifluorescence stereomicroscopy (Leica M165 FC) at three days post-injury (3 dpi). The presence of activated microglia was verified by viewing retinae of *mpeg1:eGFP* fish at 3 dpi as well. Lesioned zebrafish were allowed to recover, and regenerate their neurons until 14 dpi or 30 dpi for *XOPS:eGFP* and *trβ2:tdTomato* fish [21, 23] or until 7 dpi for *mpeg1:eGFP* fish.

*Retinal tissue dissociation*

Larvae, juveniles, and adult fish were dark-adapted for at least 12 hours, and anaesthetized with MS-222. Corneas and lenses were removed with fine forceps and scissors. The retinal tissues were dissected from either the larvae (14 dpf), juveniles (30 dpf), or adult fish, and retinal pigment epithelium (RPE) was removed from the retina cup with fine forceps. Retinae were collected into a microcentrifuge tube containing 100µL cooled (4°C) RNAse-free phosphate-buffered saline (PBS) (pH 7.4). Numbers of fish used in each experiment are listed in Table 3.2.

The following steps were designed for enzymatic dissociation of retinal cells.

- Retinae were subjected to the tissue dissociation within 2 hours after being isolated.
- Enzymatic dissociation was carried out by adding 1mL dissociation medium (Recipes for specific conditions are listed below).
- The sample mixtures were incubated at 37°C for 10 mins, and were occasionally triturated to prevent aggregation of the tissues during the incubation process.
- 150µL HI-FBS (Heat-Inactivated Fetal Bovine Serum, Gibco) was added to the mixtures to quench the enzymatic reaction.

- Visible pieces of cell aggregates from non-dissociated tissues were removed with fine forceps before and after resting the samples mixtures on ice for 3 mins.
- Samples were centrifuged with Eppendorf Centrifuge 5427R at 4000rpm for 3 mins, followed by removal of supernatant from cell pellets.
- Cells were resuspended in DNAseI solution which allows the digestion for leaked DNA in cell mixture and incubated at room temperature for 10 mins without agitation. Timing for incubation was longer for samples of regenerating retinae, as more retinae were processed in each sample (Details are described in Potential Pitfalls and Troubleshooting section).
- Samples were centrifuged with the same centrifuge as above, at 4000rpm for 3 mins followed by removal of supernatant from cell pellets.
- Cells were resuspended in 150-200µL PBS (pH=6.5) immediately before FACS.
- The resulting suspension was used for cell sorting with a SONY Cell Sorter SH800 at the Center for Reproductive Biology (CRB) FACS Core, Washington State University. The cell samples were maintained on ice for 3-4 hours prior to sorting, with no evident detrimental effects of the longer wait times.
- The samples were free of visible air bubbles which might also interfere with analytic processes.
- The entire dissociation procedure should be completed within 45 mins.

To prepare 10mL dissociation buffer (for 10 reactions),

1. Dissolve 5mg glucose and 3.3mg papain (5 U/mL) into 5mL PBS (pH=7.4).
2. Incubate at 37°C for 20 mins and cool the mixture to room temperature.
3. Different concentrations of trypsin are applied to different preparations of retina tissue.
    - Add 5mL 0.05% trypsin for adult retinae.

- Add 3mL 0.05% trypsin and 0.66mg papain (5 U/mL) in 2mL PBS (pH=7.4) for regenerating retinae.
- Add 3mL 0.05% trypsin and 2mL PBS (pH=7.4) for retina tissues of 30 dpf fish.
- Add 2mL 0.05% trypsin and 3mL PBS (pH=7.4) for retina tissues of 14 dpf fish.

4. Add 1.2mg neutral protease (0.5 U/mL).
5. Add 166uL of 6mg/mL catalase (0.1mg/mL).
6. Add 30 units of superoxide dismutase.
7. Filter with a PVDF syringe filter (Thermo Scientific) to sterilize the mixture.
8. Keep the buffer refrigerated at 4°C.

*Fluorescence-activated cell sorting (FACS)*

The primary gating strategy was based on the fluorescence intensity of cells within a sample. For the identification of target cells from tissue, the scatter characteristics (forward scatter and side scatter) of the retinal cells were also used for gating. Sorting was performed using a 100-micron nozzle. Lasers used in these experiments were 488nm and 561nm, and photomultiplier tubes (PMT) were 525/50 for GFP sorting and 600/60 for RFP, mCherry, and tdTomato sorting. In each FACS run to isolate photoreceptors or microglia, an electronic threshold value was applied to forward scatter for each cell subtype so that only events with an intensity greater than that threshold value were acquired and processed.

The dissociated cellular samples contained fluorescent photoreceptors or microglia and all other non-fluorescent retinal cells. Samples also occasionally contained cell debris produced during the tissue dissociation. Cell debris was usually smaller in size than actual cells, and could be identified and eliminated from collection by gating with side scatter parameters and collecting two adjacent populations at which cell debris region within the non-fluorescent population is closer to zero fluorescence intensity. Large aggregated events

were removed by using a gating selection referenced to the maximum forward scatter of singlet cells Some of the collected samples were analyzed by microscopy, with or without DAPI staining, to identify which gated populations included any debris or aggregates. The same strategy was practiced to set the gating boundary between non-fluorescent and fluorescent cell populations. Although the scatter characteristics of developing, regenerated and mature photoreceptors of a given photoreceptor type were distinct in some cases, fluorescence intensity roughly remained at the same magnitude. Once the two cell populations of interest (e.g. fluorescent microglia vs. other retinal cells) were identified, a gating strategy was adopted in order to ensure that fluorescent cells were clearly separated and sorted from the non-fluorescent populations.

The SH800 instrument used in this study employs a compensation system that is used to calculate the levels of different detected signals in a sample, and subsequently subtract the unwanted components from each channel. We used compensation analysis in these FACS experiments to adjust the mean value of fluorescence intensity of a non-transgenically-labeled population of cells from a transgenic fish with a predefined, non-fluorescent population of a wild-type fish or a confirmed non-fluorescent cell population. When compensated, the fluorescent-negative populations were effectively aligned into the non-fluorescent region and clearly distinguished from fluorescence-positive populations (procedures referenced to the instrument manual). Success of the compensation analysis was occasionally checked with epifluorescence microscopy of sorted cells (Sun et al., in revision). Once the gating regions for a given cell type were determined and set on the instrument panel, cells were directly sorted into 15mL Falcon Conical Centrifuge tubes (FisherScientific) containing TRIzol LS Reagent (Ambion) or lysis buffer (from Macherey-Nagel RNA kit) to reduce the risk of RNA degradation.

We wish to highlight the methods used to sort *lws1:GFP* vs. *lws2:RFP* cells from the *LWS:PAC(H)* transgenic fish. Once the GFP signal was compensated, the *lws1:GFP* population was separated from the non-GFP population. Similarly, the *lws2:RFP* population was separated from the non-RFP population using RFP signal compensation. The non-GFP and non-RFP populations then contained an overlapping population of non-fluorescent cells, which was compensated with the non-*trβ2:tdTomato* population (all LWS cones), obtained from a separate sorting experiment. Once the characteristics of the non-fluorescent cell population were determined, further alterations in compensation setting did not cause a change in scattering characteristics of the fluorescent populations (LWS1 (GFP+) and LWS2 (RFP+) cones) which helped to define the gating for the two populations. In addition, since LWS1 and LWS2 cones were almost in the same cellular size and structure, side- and forward-scattering characteristics of the populations were congruent.

Following collection of sorted cells, we opted not to use a centrifugation step for concentrating the cells. In a preliminary test, we observed that centrifugation caused a major material loss, likely due to the small mass of individual photoreceptors or perikarya, and residual charges carried in the cells after the fluorescence activation during FACS. This problem (material loss during a centrifugation step) could be ameliorated by adding 10uL 3% BSA to every 300uL solution of sorted photoreceptors.

*RNA extraction and quantitative real-time PCR (qPCR)*

RNA was extracted from sorted samples using the NucleoSpin® RNA kit (Macherey-Nagel) using the manufacturer's protocol, quantified and quality-checked on a Fragment Analyzer Automated CE System (Advanced Analytical). cDNA was synthesized using the SuperScript® kit (New England Biotech) using random hexamer primers. Gene-specific primers shown in Table 3.1 for qPCR experiments were designed using AlleleID7/84

(Premier Biosoft). qPCR amplification was done with a model 7900HT Fast Real-Time PCR System and SYBR-Green PCRMaster Mix (Applied Biosystems, Inc.). 18S was chosen as the reference transcript [44].

## Results

### *FACS analysis*

Sorting efficiency (number of target events marked for sorting/number of target events detected X 100) for all samples was maintained above 92%. The total number of instrument-detected events derived from 2 retinae of a single adult zebrafish subjected to FACS yielded approximately ~$3\times10^5$ events. However, since some of the material passing through the FACS instrument was not in a gated and collected population (e.g. cell debris, which instead entered the waste stream), 2-$2.5\times10^5$ events were usually collected.

The settings for sorting specific, fluorescently-labeled cell types were determined empirically as described in the Detailed Methods section, and reproduced in each subsequent experiment for that cell type from dissociated retinas of the corresponding transgenic zebrafish.

*SWS1 (UV) cones (sws1:eGFP+).* Sort results derived from a single adult *sws1:eGFP* fish are presented in Fig. 3.1. Fig. 3.1A shows a density plot of FSC-H (Height) versus FSC-A (Area) used to exclude aggregates. Events (98.70% efficiency; Fig. 3.1A) that fell within the pre-defined region defined by the ellipse in Fig. 3.1A were subjected to further gating discrimination by FSC-H versus fluorescence (Fig. 3.1C). Two peaks were separated based on fluorescence levels, and with compensation, the magnitude of the difference in fluorescence intensities was usually about $10^2$ (SWS1+ versus SWS1-) (Fig. 3.1B). Gates (Fig. 3.1C, F and G) were set to sort SWS1- and SWS1+ cells. A typical sorting of SWS1+

events accounted for up to 10-15% of total sorted events (G in Fig. 3.1C), while SWS1- events accounted for 80-85%. The two peaks in Fig. 1B corresponded to the events collected in the two gates presented in Fig. 3.1C, with the right gate (G) in Fig. 3.1C matching the right peak in Fig. 3.1B and the left gate (F) in Fig. 3.1C matching the left peak in Fig. 3.1B. Numbers of sorted SWS1+ events ranged from 13,000-16,000, while sorted SWS1- populations consisted of 105,000-118,000 events (Fig. 3.1D, three biological replicates shown). Ratios of SWS1+ versus SWS1- events were consistent with the percentages defined by gating shown in Fig. 3.1C.

*SWS2 cones (sws2:mCherry+).* Dissociation of retinal cells from two *sws2:mCherry+* zebrafish showed 98.91% efficiency (Fig. 3.2A). Fluorescence peaks following compensation (Fig. 3.2B) matched the gates defined for sorting (Fig. 3.2C). Gated SWS2+ events contributed to 7-9% of total sorted events, while SWS2- events accounted for 68-79% (Fig. 3.2C). SWS2+ cells showed similar FSC-H characteristics as compared with SWS1+ cells (compare Fig. 3.2C to Fig. 3.1C). The SWS2+ gate collected 11,000-14,000 cells, while there were 107,000-132,000 sorted SWS2- events (Fig. 3.2D).

*RH2-2 cones (rh2-2:eGFP+).* A sorting report of a sample of two adult *rh2-2:eGFP* fish is presented in Fig. 3.3. Sorting efficiency of the retinal tissue was excellent (99.61%) (Fig. 3.3A). A bi-fluorescence plot was used to evaluate the compensation of the eGFP+ population (Fig. 3.3B). This method is useful when the collectable (fluorescence+) cells represent low percentages of the overall cell suspension. This was anticipated because adult RH2 cones can express one of four *rh2* cone opsin genes (Chinen et al., 2003), and so the *rh2-2:eGFP*+ cones represent a fraction of the total number of RH2 cones. When appropriately compensated, the eGFP+ cells became distinguishable from the eGFP- population. With the reference to the large and defaulted fluorescence-negative cell population (on the left in Fig. 3.3B), the purity of the sorted RH2-2+ events was ensured by

the judging the 'tail' of the cell population gated at the right (K), which ideally would have as few fluorescence-negative events as possible. The gating strategy used to collect RH2-2+ and RH2-2- cells is demonstrated in Fig. 3.3C. Collected RH2-2+ events usually made up 5-8% of total sorted events, and RH2-2- events were about 86%-81% of the total (Fig. 3.3C). The numbers of sorted events in RH2-2+ and RH2-2- populations were approximately 10,000 and 150,000 respectively (Fig. 3.3D).

*LWS cones (trβ2:tdTomato+).* Sorting efficiency of *trβ2:tdTomato* zebrafish retina was 97.46% (from a single fish; Fig. 3.4A). Fluorescence intensities of two distinctive peaks were separated by a magnitude of ~$10^3$ (Fig. 3.4B). Gating strategy of two gates collecting TRβ2- cells (left gate) and TRβ2+ cells (right gate) is presented in Fig. 3.4C. To ensure purity of the TRβ2+ population, the gate was set below the FSC-A threshold with the reference to the FSC-A domain of the TRβ2- cells (shown as ~400 X 1,000 FSC-A in Fig. 3.4C). Note that Fig. 3.4C plots FSC-A versus fluorescence, rather than FSC-H versus fluorescence (as in Figs. 3.1C, 3.2C, 3.3C). Object scatter parameters of TRB2+ events in the plot of FSC-H versus fluorescence were similar to those collected within SWS1+, SWS2+, RH2-2+ gates (not shown). Numbers of sorted events were 23,000-28,000 collected in the TRB2+ population and 140,000-150,000 for the TRB2- population (Fig. 3.4D).

*LWS1 and LWS2 cones (lws:PAC(H)).* In the *lws:PAC(H)* transgenic line, LWS cones expressing the *lws1* opsin gene are GFP+, and those expressing the *lws2* opsin gene are RFP+, providing a tool for selective identification and purification of two otherwise morphologically identical cone subtypes [42]. Dissociation efficiency of retinal tissues from 4 *lws:PAC(H)* fish was 98.91% (Fig. 3.5A). Two gates set up based on fluorescence are shown in Fig. 5B, in which the upper (red fluorescence) gate (J: 14.15%) collected LWS2+ events and the gate at the bottom right (green fluorescence) (K: 5.87%) collected LWS1+ events. These gates were compensated based on both RFP and GFP fluorescence intensities, and

each gate was compared with the individual plots of FSC-A versus fluorescence (Fig. 3.5C and 3.5D). LWS1+ events constituted 7.61% of total sorted events (Fig. 3.5C), while LWS2+ events constituted 17.31% of total sorted events (Fig. 3.5D), consistent with the known relative numbers of LWS1 vs. LWS2 cones [42, 45]. These two percentages were generally consistent with those shown in gating strategy present in Fig. 3.5B. LWS1+ events (Fig. 3.5C) had scatter characteristics similar to those of the SWS1+ (Fig. 3.1C), SWS2+ (Fig. 3.2C), and RH2-2+ (Fig. 3.3C) events, while LWS2+ events were more abundant than LWS1+ events and shared scatter characteristics with TRβ2+ events (not shown). Scatter characteristics of sorted cones of different subtypes therefore remained overall, generally consistent. The LWS1+ population yielded an average of 9,500 events and the LWS2+ population yielded an average of 26,500 events (Fig. 3.5E).

*Rods (XOPS:eGFP).* Similar number of GFP+ rods were collected using this methodology as compared to the method described in Sun et al., in revision (Chapter 2). Using the methodology described in this paper, dissociation efficiency was 97.85% (Fig. 3.6A). With compensation, two peaks were separated based on fluorescence levels and shown in Fig. 3.6B. Gating strategy presented in Fig. 3.6C was different (described in Detailed Methods) from the one introduced in the study of Sun et al., in revision. The rod+ population yielded an average of 22,000 events (Fig. 3.6D).

*Rods and LWS cones of retinas of juvenile fish, and in regenerating retinas.* The dissociation and sorting method described in this paper was also successful at separating rods (using *XOPS:eGFP* retinas), and LWS cones (in *trβ2:tdTomato* retinas) from non-fluorescent retinal cells in each case, using as starting material retinas obtained from larval or juvenile fish, or retinas that had regenerated following a chemical lesion. Sorting data related to rod purification from the larval and juvenile retinas (14 dpf, 30 dpf), and regenerated retinas (14 dpi, 30 dpi) samples are shown in Figs. 3.7-10.

Dissociation efficiencies of developing retinal tissues from the *XOPS:eGFP* transgenic were 99.29% (14 dpf, Fig. 3.7A) and 99.47% (30 dpf, Fig. 3.8A). Gating strategies shown in Fig. 3.7C and 3.8C were set with the GFP compensation evaluated in Fig. 3.7B and 3.8B respectively. Compared to sorting of 30 dpf rods, or rods from undamaged adult retina, it was more challenging to obtain distinctive GFP+ vs. GFP- populations from 14 dpf retinas. The scatter characteristics of 14 dpf rods (as seen in FSC-H versus fluorescence of Fig. 3.7C) deviated from that of 30 dpf rods (see Fig. 3.8C), which implies that rods at 14 dpf may be distinct from rods of older fish in terms of soma size and internal structure. Fig. 3.7D and 3.8D present numbers of sorted GFP+ and GFP- events, in each case, GFP+ events contributed to approximately 20% of total sorted events.

Dissociation efficiencies of regenerating retinal tissues from the *XOPS:eGFP* transgenic were 98.86% (14 dpi, Fig. 3.9A) and 98.65% (30 dpi, Fig. 3.10A). GFP expression levels in two regenerating conditions were robust so that two distinguishable peaks were seen in Fig. 3.9B and 3.10B, in which peaks on the right in both situations represented the GFP+ populations and shared similar an intensity magnitude under the same compensation system. Fig. 3.9C and 3.10C show the gating strategies used to collect GFP+ and GFP- events. Compared to the case of 14 dpi samples (7.01%; Fig. 3.9C), the gated GFP+ population from 30 dpi samples contained more events (10.78%; Fig. 3.10C), which suggests that rod neurogenesis continues during the period of 14 to 30 dpi. Approximately GFP+ 20,000 cells (14 dpi, Fig. 3.9D) and 28,000 cells (30 dpi, Fig. 3.10D) were collected from the regenerating tissues.

We practiced the same approach to analyze sorted LWS cones from the 14 dpf, 30 dpf, 14 dpi, and 30 dpi *trβ2:tdTomato* samples as shown in Fig. 3.11-14. Dissociation efficiencies of these developing and regenerating tissues were shown in panels A of Figs. 3.11, 12, 13, and 14. As with adult *trβ2:tdTomato* samples, we used bi-fluorescence plots to

set and evaluate gates (Fig. 3.11C, 3.12C), so that the populations analyzed in the upper gates of Fig. 3.11B (7.32%) and 3.12B (9.76%) generally corresponded to populations collected within the right gates of Fig. 3.11C (8.55%) and 3.12C (10.91%), respectively. These two regions representing groups of similar events can be clearly seen on each of Fig. 3.11C and 3.12C plots. Two distinctive peaks can be seen in the plots of events versus fluorescence for sorting 14 and 30 dpi *trβ2:tdTomato* samples (Figs. 3.13C, 3.14C). Similar to the situation with regenerated rods, regenerated LWS cones increase in number from 14 dpi to 30 dpi (6.51% at 14 dpi; Fig. 3.13D, to 12.58% at 30 dpi; Fig. 3.14D).

*Microglia (mpeg1:eGFP) in regenerating retinas.* The strategies reported in this paper also successfully purified microglia from retinas regenerating after a chemical lesion. Sorting efficiency was high (98.97%; Fig. 3.15A). Two distinctive peaks can be seen in the fluorescence analysis, with the smaller, more highly fluorescent peak on the right representing microglia (Fig. 3.15B). Gating strategy is shown in Fig. 3.15C, in which microglia were collected with the gate on the right (4.83%). The gate on the left collected non-microglial cells as 42.28% of total events subjected to FACS. The collected fractions together represent fewer than half of the total number of events, possibly because the events that were not collected represented cellular debris present in these recently damaged retinas. Fig. 3.15D shows the number of sorted microglia and non-microglia cells, on average, 12,000 microglia were sorted from 8 regenerating retinae.

*RNA quantity and quality*

Approximately 15-30ng total RNA was yielded from RNA extraction of fluorescent samples, and ≥40ng total RNA was yielded from non-fluorescent samples. The RNA Integrity Numbers (RIN) (by 2100 Bioanalyzer) or the RNA Quality Numbers (RQN) by Fragment Analyzer of the RNA samples extracted from sorted cells in each case were greater than 8.0.

RINs or RQNs of at least 8.0 are recommended by Illumina (www.illumina.com) for downstream transcriptomic analysis using their instrumentation. Representative RIN (Figs. 3.16, 3.17) and RQN (Figs. 3.18, 3.19) electropherograms are shown for GFP+ rod samples from juvenile (Fig. 3.16) and regenerated (Fig. 3.17) *XOPS:eGFP* retina, and for adult LWS cone samples from adult *trβ2:tdTomato* retina (Fig. 3.18), and for microglial samples from regenerating *mpeg:eGFP* retina (Fig. 3.19).

*Quantitative PCR (qPCR)*

To determine the purity of the sorted photoreceptor and microglial samples, we performed qPCR analysis of transcripts known to be cell-specific, or highly enriched, or known to be absent in these cell populations. As our control, 18s (18s ribosomal RNA) was ubiquitously expressed in all fluorescent and non-fluorescent samples (Table 3.3).

Ct (cycle threshold) values for cell-specific transcripts evaluated in sorted samples are presented in Table 3.3. *Sws1:GFP*+ samples showed expression of *opn1sw1 (sws1)*, but expression of *rho*, *opn1lw1 (lws1)*, *opn1lw2 (lws2)*, and *opn1sw2 (sws2)* was not detected (N.D.) in these samples. Corresponding *sws1:GFP*- samples did not show expression of *opn1sw1*. *Sws2:mCherry*+ samples showed expression of *opn1sw2*, but expression of *rho*, *opn1lw1*, *opn1lw2*, and *opn1sw1* was not detected in these samples. Corresponding *sws2:mCherry*- samples did not show expression of *opn1sw2*. *Rh2-2:GFP*+ samples showed expression of *opn1mw2 (rh2-2)*, but expression of *rho*, *opn1lw1*, *opn1lw2*, *opn1mw1 (rh2-1)*, and *opn1mw4 (rh2-4)* was not detected, and expression of *opn1mw3 (rh2-3)* was minimal. Corresponding *Rh2-2:GFP*- samples did not show expression of *opn1mw2*. *Lws1:GFP*+ samples showed expression of *opn1lw1*, but expression of *rho*, *opn1mw1*, and *opn1mw2* was not detected in these samples, and expression of *opn1lw2* was extremely low (with a very high Ct). Corresponding *lws2:RFP*+ samples showed expression of *opn1lw2*, but

expression of *rho*, *opn1lw1*, *opn1mw1*, and *opn1mw2* was not detected. *Xops:eGFP*+ samples of all conditions showed expression of *rho*, but expression of *opn1lw1*, *opn1lw2*, and *opn1sw1* was either extremely low or not detected. Corresponding *xops:eGFP*- samples did not show expression of *rho*, while *nrl* transcripts were expressed in all *GFP*+ and *GFP*- samples but were enriched in *GFP*+ samples. *Trβ2:tdTomato*+ samples of all conditions showed expressions of *opn1lw1* and *opn1lw2*, but expression of *rho*, *opn1mw1*, and *opn1mw2* was minimal or not detected. Corresponding *trβ2:tdTomato*- samples showed little or no expression of *opn1lw1* and *opn1lw2*. Expression of *nr2e3* and *thrb* was detected in all samples that were evaluated for the presence of these transcripts.

As shown in Table 3.4, *mpeg1:GFP*+ samples showed enriched expression of microglial transcripts *L-plastin* and *mpeg1.2* compared to those in *mpeg1:GFP*- samples, but expression of photoreceptor transcripts *rho* and *opn1lw2* were not detected in *GFP*+ samples.

## Potential Pitfalls and Troubleshooting

### *Presence of cell aggregates*

The incubation time for tissue dissociation may require adjustment depending on the sample. In general, a dissociation protocol that is cell survival-friendly, is likely to produce more aggregates containing a combination of fluorescent and non-fluorescent cells. Such a protocol then creates additional drawbacks because the presence of aggregates may adversely affect the accuracy of the FACS instrument compensation settings. For the method and sample types described in this paper, the dissociation step required 10 minutes. If tissues weigh more than ~100mg (approximately equivalent to the weight of 10 retinae from adult fish), incubation time for dissociation can be set longer, up to 15 minutes. Pilot experiments should be used to determine optimum incubation time. For example, after 10 to

15 minutes of incubation, suspended cells can be stained with DAPI and viewed with epifluorescence microscopy to evaluate dissociation efficiency (presence or absence of aggregates), and, if desired, cell survival. Our preliminary experiments determined that incubation with the dissociation protocols described in this paper should not exceed 20 minutes, otherwise cell survival was compromised (not shown). Dissociated cells generally survive well during 10 to 15 minutes of incubation. For experiments using less than ~100 mg of tissue, we recommend using the indicated incubation time but changing ratios of chemicals for the dissociation of photoreceptors and microglia.

*Insufficient materials for downstream applications*

The workflow described in this paper provides a sufficient number of sorted events from a rather small number of suspended cells after tissue dissociation (Table 3.2). For the purpose of RNA extraction and analysis of gene expression, the number of sorted events was well-correlated to the RNA yield. For example, this methodology can work for as few as ~9,000 collected cells to yield ~15ng RNA with the suggested protocols for TRIzol® LS Reagent (ThermoFisher) or NucleoSpin® RNA XS kit (Macherey-Nagel), while ~30ng RNA can usually be yielded from sorted samples with ~25,000-30,000 cells. A simple solution for insufficient sorted materials for downstream applications such as RNA extraction is using more transgenic fish to increase the sorting yield. If fish resource is limited, a possible troubleshooting method is to improve the dissociation efficiency to reduce the abundance of aggregates. For the proposed dissociation protocol in this paper, an increased concentration of trypsin or neutral protease would boost the dissociation power. However, this adjustment carries risk of the generation of more cell debris and may jeopardize cell survival.

*Inconsistent sorting of cell populations during a FACS run*

An inconsistent sorting of cell populations over the time of a single FACS run is likely to result in decreased purity of the sorted cells. Such inconsistency may result from the fluorescence fading during the sorting process, and/or quenching of signal by cell death, photobleaching, and/or high stickiness of the cell suspension due to leaked DNA, which in turn contributes to aggregate formation.

Besides using DAPI staining to evaluate cell integrity and survival of collected cells, a drop of DRAQ7 DROP & GO™ (BioStatus) can be added to the cell mixture to label dead cells (not shown), as a supplemental strategy to monitor cell attributes during a sort. DRAQ7 is a fluorescent DNA dye that stains nuclei of permeabilised cells. For samples expressing mCherry, RFP, tdTomato, or other red/far red fluorophores, the usage of DRAQ7, which also fluoresces in the red/far red, is not recommended. Photobleaching can be minimized by storing the samples in a dark environment (e.g. keeping on ice in a styrofoam box) prior to FACS. In the protocols described here, leaked DNA is removed by the DNAseI reaction. However, we noted that samples of regenerating or regenerated retinas always had stickier solutions than other samples, likely due to the presence of damaged cells and cell debris. In such situations, longer incubations with rDNAse may reduce stickiness and therefore signal quenching.

To evaluate sorting consistency using the protocols described here, sorted events were collected in different quantities, and/or at different times during a sorting run, and compared. Figs. 3.20-22 present sorting reports for 10,000 sorted events (Fig. 3.20), the first 100,000 and second 100,000 sorted events (Fig. 3.21), and 300,000 sorted events (Fig. 3.22), all of which show excellent consistency for sorting the given cell types (compare to the reports shown in the Result section).

*Low sorting efficiency*

A low sorting efficiency (<90%) may result from uneven distribution of aggregates in a cell suspension. There are three considerations for this problematic situation: (1) The stream of flow cytometry can be run with a lower speed (or air pressure). A typical speed is <500 events/second. (2) Cell samples can be diluted before FACS to reduce the concentrations of aggregates or cell clusters. (3) Post-sort analysis can be performed to evaluate the purity of sorted fluorescent cells. Fig. 23 provides an example of such an analysis.

*Collection of false-positive artifacts by using fluorescence intensity as the only sorting parameter.*

Using fluorescence intensity as the primary gating method can lead to the increased risk of collecting false-positive artifacts such as aggregates and/or the remains of broken cells. In the methodology described in this paper, we used a gating method for collection of photoreceptors and microglia based on FSC-H/A and SSC characteristics in addition to straightforward demarcation with fluorescence intensities. In addition, the number of events versus fluorescence intensity should be consistent with known proportions of targeted cell population vs. entire sample (e.g. from histological studies).

*Limitations of the instrumentation.*

A disadvantage of standard, commercially-available flow sorters is that it is almost impossible to separate a clean population of co-labeled cells (e.g. GFP and RFP) from singly-labeled cells which have similar object scatter parameters.

As a final consideration, the determination of various gating strategies requires not only a suitable flowcytometric sorter, but also investigator knowledge of the cell biology of the sorted samples, properly validated protocols, and experience in troubleshooting.

## Discussion

In this paper, we demonstrate and illustrate a multi-step methodology to obtain purified samples of specific retinal cell types, suitable for the preparation of high-quality RNA for downstream gene expression analysis. This workflow was successful for starting material obtained from adult, juvenile, or regenerating retina, and was successful for isolating specific photoreceptor subtypes and for isolating microglia. These cell types represent distinct target populations in terms of morphology, position within the retina, and associations with surrounding cells. Flow cytometry and cell sorting techniques were optimized to increase sorting efficiency and reduce sample loss, and various gating strategies were evaluated based upon scatter and fluorescence characteristics of fluorescent versus non-fluorescent populations, as well as with those of the non-fluorescent controls used for compensation.

We are aware of only two previous reports of FACS sorting of zebrafish photoreceptors – isolation of cones [46], and our prior study in which rods were isolated (Sun et al., in revision), and none for zebrafish retinal microglia. The protocol described here represents an improvement upon these methods, due to the requirement for far less starting material, and therefore fewer fish, in comparison to the approach of [46]. For example, one adult *trβ2:tdTomato* fish (2 retinae) yielded approximately 25,000 LWS cones and ~25-30ng RNA in the present study, while ~1,000,000 cones (of all subtypes) were sorted from 30 retinae collected from adult *3.2gnat2:EGFP* (of all subtypes), and ~80ng RNA was subsequently extracted in the Glaviano study. The current protocol is also more versatile than our prior approach (Sun et al., in revision), most importantly due to the use of the SH800 FACS sorter, with additional lasers and the compensation system to allow efficient sorting of a wider range of fluorescent samples. Both strategies yielded favorable outcomes

for the downstream gene expression analysis, such as RNA-seq. Isolation of specific photoreceptor subtypes and microglia with high purity and in sufficient quantities for downstream studies of cell-specific gene expression represents a useful research objective. Knowledge of physiological and pathophysiological features of the transcriptomes of mature, developing, and regenerated rod and cone photoreceptors is currently incomplete, although this information is critical in identifying regulatory genes that may be involved in photoreceptor development, degenerations, and regeneration, and in understanding regulation of morphological maturation of these two cell populations. The technique described in this paper may be practiced for the downstream experiments of next-generation sequencing which advances the characterization of molecular regulators specific to and enriched in photoreceptors and microglia. Furthermore, the zebrafish model provides outstanding advantages in potentially screening numerous compounds and drugs for the therapeutic applications in human diseases. The methodology described here can also be applied to the assessment of drug treatments affecting a given photoreceptor subtype.

References


1. Bilotta J, Saszik S: **The zebrafish as a model visual system**. *International journal of developmental neuroscience : the official journal of the International Society for Developmental Neuroscience* 2001, **19**(7):621-629.
2. Link BA, Collery RF: **Zebrafish Models of Retinal Disease**. *Annual Review of Vision Science* 2015, **1**(1):125-153.
3. Raymond PA, Barthel LK, Rounsifer ME, Sullivan SA, Knight JK: **Expression of rod and cone visual pigments in goldfish and zebrafish: a rhodopsin-like gene is expressed in cones**. *Neuron* 1993, **10**(6):1161-1174.
4. Fleisch VC, Neuhauss SC: **Visual behavior in zebrafish**. *Zebrafish* 2006, **3**(2):191-201.
5. Allison WT, Barthel LK, Skebo KM, Takechi M, Kawamura S, Raymond PA: **Ontogeny of cone photoreceptor mosaics in zebrafish**. *The Journal of comparative neurology* 2010, **518**(20):4182-4195.
6. Fadool JM: **Development of a rod photoreceptor mosaic revealed in transgenic zebrafish**. *Developmental biology* 2003, **258**(2):277-290.
7. Chinen A, Hamaoka T, Yamada Y, Kawamura S: **Gene duplication and spectral diversification of cone visual pigments of zebrafish**. *Genetics* 2003, **163**(2):663-675.
8. Morrow JM, Lazic S, Chang BSW: **A novel rhodopsin-like gene expressed in zebrafish retina**. *Visual neuroscience* 2011, **28**(4):325-335.
9. Takechi M, Kawamura S: **Temporal and spatial changes in the expression pattern of multiple red and green subtype opsin genes during zebrafish development**. *The Journal of experimental biology* 2005, **208**(Pt 7):1337-1345.
10. Nelson SM, Frey RA, Wardwell SL, Stenkamp DL: **The developmental sequence of gene expression within the rod photoreceptor lineage in embryonic zebrafish**. *Developmental dynamics : an official publication of the American Association of Anatomists* 2008, **237**(10):2903-2917.
11. Hennig AK, Peng GH, Chen S: **Regulation of photoreceptor gene expression by Crx-associated transcription factor network**. *Brain research* 2008, **1192**:114-133.
12. Qian J, Esumi N, Chen Y, Wang Q, Chowers I, Zack DJ: **Identification of regulatory targets of tissue-specific transcription factors: application to retina-specific gene regulation**. *Nucleic Acids Research* 2005, **33**(11):3479-3491.
13. Saszik S, Bilotta J, Givin CM: **ERG assessment of zebrafish retinal development**. *Visual neuroscience* 1999, **16**(5):881-888.
14. Neuhauss SC: **Behavioral genetic approaches to visual system development and function in zebrafish**. *Journal of neurobiology* 2003, **54**(1):148-160.
15. Bernardos RL, Barthel LK, Meyers JR, Raymond PA: **Late-stage neuronal progenitors in the retina are radial Muller glia that function as retinal stem cells**. *The Journal of neuroscience : the official journal of the Society for Neuroscience* 2007, **27**(26):7028-7040.
16. Suliman T, Novales Flamarique I: **Visual pigments and opsin expression in the juveniles of three species of fish (rainbow trout, zebrafish, and killifish) following prolonged exposure to thyroid hormone or retinoic acid**. *The Journal of comparative neurology* 2014, **522**(1):98-117.
17. Fimbel SM, Montgomery JE, Burket CT, Hyde DR: **Regeneration of inner retinal neurons after intravitreal injection of ouabain in zebrafish**. *The Journal of neuroscience : the official journal of the Society for Neuroscience* 2007, **27**(7):1712-1724.
18. Kassen SC, Ramanan V, Montgomery JE, C TB, Liu CG, Vihtelic TS, Hyde DR: **Time course analysis of gene expression during light-induced photoreceptor cell death and regeneration in albino zebrafish**. *Developmental neurobiology* 2007, **67**(8):1009-1031.
19. Nagashima M, Barthel LK, Raymond PA: **A self-renewing division of zebrafish Muller glial cells generates neuronal progenitors that require N-cadherin to regenerate retinal neurons**. *Development (Cambridge, England)* 2013, **140**(22):4510-4521.

20. Raymond PA, Barthel LK, Bernardos RL, Perkowski JJ: **Molecular characterization of retinal stem cells and their niches in adult zebrafish**. *BMC developmental biology* 2006, **6**:36.
21. Sherpa T, Lankford T, McGinn TE, Hunter SS, Frey RA, Sun C, Ryan M, Robison BD, Stenkamp DL: **Retinal regeneration is facilitated by the presence of surviving neurons**. *Developmental neurobiology* 2014, **74**(9):851-876.
22. McGinn TE, Mitchell DM, Meighan PC, Partington N, Leoni DC, Jenkins CE, Varnum MD, Stenkamp DL: **Restoration of Dendritic Complexity, Functional Connectivity, and Diversity of Regenerated Retinal Bipolar Neurons in Adult Zebrafish**. *The Journal of Neuroscience* 2017.
23. Sherpa T, Fimbel SM, Mallory DE, Maaswinkel H, Spritzer SD, Sand JA, Li L, Hyde DR, Stenkamp DL: **Ganglion Cell Regeneration Following Whole-Retina Destruction in Zebrafish**. *Developmental neurobiology* 2008, **68**(2):166-181.
24. McCarthy CA, Widdop RE, Deliyanti D, Wilkinson-Berka JL: **Brain and retinal microglia in health and disease: an unrecognized target of the renin-angiotensin system**. *Clinical and experimental pharmacology & physiology* 2013, **40**(8):571-579.
25. Ma W, Zhao L, Wong WT: **Microglia in the Outer Retina and their Relevance to Pathogenesis of Age-Related Macular Degeneration (AMD)**. *Adv Exp Med Biol* 2012, **723**:37-42.
26. Couturier A, Bousquet E, Zhao M, Naud MC, Klein C, Jonet L, Tadayoni R, de Kozak Y, Behar-Cohen F: **Anti-vascular endothelial growth factor acts on retinal microglia/macrophage activation in a rat model of ocular inflammation**. *Molecular Vision* 2014, **20**:908-920.
27. Li L, Eter N, Heiduschka P: **The microglia in healthy and diseased retina**. *Experimental eye research* 2015, **136**:116-130.
28. Lakowski J, Han YT, Pearson RA, Gonzalez-Cordero A, West EL, Gualdoni S, Barber AC, Hubank M, Ali RR, Sowden JC: **Effective transplantation of photoreceptor precursor cells selected via cell surface antigen expression**. *Stem cells (Dayton, Ohio)* 2011, **29**(9):1391-1404.
29. Sharma YV, Cojocaru RI, Ritter LM, Khattree N, Brooks M, Scott A, Swaroop A, Goldberg AF: **Protective gene expression changes elicited by an inherited defect in photoreceptor structure**. *PloS one* 2012, **7**(2):e31371.
30. Feodorova Y, Koch M, Bultman S, Michalakis S, Solovei I: **Quick and reliable method for retina dissociation and separation of rod photoreceptor perikarya from adult mice**. *MethodsX* 2015, **2**:39-46.
31. Muranishi Y, Sato S, Inoue T, Ueno S, Koyasu T, Kondo M, Furukawa T: **Gene expression analysis of embryonic photoreceptor precursor cells using BAC-Crx-EGFP transgenic mouse**. *Biochemical and biophysical research communications* 2010, **392**(3):317-322.
32. Cheng H, Aleman TS, Cideciyan AV, Khanna R, Jacobson SG, Swaroop A: **In vivo function of the orphan nuclear receptor NR2E3 in establishing photoreceptor identity during mammalian retinal development**. *Human molecular genetics* 2006, **15**(17):2588-2602.
33. Lamba DA, McUsic A, Hirata RK, Wang PR, Russell D, Reh TA: **Generation, purification and transplantation of photoreceptors derived from human induced pluripotent stem cells**. *PloS one* 2010, **5**(1):e8763.
34. Glaviano A, Smith AJ, Blanco A, McLoughlin S, Cederlund ML, Heffernan T, Sapetto-Rebow B, Alvarez Y, Yin J, Kennedy BN: **A method for isolation of cone photoreceptors from adult zebrafish retinae**. *BMC Neuroscience* 2016, **17**(1):71.
35. Qin Z, Barthel LK, Raymond PA: **Genetic evidence for shared mechanisms of epimorphic regeneration in zebrafish**. *Proc Natl Acad Sci U S A* 2009, **106**(23):9310-9315.
36. Sifuentes CJ, Kim JW, Swaroop A, Raymond PA: **Rapid, Dynamic Activation of Muller Glial Stem Cell Responses in Zebrafish**. *Investigative ophthalmology & visual science* 2016, **57**(13):5148-5160.
37. Westerfield M: **The Zebrafish Book. A Guide for the Laboratory Use of Zebrafish (Danio rerio)**, 5th edn. Eugene: University of Oregon Press; 2007.

38. Suzuki SC, Bleckert A, Williams PR, Takechi M, Kawamura S, Wong RO: **Cone photoreceptor types in zebrafish are generated by symmetric terminal divisions of dedicated precursors**. *Proc Natl Acad Sci U S A* 2013, **110**(37):15109-15114.
39. Tsujimura T, Masuda R, Ashino R, Kawamura S: **Spatially differentiated expression of quadruplicated green-sensitive RH2 opsin genes in zebrafish is determined by proximal regulatory regions and gene order to the locus control region**. *BMC genetics* 2015, **16**:130.
40. Takechi M, Hamaoka T, Kawamura S: **Fluorescence visualization of ultraviolet-sensitive cone photoreceptor development in living zebrafish**. *FEBS Letters* 2003, **553**(1-2):90-94.
41. Salbreux G, Barthel LK, Raymond PA, Lubensky DK: **Coupling Mechanical Deformations and Planar Cell Polarity to Create Regular Patterns in the Zebrafish Retina**. *PLOS Computational Biology* 2012, **8**(8):e1002618.
42. Tsujimura T, Hosoya T, Kawamura S: **A Single Enhancer Regulating the Differential Expression of Duplicated Red-Sensitive Opsin Genes in Zebrafish**. *PLoS Genetics* 2010, **6**(12):e1001245.
43. Ellett F, Pase L, Hayman JW, Andrianopoulos A, Lieschke GJ: **mpeg1 promoter transgenes direct macrophage-lineage expression in zebrafish**. *Blood* 2011, **117**(4):e49-56.
44. Mitchell DM, Stevens CB, Frey RA, Hunter SS, Ashino R, Kawamura S, Stenkamp DL: **Retinoic Acid Signaling Regulates Differential Expression of the Tandemly-Duplicated Long Wavelength-Sensitive Cone Opsin Genes in Zebrafish**. *PLoS Genetics* 2015, **11**(8):e1005483.
45. Mitchell DM, Stevens CB, Frey RA, Hunter SS, Ashino R, Kawamura S, Stenkamp DL: **Retinoic Acid Signaling Regulates Differential Expression of the Tandemly-Duplicated Long Wavelength-Sensitive Cone Opsin Genes in Zebrafish**. *PLoS Genet* 2015, **11**(8):e1005483.
46. Glaviano A, Smith AJ, Blanco A, McLoughlin S, Cederlund ML, Heffernan T, Sapetto-Rebow B, Alvarez Y, Yin J, Kennedy BN: **A method for isolation of cone photoreceptors from adult zebrafish retinae**. *BMC Neuroscience* 2016, **17**:71.

## Figures and Tables

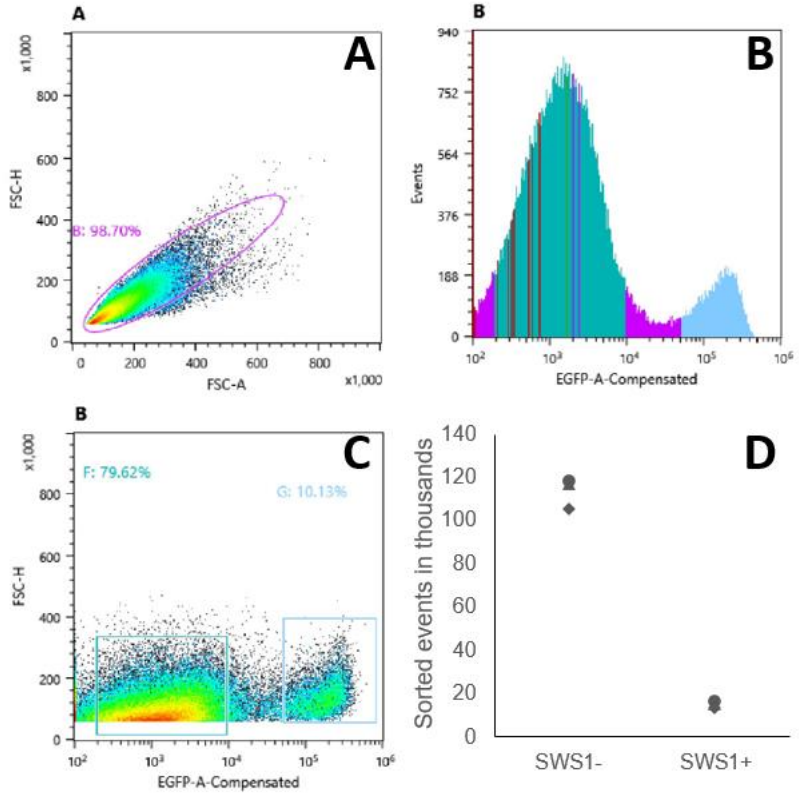


***Figure 3.1.*** A-C. Representative (100,000 sorted events) sorting reports of adult *SWS1:eGFP* fish retinal tissue. The eGFP+ LWS cone population can be gated by using eGFP expression and scatter characteristics. A. Forward scatter (FSC-H) vs. (FSC-A) plot demonstrates effective dissociation of retinal cells. The ellipse indicates the population of dissociated cells subjected to sorting. B. The eGFP- cells and the eGFP+ cells appear in two distinctive peaks. C. Gating strategy, with sorting percentage of the eGFP+ cells indicated. Gates are shown with two rectangles. D. Numbers of sorted events collected in eGFP- (SWS1-) and eGFP+ (SWS1+) cell populations for the three biological replicates. Letter A at upper left in Panel A indicated all events prior to sorting. Letter B at upper left in Panel B and C indicated the sorting of events collected in the ellipse shown in Panel A. Different colors shown in Panel B were assigned by the machine testing different gates, and are not relevant in the data interpretation.

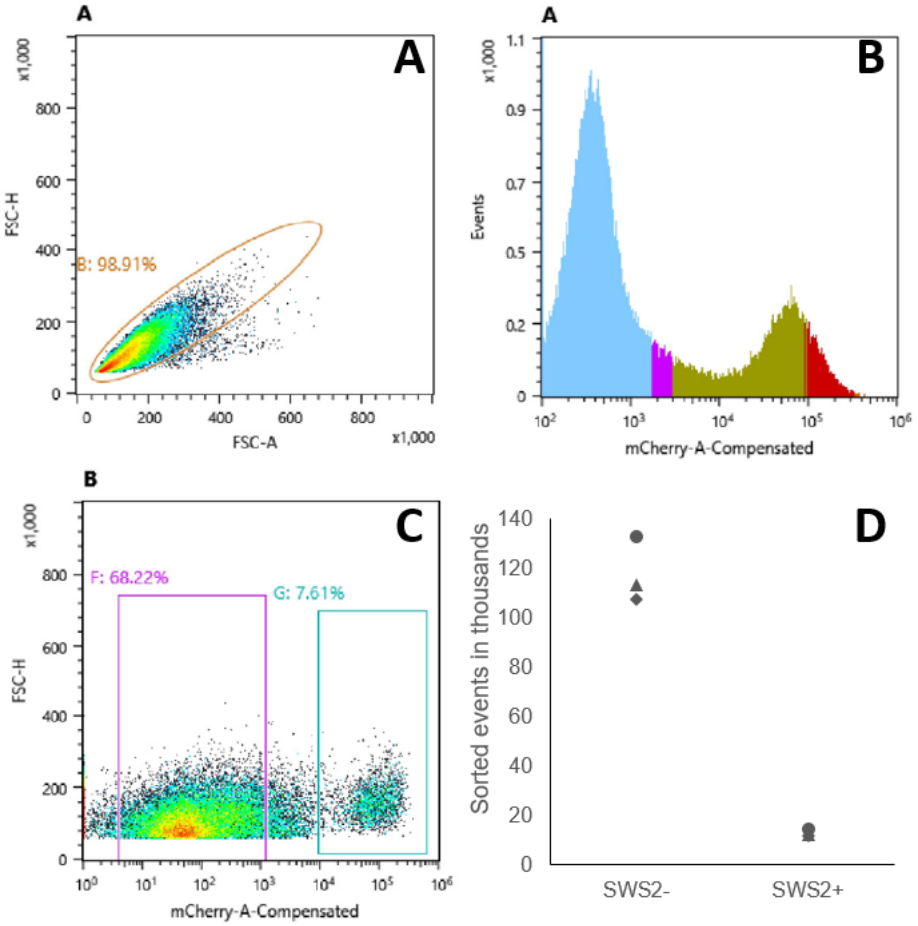


***Figure 3.2.*** A-C. Representative (100,000 sorted events) sorting reports of adult *SWS2:mCherry* fish retinal tissue. The mCherry+ LWS cone population can be gated with the mCherry expression and scatter characteristics. A. Forward scatter (FSC-H) vs. (FSC-A) plot demonstrates effective dissociation of retinal cells. The ellipse indicates the population of dissociated cells subjected to sorting. B. The mCherry- cells and the mCherry+ cells appear in two distinctive peaks. C. Gating strategy, with sorting percentage of the mCherry+ cells indicated. Gates are shown with two rectangles. D. Numbers of sorted events collected in mCherry- (SWS2-) and mCherry+ (SWS2+) cell populations for the three biological replicates. Letter A at upper left in Panel A and B indicated all events prior to sorting. Letter B at upper left in Panel C indicated the sorting of events collected in the ellipse shown in Panel A. Different colors shown in Panel B were assigned by the machine testing different gates, and are not relevant in the data interpretation.

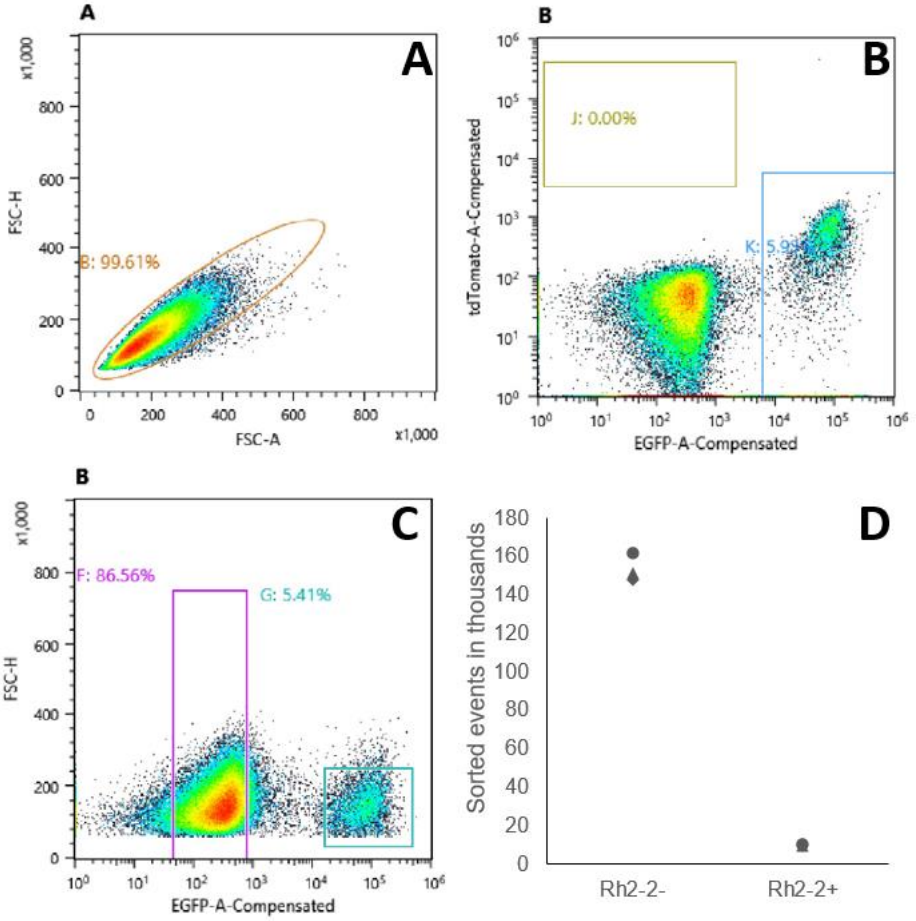


***Figure 3.3.*** A-C. Representative (100,000 sorted events) sorting reports of adult *rh2-2:eGFP* fish retinal tissue. The eGFP+ rod population can be gated with the eGFP expression and scatter characteristics. A. Forward scatter (FSC-H) vs. (FSC-A) plot demonstrates effective dissociation of retinal cells. The ellipse indicates the population of dissociated cells subjected to sorting. B. Bi-fluorescence plot shows the eGFP+ cells as a distinctive population. C. Gating strategy, with sorting percentage of the eGFP+ cells indicated. Gates are shown with two rectangles. D. Numbers of sorted events collected in eGFP- (rh2-2-) and eGFP+ (rh2-2+) cell populations for the three biological replicates. Letter A at upper left in Panel A indicated all events prior to sorting. Letter B at upper left in Panel B and C indicated the sorting of events collected in the ellipse shown in Panel A.

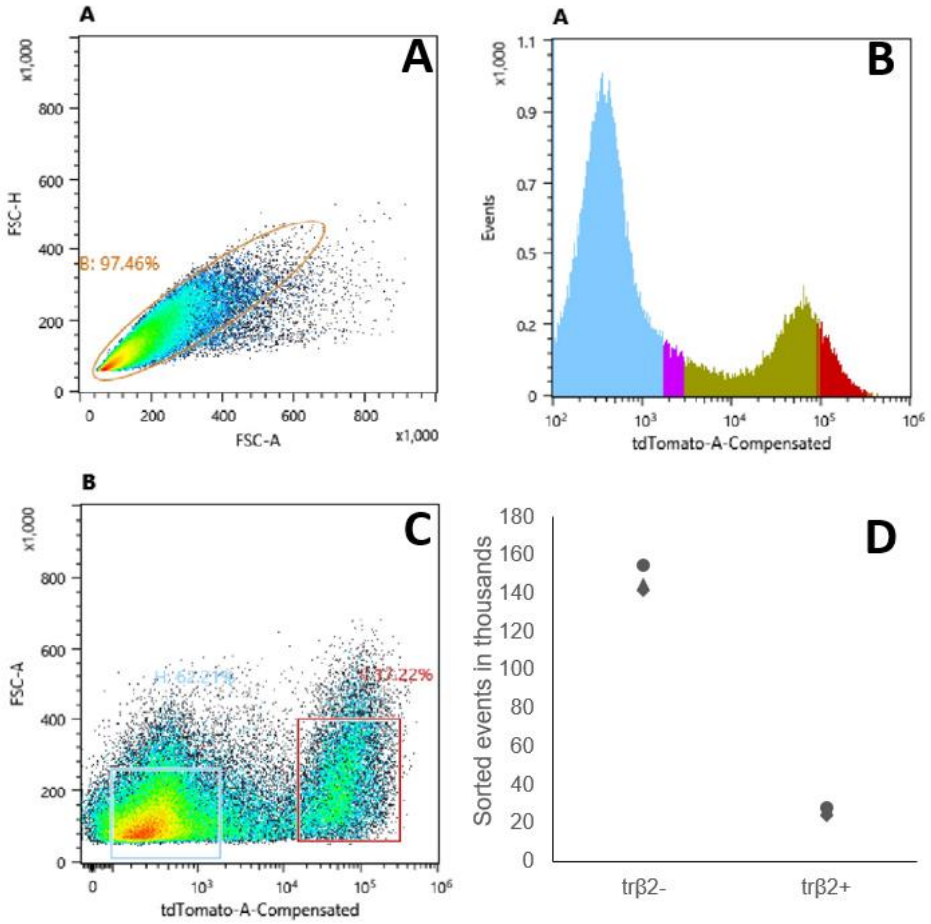


***Figure 3.4.*** A-C. Representative (100,000 sorted events) sorting reports of adult *trβ2:tdTomato* fish retinal tissue. The tdTomato+ LWS cone population can be gated with the tdTomato expression and scatter characteristics. A. Forward scatter (FSC-H) vs. (FSC-A) plot demonstrates effective dissociation of retinal cells. The ellipse indicates the population of dissociated cells subjected to sorting. B. The tdTomato- cells and tdTomato+ cells appear in two distinctive peaks. C. Gating strategy, with sorting percentage of the tdTomato+ cells indicated. Gates are shown with two rectangles. D. Numbers of sorted events collected in tdTomato- (trβ2-) and tdTomato+ (trβ2+) cell populations for the three biological replicates. Letter A at upper left in Panel A and B indicated all events prior to sorting. Letter B at upper left in Panel C indicated the sorting of events collected in the ellipse shown in Panel A. Different colors shown in Panel B were assigned by the machine testing different gates, and are not relevant in the data interpretation.

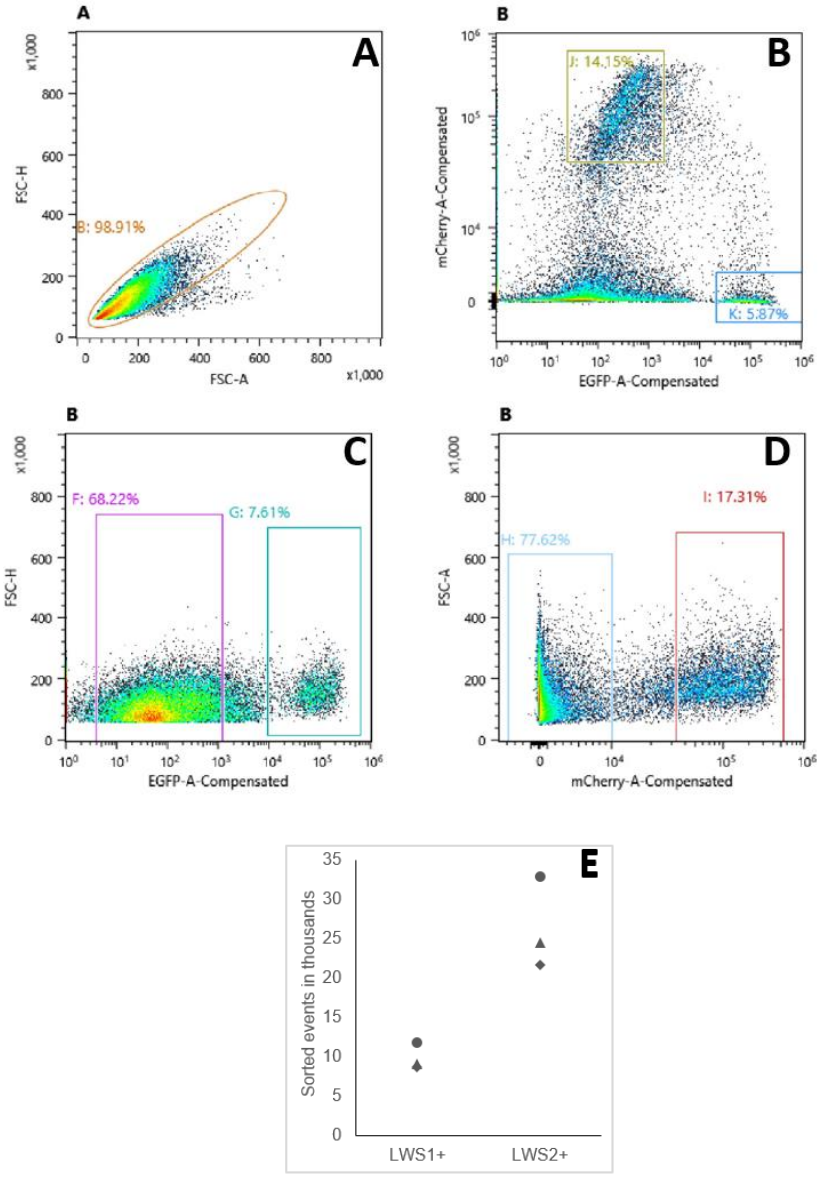


***Figure 3.5.*** A-D. Representative (100,000 sorted events) sorting reports of adult *lws:Pac(H)* fish retinal tissue. The GFP+ LWS1 cone and RFP+ LWS2 cone populations can be gated with the fluorescence expressions and scatter characteristics. A. Forward scatter (FSC-H) vs. (FSC-A) plot demonstrates effective dissociation of retinal cells. B. Gating Strategy, with the GFP+ cells and the RFP+ cells appearing as two distinctive populations. C. FSC-H vs fluorescence plot shows the percentage of the GFP+ cells. D. FSC-A vs fluorescence plot shows the percentage of the RFP+ cells. E. Numbers of sorted events collected in GFP+ (LWS1+) and RFP+ (LWS2+) cell populations for the three biological replicates. Letter A at upper left in Panel A indicated all events prior to sorting. Letter B at upper left in Panel B, C, D indicated the sorting of events collected in the ellipse shown in Panel A.

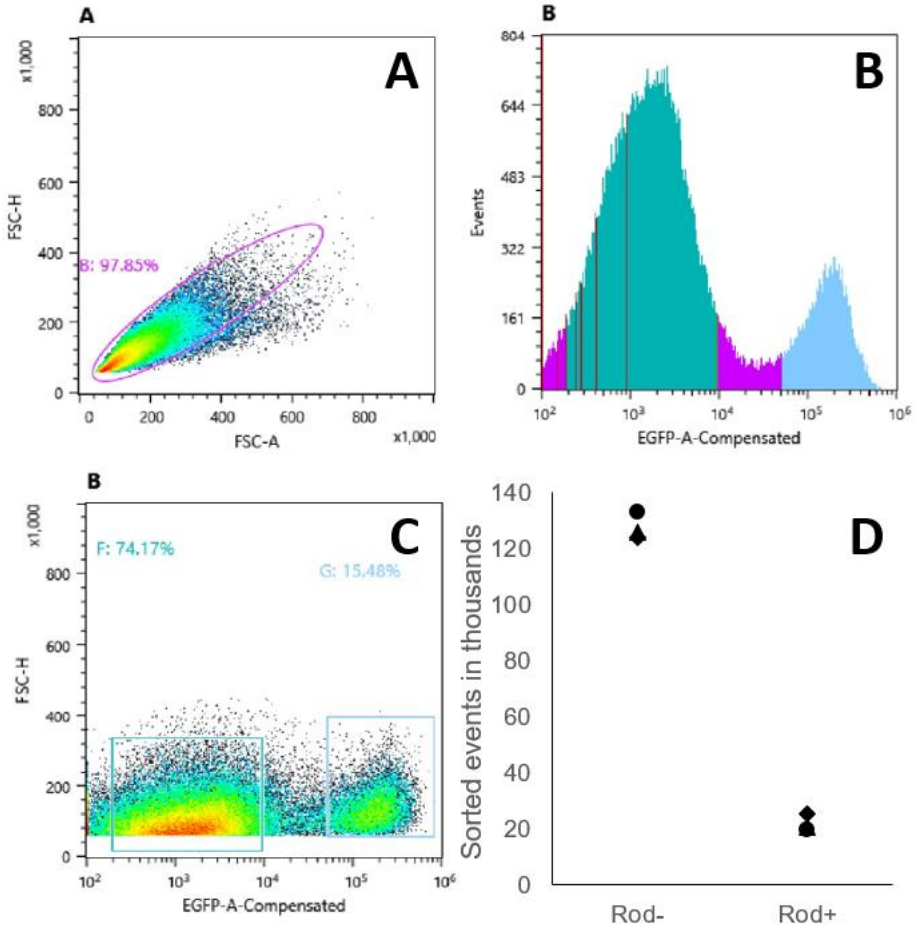


***Figure 3.6.*** A-C. Representative (100,000 sorted events) sorting reports of adult *XOPS:eGFP* fish retinal tissue. The eGFP+ rod population can be gated with the eGFP expression and scatter characteristics. A. Forward scatter (FSC-H) vs. (FSC-A) plot demonstrates effective dissociation of retinal cells. The ellipse indicates the population of dissociated cells subjected to sorting. B. Bi-fluorescence plot shows the eGFP+ cells as a distinctive population. C. Gating strategy, with sorting percentage of the eGFP+ cells indicated. Gates are shown with two rectangles. D. Numbers of sorted events collected in eGFP- (rod-) and eGFP+ (rod+) cell populations for the three biological replicates. Letter A at upper left in Panel A indicated all events prior to sorting. Letter B at upper left in Panel B and C indicated the sorting of events collected in the ellipse shown in Panel A. Different colors shown in Panel B were assigned by the machine testing different gates, and are not relevant in the data interpretation.

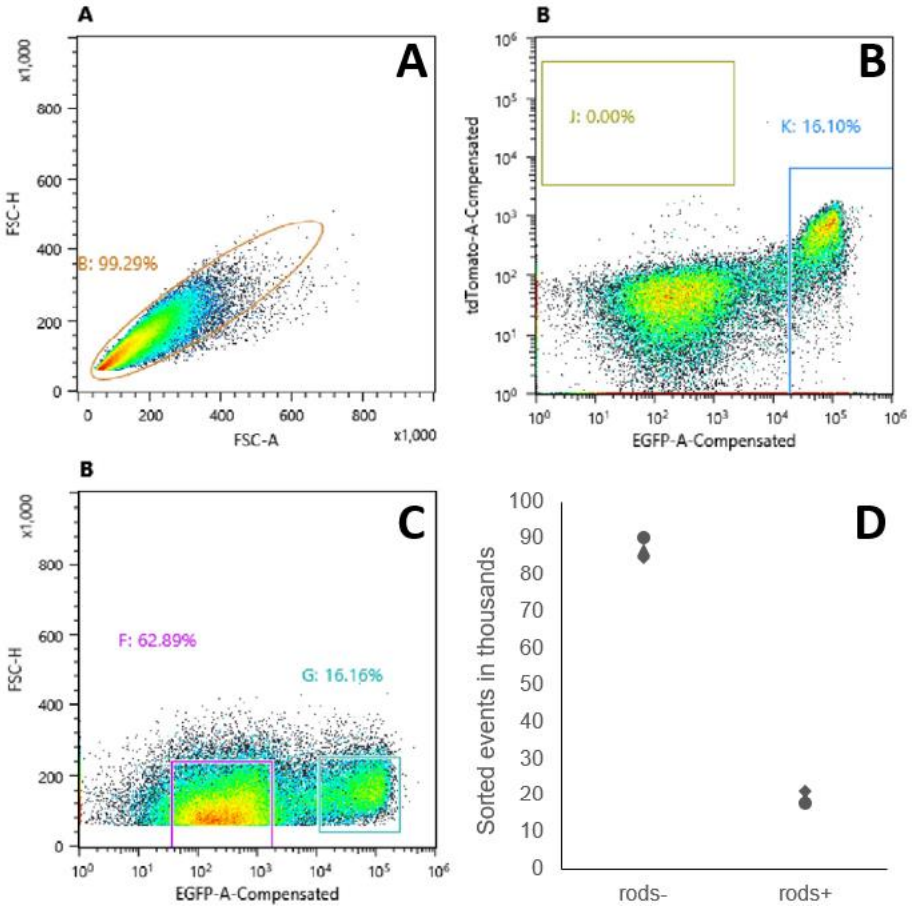


***Figure 3.7.*** A-C. Representative (100,000 sorted events) sorting reports of 14 dpf *XOPS:eGFP* fish retinal tissue. The eGFP+ rod population can be gated with the eGFP expression and scatter characteristics. A. Forward scatter (FSC-H) vs. (FSC-A) plot demonstrates effective dissociation of retinal cells. The ellipse indicates the population of dissociated cells subjected to sorting. B. Bi-fluorescence plot shows the eGFP+ cells as a distinctive population. C. Gating strategy, with sorting percentage of the eGFP+ cells indicated. Gates are shown with two rectangles. D. Numbers of sorted events collected in eGFP- (rod-) and eGFP+ (rod+) cell populations for the three biological replicates. Letter A at upper left in Panel A indicated all events prior to sorting. Letter B at upper left in Panel B and C indicated the sorting of events collected in the ellipse shown in Panel A.

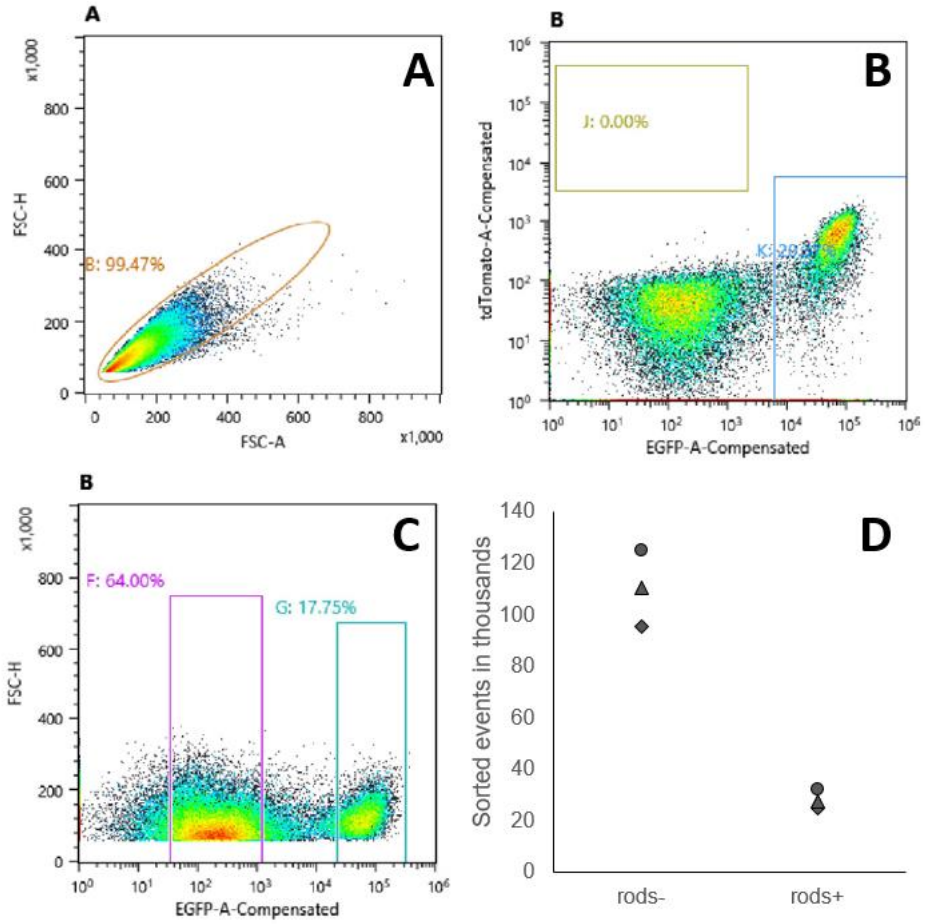


***Figure 3.8.*** A-C. Representative (100,000 sorted events) sorting reports of 30 dpf *XOPS:eGFP* fish retinal tissue. The eGFP+ rod population can be gated with the eGFP expression and scatter characteristics. A. Forward scatter (FSC-H) vs. (FSC-A) plot demonstrates effective dissociation of retinal cells. The ellipse indicates the population of dissociated cells subjected to sorting. B. Bi-fluorescence plot shows the eGFP+ cells as a distinctive population. C. Gating strategy, with sorting percentage of the eGFP+ cells indicated. Gates are shown with two rectangles. D. Numbers of sorted events collected in eGFP- (rod-) and eGFP+ (rod+) cell populations for the three biological replicates. Letter A at upper left in Panel A indicated all events prior to sorting. Letter B at upper left in Panel B and C indicated the sorting of events collected in the ellipse shown in Panel A.

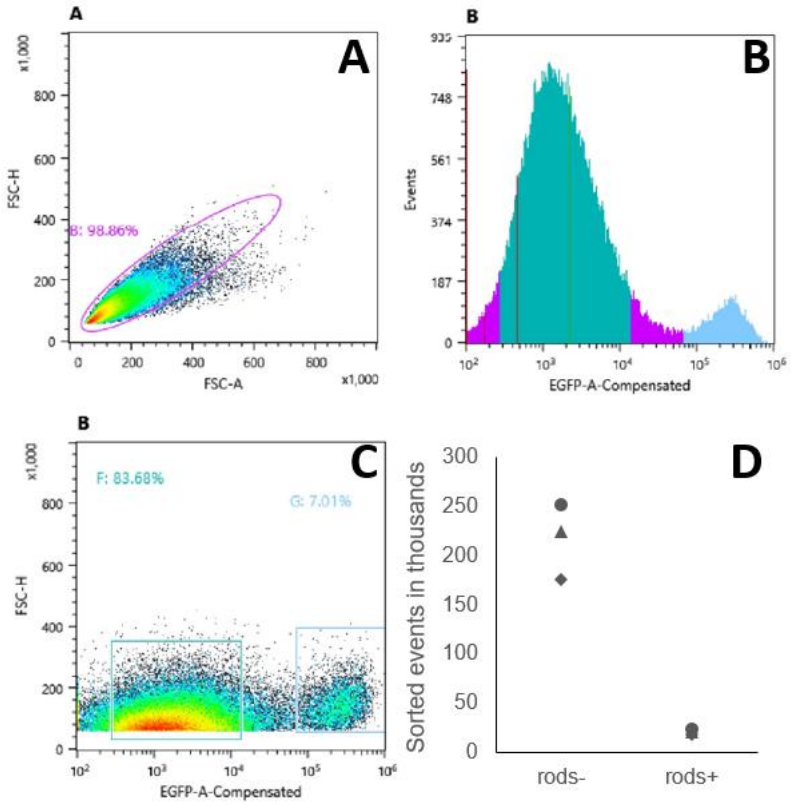


***Figure 3.9.*** A-C. Representative (100,000 sorted events) sorting reports of 14 dpi *XOPS:eGFP* fish retinal tissue. The eGFP+ LWS cone population can be gated with the eGFP expression and scatter characteristics. A. Forward scatter (FSC-H) vs. (FSC-A) plot demonstrates effective dissociation of retinal cells. The ellipse indicates the population of dissociated cells subjected to sorting. B. The eGFP- cells and the eGFP+ cells appear in two distinctive peaks. C. Gating strategy, with sorting percentage of the eGFP+ cells indicated. Gates are shown with two rectangles. D. Numbers of sorted events collected in eGFP- (rod-) and eGFP+ (rod+) cell populations for the three biological replicates. Letter A at upper left in Panel A indicated all events prior to sorting. Letter B at upper left in Panel B and C indicated the sorting of events collected in the ellipse shown in Panel A. Different colors shown in Panel B were assigned by the machine testing different gates, and are not relevant in the data interpretation.

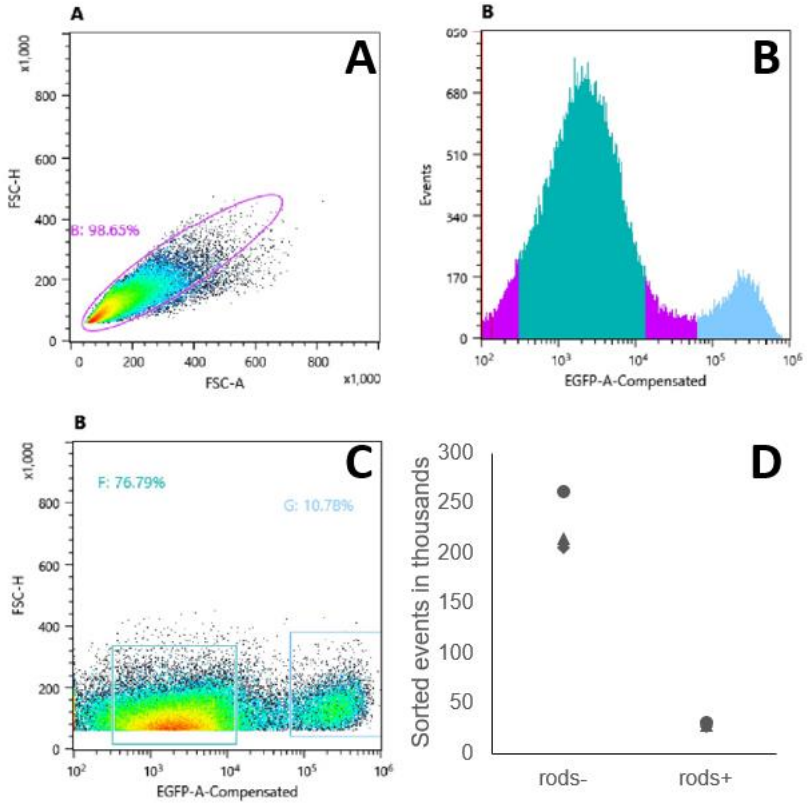


***Figure 3.10.*** A-C. Representative (100,000 sorted events) sorting reports of 30 dpi *XOPS:eGFP* fish retinal tissue. The eGFP+ LWS cone population can be gated with the eGFP expression and scatter characteristics. A. Forward scatter (FSC-H) vs. (FSC-A) plot demonstrates effective dissociation of retinal cells. The ellipse indicates the population of dissociated cells subjected to sorting. B. The eGFP- cells and the eGFP+ cells appear in two distinctive peaks. C. Gating strategy, with sorting percentage of the eGFP+ cells indicated. Gates are shown with two rectangles. D. Numbers of sorted events collected in eGFP- (rod-) and eGFP+ (rod+) cell populations for the three biological replicates. Letter A at upper left in Panel A indicated all events prior to sorting. Letter B at upper left in Panel B and C indicated the sorting of events collected in the ellipse shown in Panel A. Different colors shown in Panel B were assigned by the machine testing different gates, and are not relevant in the data interpretation.

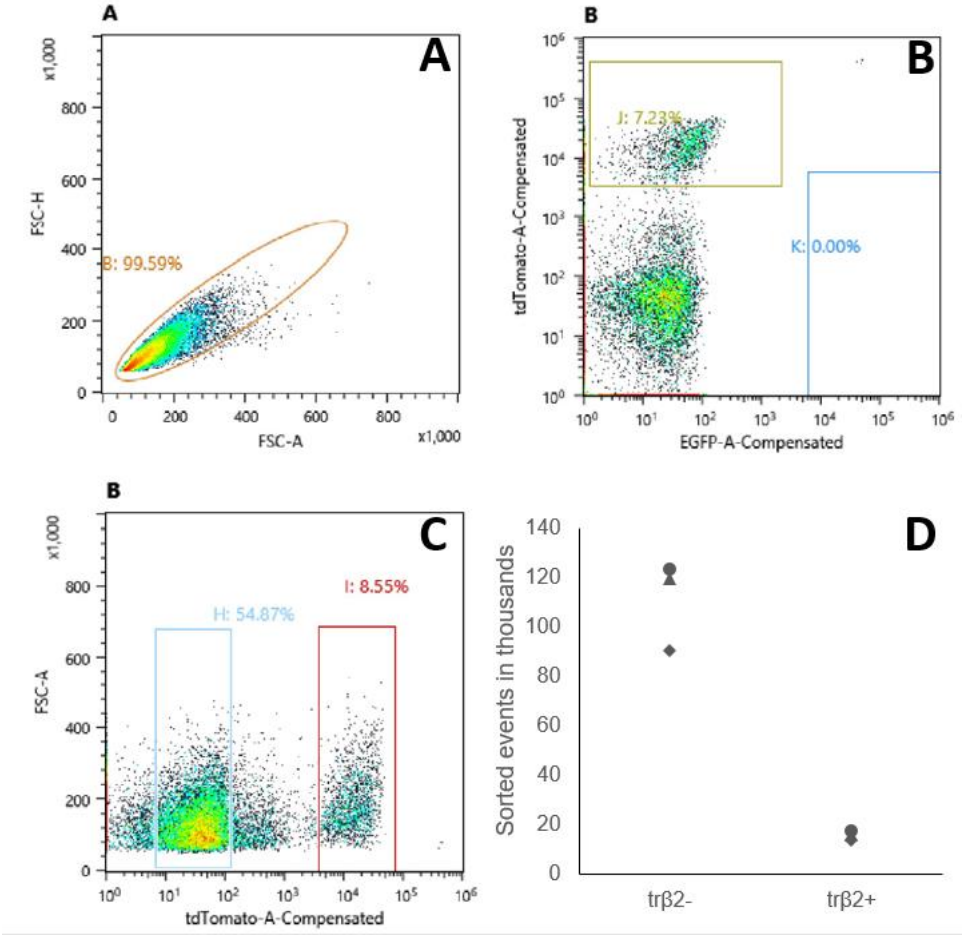


***Figure 3.11.*** A-C. Representative (100,000 sorted events) sorting reports of 14 dpf *trβ2:tdTomato* fish retinal tissue. The tdTomato+ LWS cone population can be gated with the tdTomato expression and scatter characteristics. A. Forward scatter (FSC-H) vs. (FSC-A) plot demonstrates effective dissociation of retinal cells. The ellipse indicates the population of dissociated cells subjected to sorting. B. Bi-fluorescence plot shows the tdTomato+ cells as a distinctive population. C. Gating strategy, with sorting percentage of the tdTomato+ cells indicated. Gates are shown with two rectangles. D. Numbers of sorted events collected in tdTomato- (trβ2-) and tdTomato+ (trβ2+) cell populations for the three biological replicates. Letter A at upper left in Panel A indicated all events prior to sorting. Letter B at upper left in Panel B and C indicated the sorting of events collected in the ellipse shown in Panel A.

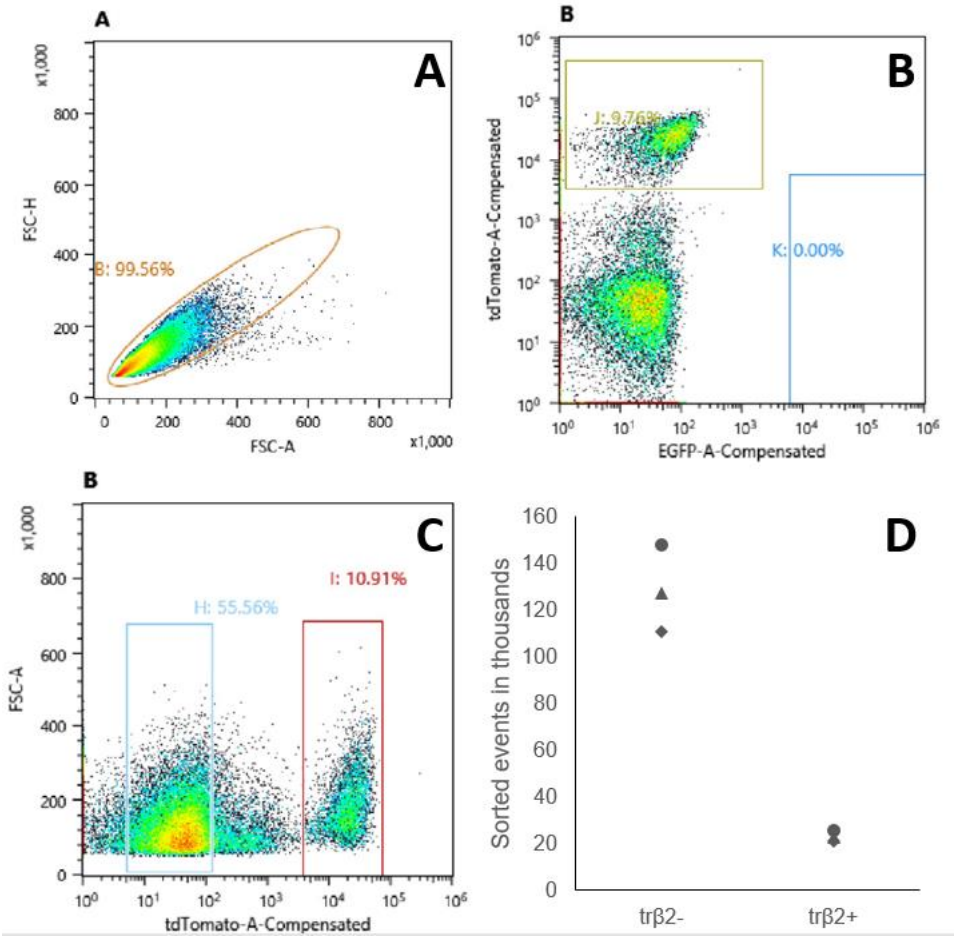


***Figure 3.12.*** A-C. Representative (100,000 sorted events) sorting reports of 30 dpf *trβ2:tdTomato* fish retinal tissue. The tdTomato+ LWS cone population can be gated with the tdTomato expression and scatter characteristics. A. Forward scatter (FSC-H) vs. (FSC-A) plot demonstrates effective dissociation of retinal cells. The ellipse indicates the population of dissociated cells subjected to sorting. B. Bi-fluorescence plot shows the tdTomato+ cells as a distinctive population. C. Gating strategy, with sorting percentage of the tdTomato+ cells indicated. Gates are shown with two rectangles. D. Numbers of sorted events collected in tdTomato- (trβ2-) and tdTomato+ (trβ2+) cell populations for the three biological replicates. Letter A at upper left in Panel A indicated all events prior to sorting. Letter B at upper left in Panel B and C indicated the sorting of events collected in the ellipse shown in Panel A.

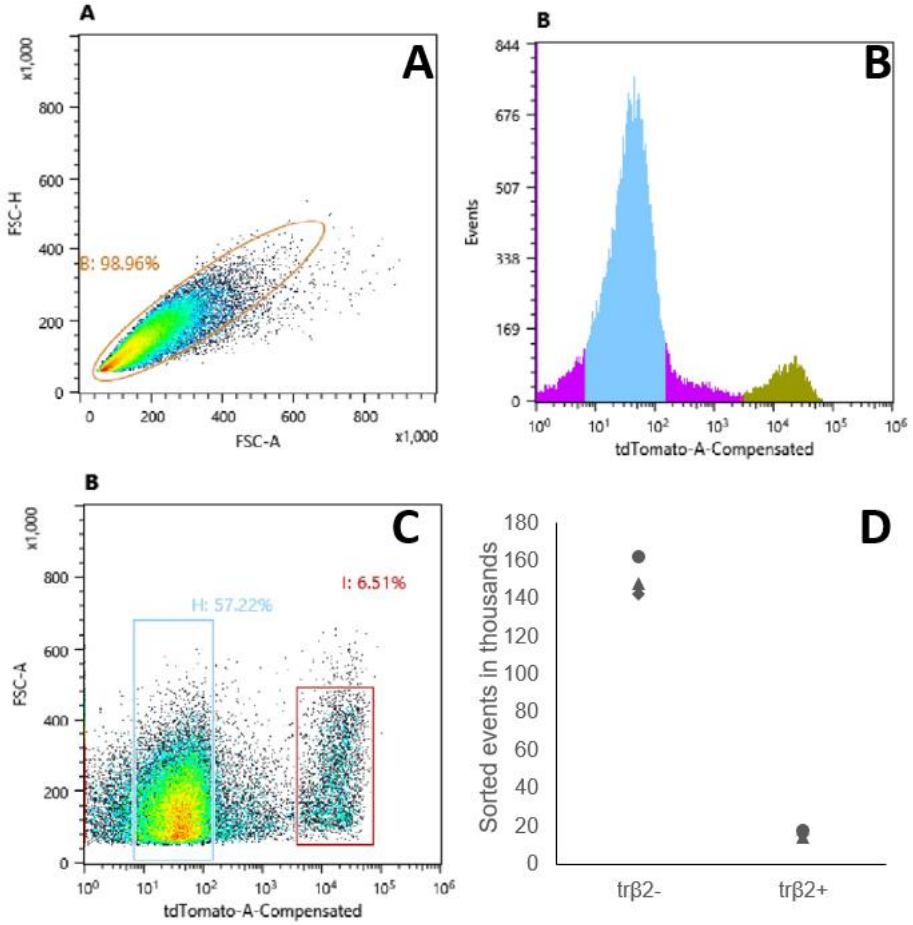


***Figure 3.13.*** A-C. Representative (100,000 sorted events) sorting reports of 14 dpi *trβ2:tdTomato* fish retinal tissue. The tdTomato+ LWS cone population can be gated with the tdTomato expression and scatter characteristics. A. Forward scatter (FSC-H) vs. (FSC-A) plot demonstrates effective dissociation of retinal cells. The ellipse indicates the population of dissociated cells subjected to sorting. B. The tdTomato- cells and the tdTomato+ cells appear in two distinctive peaks. C. Gating strategy, with sorting percentage of the tdTomato+ cells indicated. Gates are shown with two rectangles. D. Numbers of sorted events collected in tdTomato- (trβ2-) and tdTomato+ (trβ2+) cell populations for the three biological replicates. Letter A at upper left in Panel A indicated all events prior to sorting. Letter B at upper left in Panel B and C indicated the sorting of events collected in the ellipse shown in Panel A. Different colors shown in Panel B were assigned by the machine testing different gates, and are not relevant in the data interpretation.

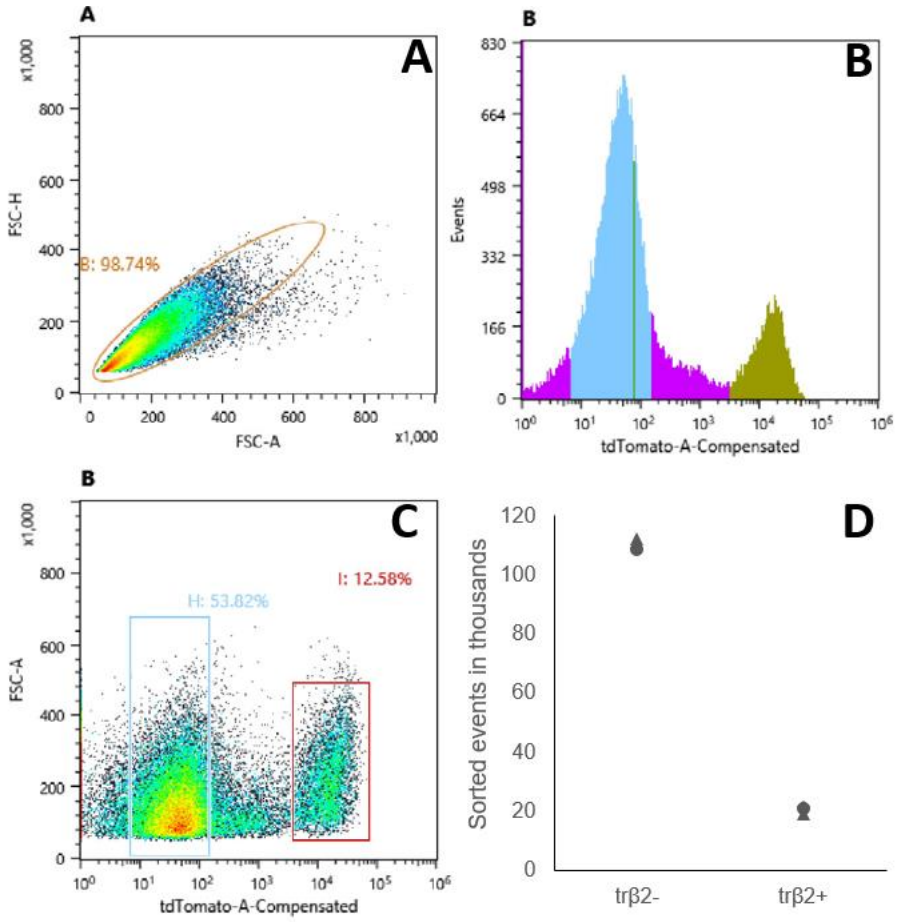


***Figure 3.14.*** A-C. Representative (100,000 sorted events) sorting reports of 30 dpi *trβ2:tdTomato* fish retinal tissue. The tdTomato+ LWS cone population can be gated with the tdTomato expression and scatter characteristics. A. Forward scatter (FSC-H) vs. (FSC-A) plot demonstrates effective dissociation of retinal cells. The ellipse indicates the population of dissociated cells subjected to sorting. The ellipse indicates the population of dissociated cells subjected to sorting. B. The tdTomato- cells and the tdTomato+ cells appear in two distinctive peaks. C. Gating strategy, with sorting percentage of the tdTomato+ cells indicated. Gates are shown with two rectangles. D. Numbers of sorted events collected in tdTomato- (trβ2-) and tdTomato+ (trβ2+) cell populations for the three biological replicates. Letter A at upper left in Panel A all events prior to sorting. Letter B at upper left in Panel B and C indicated the sorting of events collected in the ellipse shown in Panel A. Different colors shown in Panel B were assigned by the machine testing different gates, and are not relevant in the data interpretation.

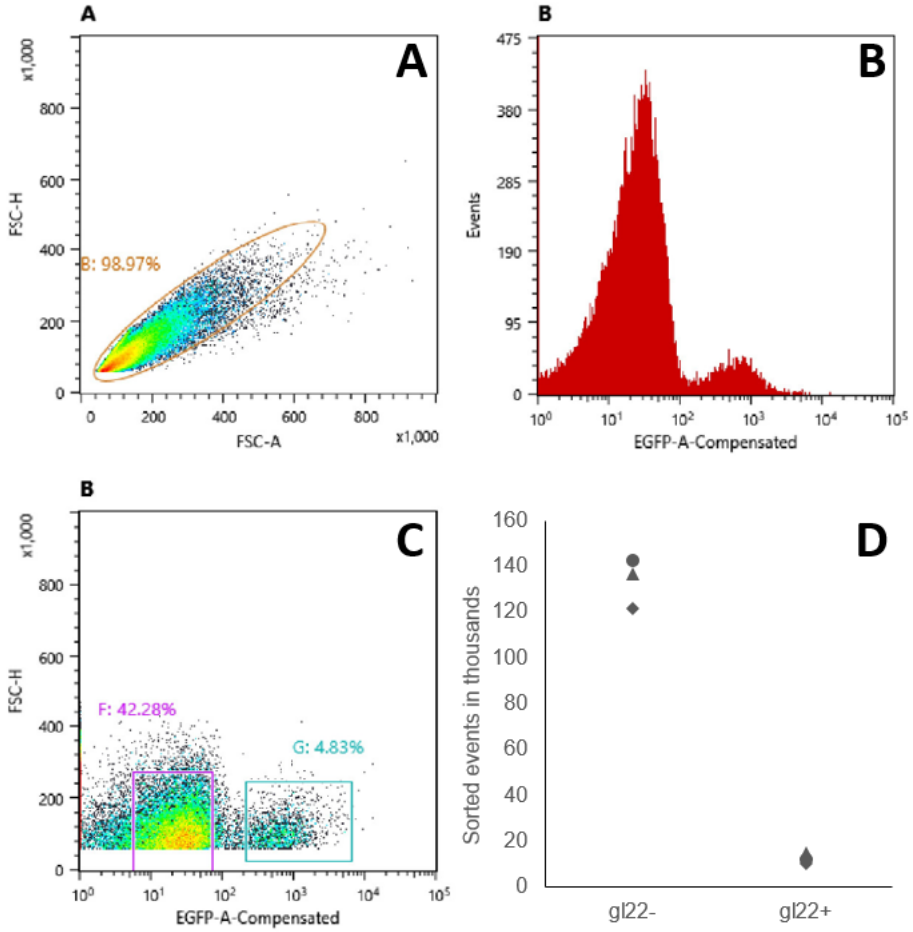


***Figure 3.15.*** A-C. Representative (100,000 sorted events) sorting reports of 7 dpi *gl22:eGFP* fish retinal tissue. The eGFP+ microglia population can be gated with the eGFP expression and scatter characteristics. A. Forward scatter (FSC-H) vs. (FSC-A) plot demonstrates effective dissociation of retinal cells. The ellipse indicates the population of dissociated cells subjected to sorting. B. eGFP- cells and eGFP+ cells appear in two distinctive peaks. C. Gating strategy, with sorting percentage of the eGFP+ cells indicated. Gates are shown with two rectangles. D. Numbers of sorted events collected in eGFP- (gl22-) and eGFP+ (gl22+) cell populations for the three biological replicates. Letter A at upper left in Panel A indicated all events prior to sorting. Letter B at upper left in Panel B and C indicated the sorting of events collected in the ellipse shown in Panel A.

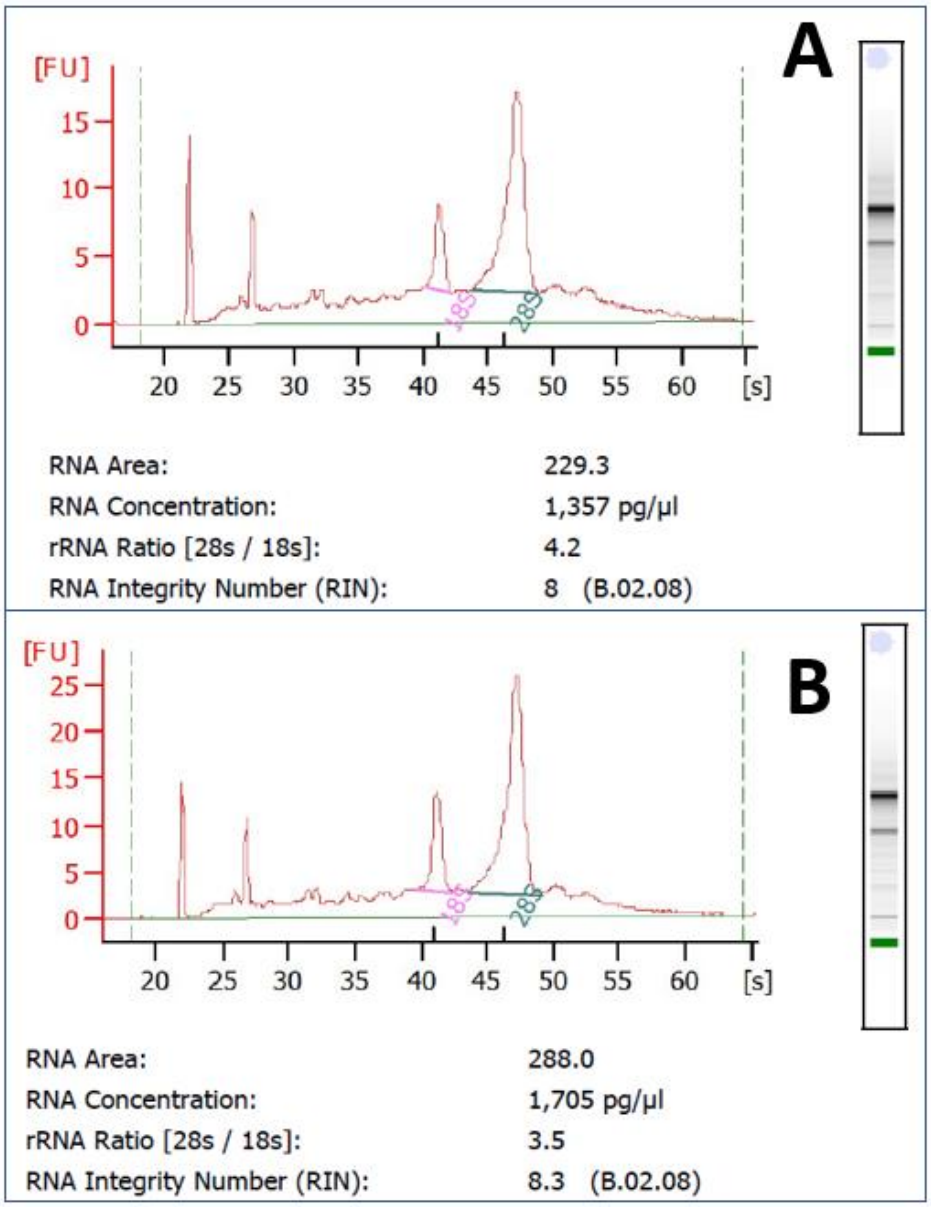


***Figure 3.16.*** Quality check of 14 dpf rod+ and rod- RNA samples by Bioanalyzer 2100. Peaks of 18s and 28s RNA as well as the RIN number of Rod+ RNA sample are shown in A. Peaks of 18s and 28s RNA as well as the RIN number of Rod- RNA sample are shown B.

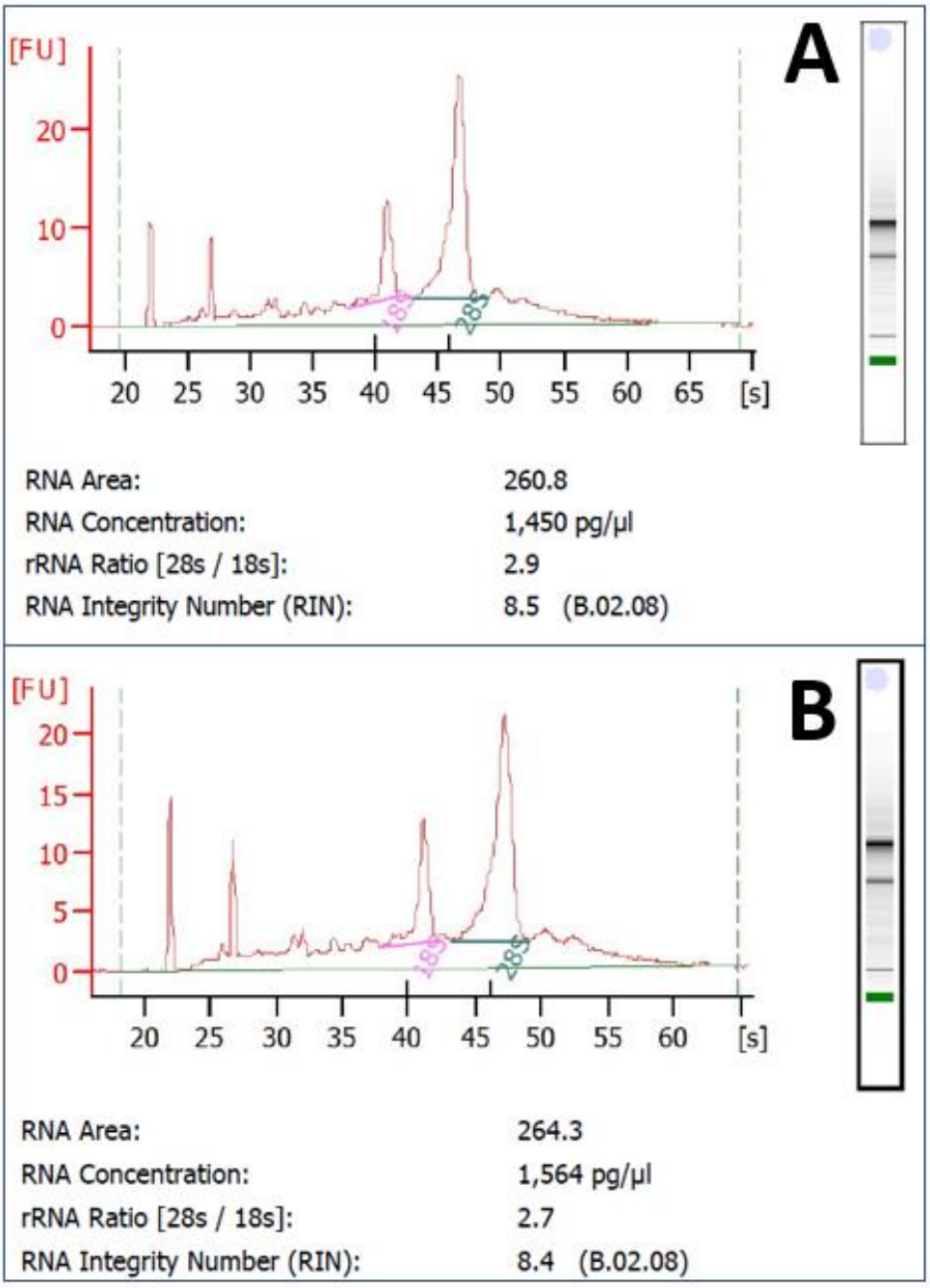


***Figure 3.17.*** Quality check of 14 dpi rod+ and rod- RNA samples by Bioanalyzer 2100. Peaks of 18s and 28s RNA as well as the RIN number of Rod+ RNA sample are shown in A. Peaks of 18s and 28s RNA as well as the RIN number of Rod- RNA sample are shown in B.

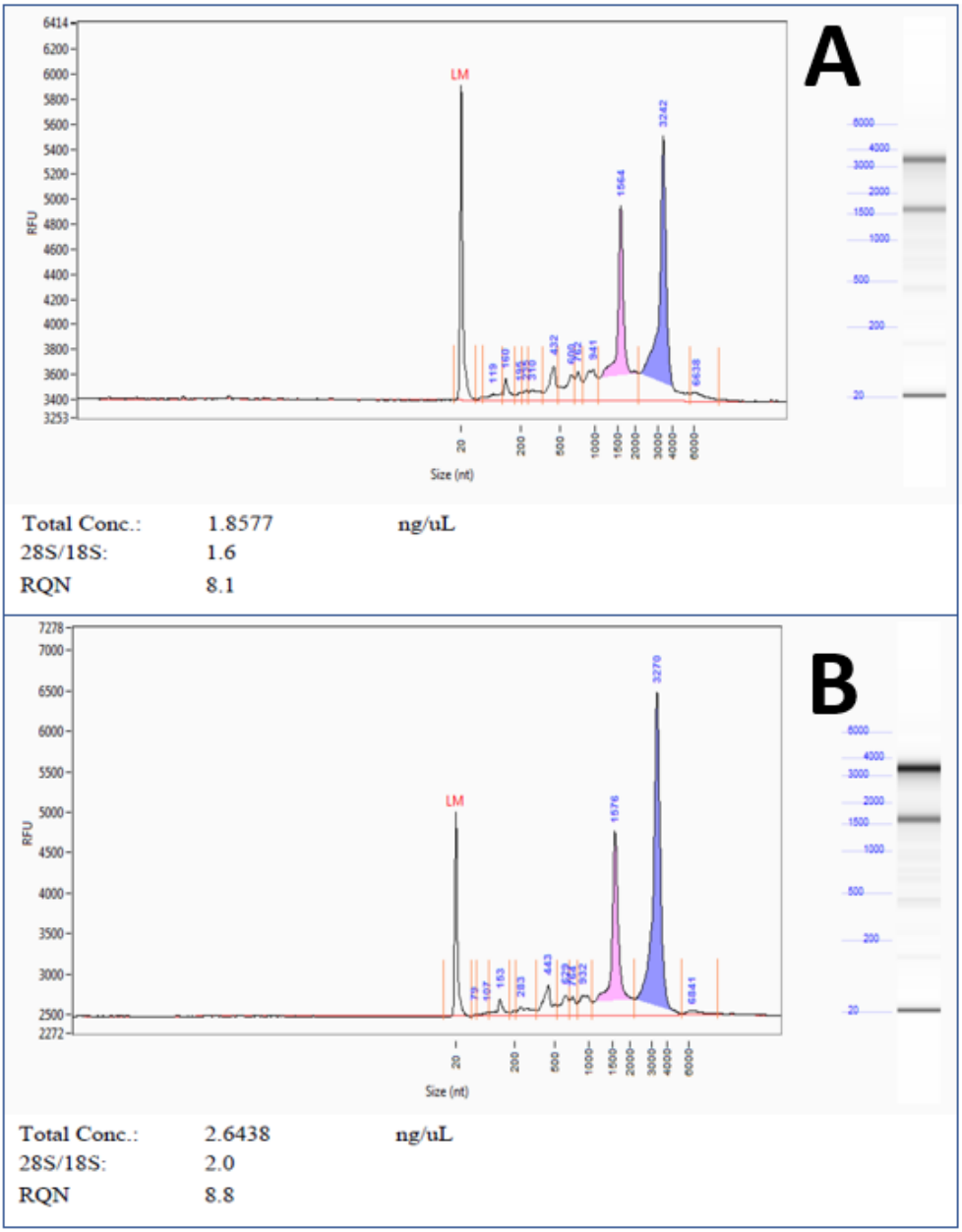


***Figure 3.18.*** Quality check of adult TRB2+ (LWS cones) and TRB2- RNA samples by Fragment Analyzer. Peaks of 18s and 28s RNA as well as the RQN number of TRB2+ RNA sample are shown in A. Peaks of 18s and 28s RNA as well as the RQN number of TRB2- RNA sample are shown in B.

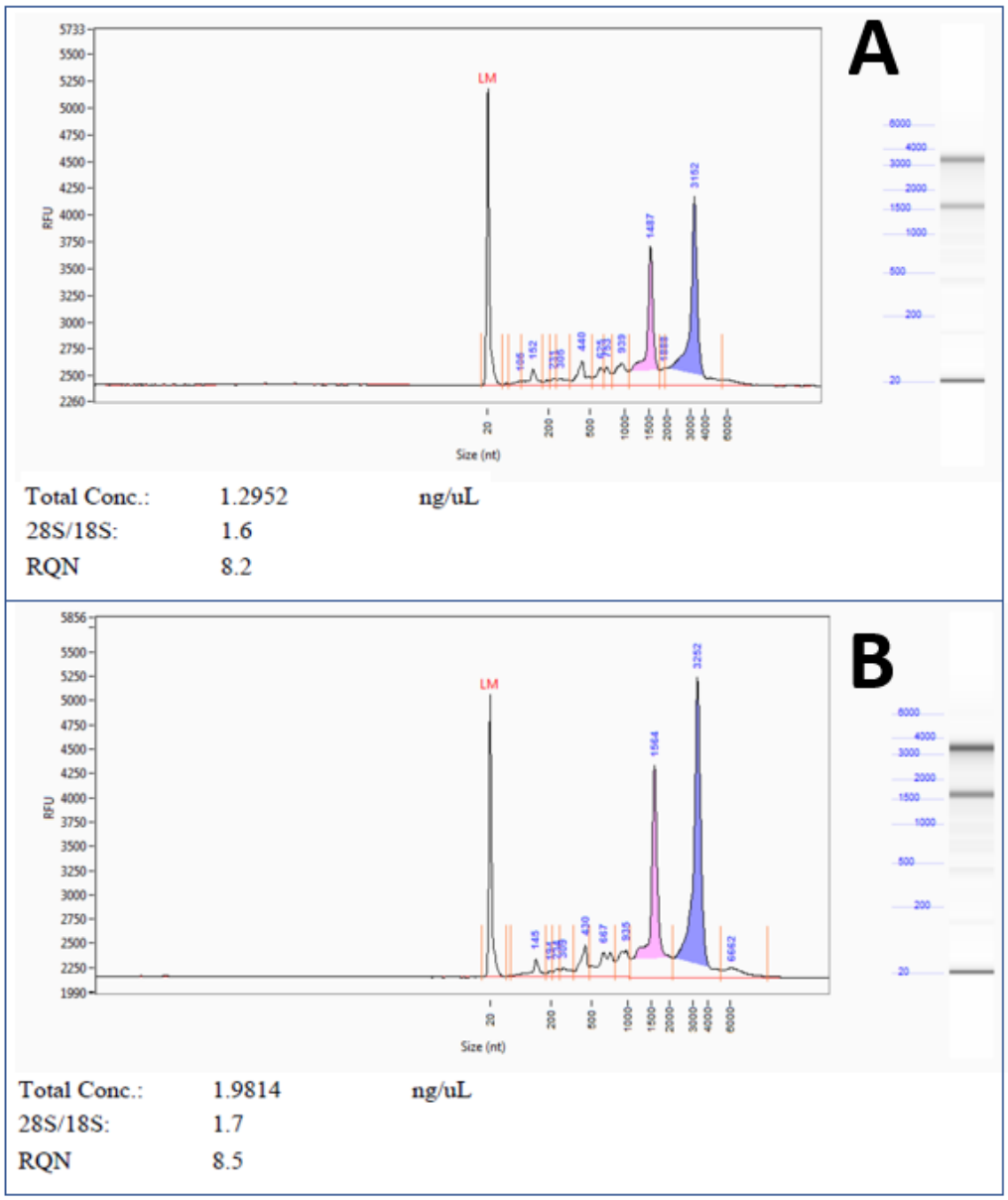


***Figure 3.19.*** Quality check of adult Mpeg1+ (microglia) and Mpeg1- RNA samples by Fragment Analyzer. Peaks of 18s and 28s RNA as well as the RQN number of MPEG1+ RNA sample are shown in A. Peaks of 18s and 28s RNA as well as the RQN number of MPEG1- RNA sample are shown in B.

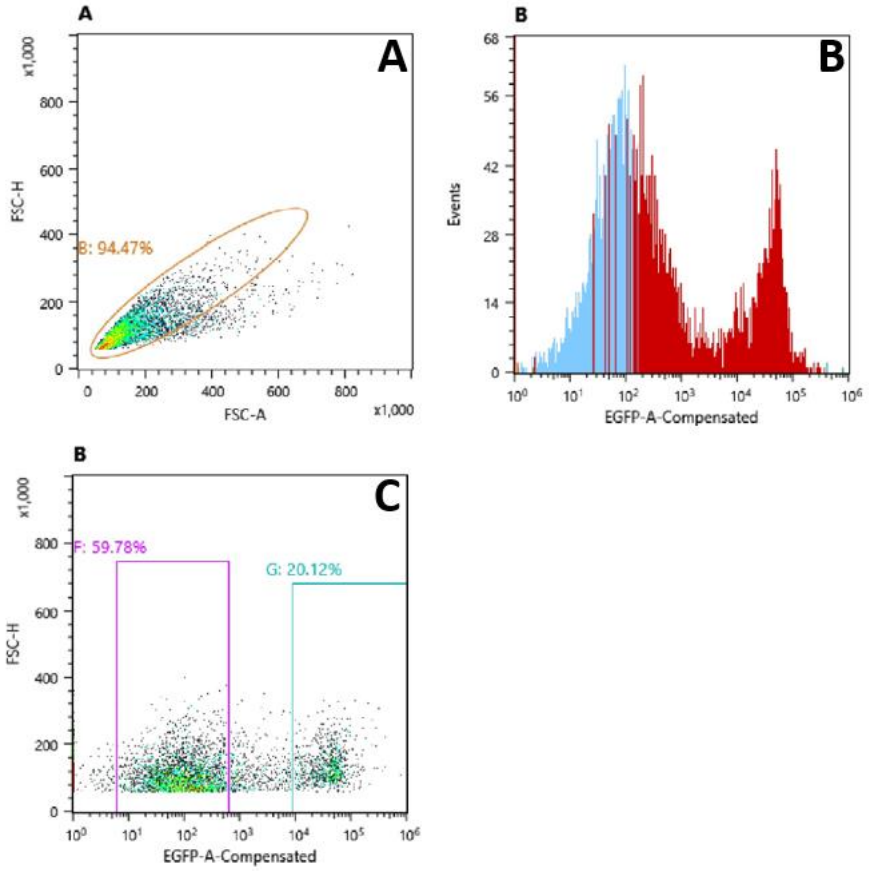


***Figure 3.20.*** The first 10,000 sorted events of adult *XOPS:eGFP* fish retina tissue. This sorting report is generally consistent (A and B) to that of 100,000 sorted events. Sorted rod photoreceptors usually contribute to 15-25% of total sorted events (see gating strategy in C). Different colors shown in Panel B were assigned by the machine testing different gates, and are not relevant in the data interpretation.

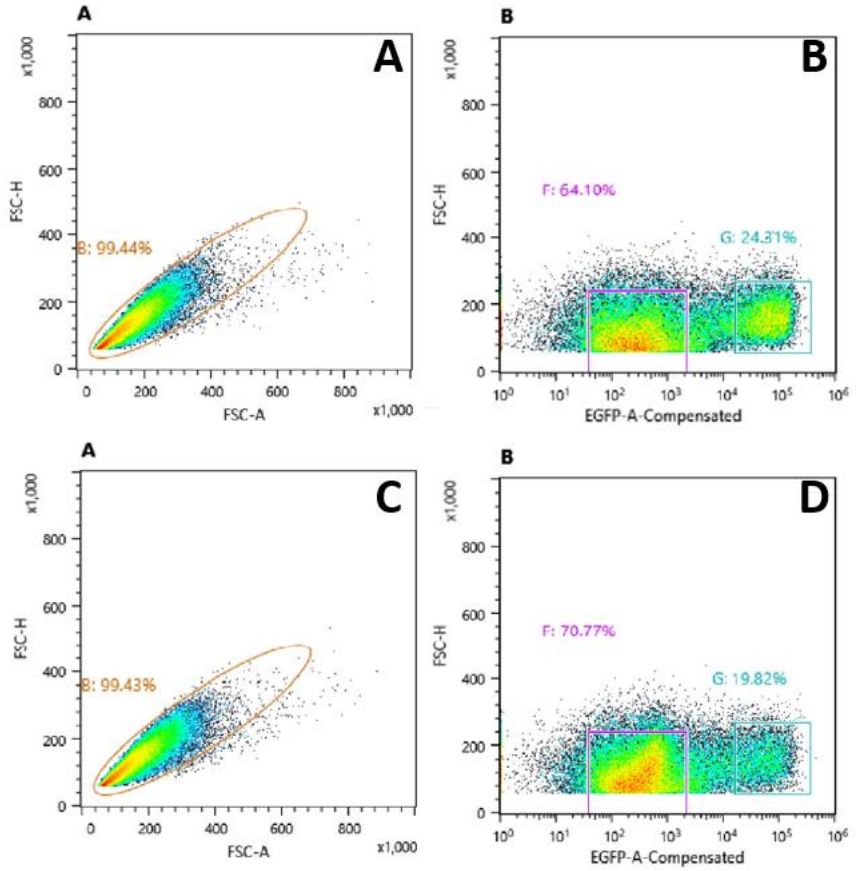


***Figure 3.21.*** A comparison of reports of the first 100,000 sorted events vs. the second 100,000 sorted events from the same adult *XOPS:eGFP* fish retinal sample. The first 100,000 sorted events (A and B) had similar sorting percentages to the second 100,000 sorting events (C and D) using the same gating strategy.

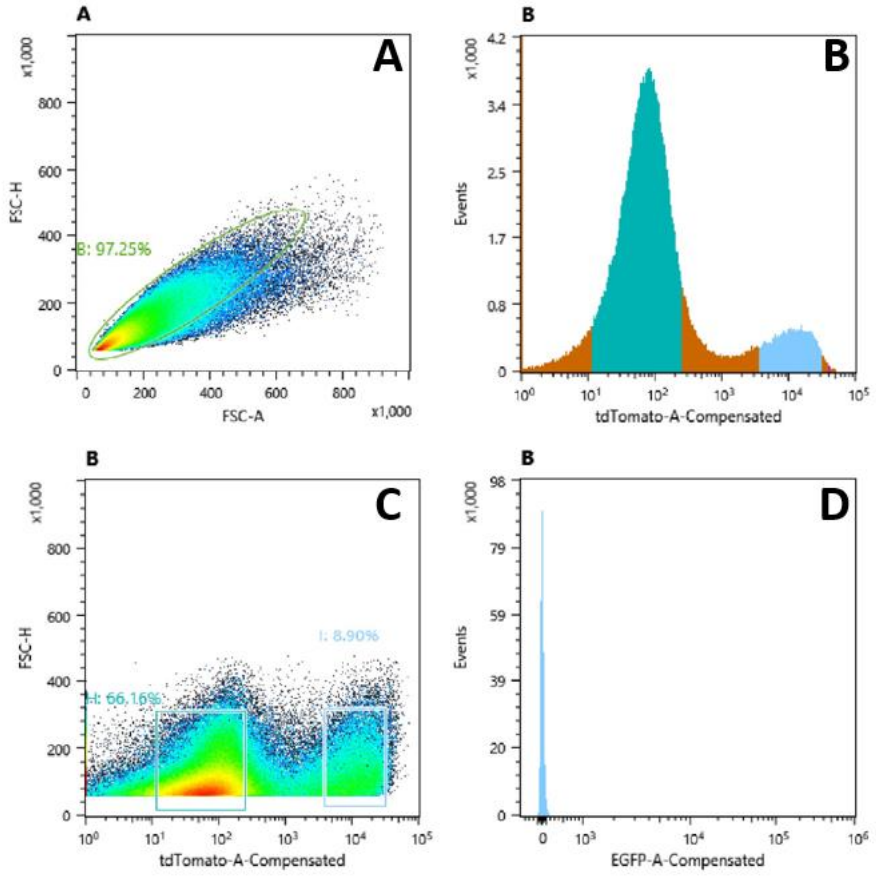


***Figure 3.22.*** A report of 300,000 sorted events with 30 dpi *trβ2:tdTomato* fish retina tissue. Dissociation of retina tissue was effectively performed as illustrated in (A, as FSC-H versus FSC-A). (B) shows two distinctive peaks of trβ2+ and trβ2- populations. Gating strategy and sorting percentages are presented in (C). (D) proves the effectiveness of the compensation system. Different colors shown in Panel B were assigned by the machine testing different gates, and are not relevant in the data interpretation.

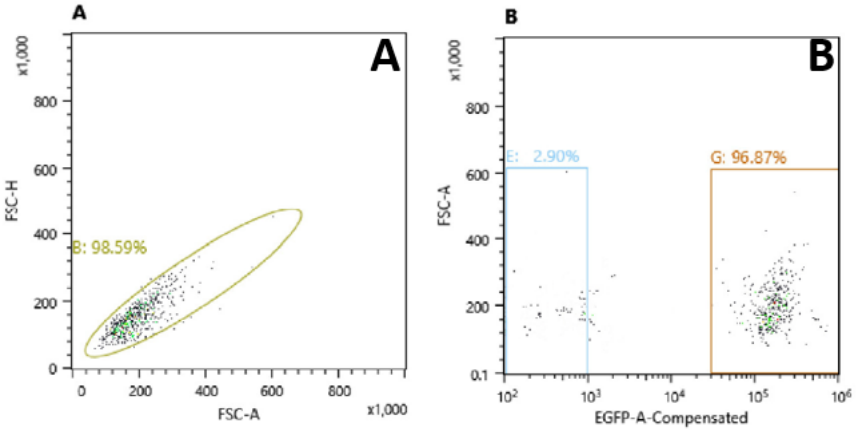


***Figure 3.23.*** A post-sorting analysis of a rod+ sorted sample of 30 dpi *XOPS:eGFP* fish retina tissue. The checking on the sorted samples gives a consistent FSC-H versus FSC-A plot (A) to the primary sorting and a proof of the sample purity (B).

**Table 3.1. Primers used for qPCR experiments**

| Gene | Sense Primer 5' -> 3' | Anti-sense Primer 5'-> 3' |
|---|---|---|
| Lplastin | GCAGTGGGTGAACGAAACAC | TCGAGATCGCATACTTGGCG |
| mpeg1.1 | CATGTCGTGGCTGGAACAGA | ATGGTTACGGACTTGAACCCG |
| nr2e3 | CTTGCTCAACATATTCAC | GGAAGGAGAAGTAATAGTC |
| opn1lw1 | CCCACACTGCATCTCGACAA | AAGGTATTCCCCATCACTCCAA |
| opn1lw2 | AGAGGGAAGAACTGGACTTTCAGA | TTCAGAGGAGTTTTGCCTACATATGT |
| opn1sw1 | GAGTCACATTCAGTCTTG | GTCTATCAGCACACTTATC |
| opn1sw2 | ATCTGGGTGGTTTCCAACCG | ACAGGAGCGGAACTGTTTGTT |
| opn1mw1 | CAGCCCAGCACAAGAAACTC | AGAGCAACCTGACCTCCAAGT |
| opn1mw2 | TTTTTGGCTGGTCCCGATACA | CAGGAACGCAGAAATGACAGC |
| opn1mw3 | TGCTTTCGCTGGGATTGGATT | CCCTCTGGAATATACCTTGACCA |
| opn1mw4 | CACGCTTTCGCAGGATGC | CGGAATATACCTGGGCCAAC |
| rho | ACTTCCGTTTCGGGGAGAAC | GAAGGACTCGTTGTTGACAC |
| thrb | TCTGGTCTGATGAGTCTA | GTATTAGCCTGGTGATGA |
| 18S | GAACGCCACTTGTCCCTCTA | GTTGGTGGAGCGATTTGTCT |

**Table 3.2. Summary of fish samples used in each FACS experiment**

| Transgenic lines | Retinae/Sample | Ages | An example of RNA yielding/sample | |
|---|---|---|---|---|
| *sws1:GFP* | 2 | 10mo | 21ng for GFP+ | 32ng for GFP- |
| *sws2:mcherry* | 4 | 10mo | 16ng for mcherry+ | 30ng for mcherry- |
| *rh2-2:GFP* | 4 | 10mo | 15ng for GFP+ | 44ng for GFP- |
| *trβ2:tdTomato* | 2 | 1yo | 26ng for tdTomato+ | 48ng for tdTomato- |
| *lws:Pac(H)* | 8 | 10mo | 19ng for GFP+ | 21ng for RFP+ |
| *XOPS:eGFP* | 2 | 1yo | 24ng for GFP+ | 45ng for RFP+ |
| 14dpf *XOPS:eGFP* | 30-40 | N.A. | 17ng for GFP+ | 33ng for GFP- |
| 30dpf *XOPS:eGFP* | 20 | N.A. | 27ng for GFP+ | 49ng for GFP- |
| 14dpi *XOPS:eGFP* | 3 | 1yo | 25ng for GFP+ | 39ng for GFP- |
| 30dpi *XOPS:eGFP* | 2 | 1yo | 19ng for GFP+ | 33ng for GFP- |
| 14dpf *trβ2:tdTomato* | 30-40 | N.A. | 18ng for tdTomato+ | 43ng for tdTomato- |
| 30dpf *trβ2:tdTomato* | 20 | N.A. | 22ng for tdTomato+ | 50ng for tdTomato- |
| 14dpi *trβ2:tdTomato* | 3 | 1yo | 27ng for tdTomato+ | 57ng for tdTomato- |
| 30dpi *trβ2:tdTomato* | 2 | 1yo | 20ng for tdTomato+ | 45ng for tdTomato- |
| *mpeg1:eGFP* | 8 | 8mo | 14ng for GFP+ | 29ng for GFP- |

## Table 3.3. qPCR analysis of sorted photoreceptor samples

| Sorted samples | Cycle threshold (Ct) values | | | | | | | |
|---|---|---|---|---|---|---|---|---|
| | *rho* | *opn1lw1* | *opn1lw2* | *opn1sw1* | *opn1sw2* | *nr2e3* | *thrb* | *18s* |
| SWS1:GFP+ | N.D. | N.D. | N.D. | 24.38 | N.D. | 24.72 | 24.83 | 17.42 |
| SWS1:GFP- | 18.83 | 21.19 | 20.76 | N.D. | 25.09 | 21.61 | 25.03 | 17.08 |
| | *rho* | *opn1lw1* | *opn1lw2* | *opn1sw1* | *opn1sw2* | *nr2e3* | *thrb* | *18s* |
| SWS2:mcherry+ | N.D. | N.D. | N.D. | N.D. | 24.26 | 25.84 | 25.92 | 16.89 |
| SWS2:mcherry- | 20.11 | 22.03 | 21.97 | 24.17 | N.D. | 23.17 | 25.43 | 16.41 |
| | *rho* | *opn1lw1* | *opn1lw2* | *opn1mw1* | *opn1mw2* | *opn1mw3* | *opn1mw4* | *18s* |
| Adult Rh2-2:GFP+ | N.D. | N.D. | N.D. | N.D. | 23.84 | 38.82 | N.D. | 16.46 |
| Adult Rh2-2:GFP- | 19.56 | 23.74 | 21.86 | 22.94 | N.D. | 24.27 | 26.52 | 16.03 |
| | *rho* | *opn1lw1* | *opn1lw2* | *opn1sw1* | *opn1mw1* | *nr2e3* | *thrb* | *18s* |
| Adult trβ2:tdTomato+ | N.D. | 21.33 | 20.27 | N.D. | N.D. | 24.92 | 23.55 | 15.28 |
| Adult trβ2:tdTomato- | 20.08 | N.D. | 38.13 | 23.85 | 24.31 | 22.36 | 25.94 | 15.01 |
| | *rho* | *opn1lw1* | *opn1lw2* | *opn1mw1* | *opn1mw2* | *nr2e3* | *thrb* | *18s* |
| LWS1:GFP+ | N.D. | 26.54 | 38.91 | N.D. | N.D. | 29.72 | 25.73 | 20.72 |
| LWS2:RFP+ | N.D. | N.D. | 26.35 | N.D. | N.D. | 28.89 | 25.98 | 21.18 |
| | *rho* | *opn1lw1* | *opn1lw2* | *opn1sw1* | *nrl* | *nr2e3* | *thrb* | *18s* |
| 14dpf XOPS:eGFP+ | 19.86 | N.D. | N.D. | 37.26 | 22.57 | 24.39 | 27.75 | 18.98 |
| 14dpf XOPS:eGFP- | N.D. | 22.77 | 22.18 | 23.09 | 27.98 | 26.92 | 24.88 | 18.42 |
| | *rho* | *opn1lw1* | *opn1lw2* | *opn1sw1* | *nrl* | *nr2e3* | *thrb* | *18s* |
| 30dpf XOPS:eGFP+ | 20.37 | N.D. | N.D. | N.D. | 23.76 | 25.39 | 26.48 | 18.19 |
| 30dpf XOPS:eGFP- | N.D. | 21.66 | 20.89 | 23.44 | 28.61 | 28.76 | 24.11 | 17.88 |
| | *rho* | *opn1lw1* | *opn1lw2* | *opn1sw1* | *nrl* | *nr2e3* | *thrb* | *18s* |
| 14dpi XOPS:eGFP+ | 18.65 | N.D. | N.D. | 38.57 | 23.47 | 25.39 | 26.55 | 16.95 |
| 14dpi XOPS:eGFP- | N.D. | 20.12 | 19.74 | 20.53 | 28.61 | 28.52 | 24.28 | 16.42 |
| | *rho* | *opn1lw1* | *opn1lw2* | *opn1sw1* | *nrl* | *nr2e3* | *thrb* | *18s* |
| 30dpi XOPS:eGFP+ | 19.30 | N.D. | N.D. | N.D. | 25.31 | 26.41 | 28.69 | 17.01 |
| 30dpi XOPS:eGFP- | N.D. | 21.35 | 20.53 | 22.20 | 27.67 | 28.72 | 25.02 | 16.56 |
| | *rho* | *opn1lw1* | *opn1lw2* | *opn1sw1* | *opn1mw1* | *nr2e3* | *thrb* | *18s* |
| 14dpf trβ2:tdTomato+ | N.D. | 22.89 | 21.91 | N.D. | 38.60 | 27.46 | 23.84 | 19.04 |
| 14dpf trβ2:tdTomato- | 21.25 | N.D. | 37.11 | 22.66 | 23.72 | 25.23 | 25.39 | 18.63 |
| | *rho* | *opn1lw1* | *opn1lw2* | *opn1sw1* | *opn1mw1* | *nr2e3* | *thrb* | *18s* |
| 30dpf trβ2:tdTomato+ | N.D. | 21.91 | 21.34 | N.D. | N.D. | 26.16 | 24.40 | 18.12 |
| 30dpf trβ2:tdTomato- | 21.08 | N.D. | N.D. | 22.78 | 23.59 | 24.58 | 25.56 | 17.79 |
| | *rho* | *opn1lw1* | *opn1lw2* | *opn1sw1* | *opn1mw1* | *nr2e3* | *thrb* | *18s* |
| 14dpi trβ2:tdTomato+ | N.D. | 20.97 | 20.81 | N.D. | N.D. | 27.87 | 24.53 | 18.80 |
| 14dpi trβ2:tdTomato- | 21.42 | N.D. | N.D. | 23.75 | 23.68 | 26.91 | 25.60 | 18.03 |
| | *rho* | *opn1lw1* | *opn1lw2* | *opn1sw1* | *opn1mw1* | *nr2e3* | *thrb* | *18s* |
| 30dpi trβ2:tdTomato+ | N.D. | 23.66 | 22.45 | N.D. | N.D. | 27.33 | 26.85 | 18.24 |
| 30dpi trβ2:tdTomato- | 21.53 | N.D. | 37.68 | 23.99 | 24.50 | 25.72 | 28.11 | 17.12 |

**Table 3.4. qPCR analysis of sorted microglia samples**

| Sorted samples | Cycle threshold (Ct) values | | | | |
|---|---|---|---|---|---|
| | *rho* | *opn1lw2* | *L-plastin* | *mpeg1.1* | *18s* |
| 7dpi mpeg1:eGFP+ | N.D. | N.D. | 21.56 | 22.28 | 14.61 |
| 7dpi mpeg1:eGFP- | 20.31 | 22.24 | 37.49 | 38.77 | 13.94 |

**Chapter 4: Zebrafish rxrga mutants: generation, validation, and preliminary characterization of opsin expression phenotype.**

Chi Sun, Carlos Galicia, and Deborah L. Stenkamp

Publication status: unpublished

Abstract

Background: Retinoid X receptors (RXR) are nuclear hormone receptors that form homo- or heterodimers with other receptors such as thyroid hormone receptors. In the presence of ligand (e.g. retinoids or thyroid hormone), dimers bind to DNA response elements, promoting transcription of target genes. RXRγ specifically is required for cone photoreceptor patterning in mice, where it is cone-specific [1]. The zebrafish genome harbors two *RXRγ* genes, *RXRγa* and *RXRγb*. We detected expression of *RXRγa* and *RXRγb* transcripts in purified rods by RNA-seq (Sun et al., in revision). In addition, an RXR-selective agonist regulated differential expression of the tandemly-duplicated long wavelength-sensitive (*lws*) cone opsins [2].

Results: We generated *RXRγa* mutant zebrafish to study further RXRγ functions. *RXRγa* (exons 1, 3) were targeted by CRISPR/Cas9. *RXRγa* indels were characterized in F0 and F1 adults by an Ampli-Seq. We shortlised mutant alleles in *RXRγa* exon 3 that are predicted to result in premature stop codons or significant changes to the DNA-binding domain. By comparing to WT controls, qPCR studies of selected *RXRγa* mutants at 7 days post-fertilization (dpf) and adult ages showed undetectable levels of *RXRγa* transcripts and greatly reduced expression of cone opsins *lws1*, *lws2*, *rh2-1*, *rh2-2*, *rh2-3*, and *rh2-4*.

Conclusion: RXRγa may regulate expression of specific rod and cone opsins in zebrafish.

Introduction

The spatial arrangement of zebrafish photoreceptors presents a regular neuronal mosaic. The wavelength sensitivity of a photoreceptor subtype is determined by the photopigment that is responsible for light absorption and is composed of an opsin and a chromophore. Zebrafish expresses 10 different opsins, as each coded by a separate gene [3-5]. There are two tandemly-duplicated Lws-opsin (*lws-1* and *-2*) and four tandemly-quadruplicated Mws-opsin genes (*rh2-1*, *rh2-2*, *rh2-3*, and *rh2-4*), in contrast to Sws1- and Sws2-opsins, which are each encoded by a single gene (*sws-1* and *-2*, respectively). The opsin of rods is coded by *rh1* gene, and *rhol* (*rhodopsin-like*) is also expressed in rods. The expression of these opsins at given developmental stages may follow a spatiotemporal pattern, at which some opsins are expressed at specific locations of the retina [6, 7]. Unlike the case that other retinal cells are generated at cilia marginal zone (CMZ), neurogenesis of rod photoreceptors takes place in the outer nuclear layer of the adult zebrafish [8].

For photoreceptor cells, cones usually exit from the mitotic cycle and commit to the photoreceptor lineage earlier than rods. In zebrafish, cone progenitors are produced by the asymmetric division, giving rise to a cone and another retinal cell type before the dedicated precursors are generated [9, 10]. Cone photoreceptors of the same type are produced by symmetric division of dedicated precursors. At the early stage of development, newly generated rods and cones remain morphologically indistinct, which has hindered direct studies of the events that generate photoreceptor diversity. By 48-50hfp, the photoreceptor cell layer can be identified in histological sections. Rods express opsin around 50 hpf, shortly followed by red and blue cones. Outer segments of rods and cones appear at a small patch of the ventral retina around 60 hpf [11]. At 4 dpf (days post fertilization), photoreceptor subtypes already become morphologically distinct [12, 13].

Retinoids are vitamin A metabolites that are vital signaling components for the development and maintenance of the visual system [14-16]. Retinoic acid (RA) is a major metabolite of vitamin A and is involved in early eye morphogenesis, including closure of optic fissure [17, 18] and retinal patterning [19-21]. At the stage of retinal cell differentiation, RA is known to regulate the development of photoreceptors [22, 23], and may favor retinal progenitor cells toward photoreceptor cell fate [24] and accelerate photoreceptor differentiation [25]. However, RA induces apoptosis to developing photoreceptors with the presence of RPE during cell differentiation [26]. In zebrafish, RA treatment promotes rod differentiation but delays cone maturation, while rod differentiation is impeded with the inhibition of endogenous RA synthesis [27]. Also, RA signaling regulates the opsin transcription in photoreceptors [28], and cell fate choices of photoreceptors during embryonic development [2, 29]. Endogenous RA signaling in zebrafish retina regulates differential expression of the *lws* genes in postmitotic cones by switching from *lws2* to *lws1* expression in response to RA treatment [30].

Vitamin A is stored in the form of all-trans-retinyl esters and carotenoids in mammals [31]. Retinol binds with retinol binding protein 4 (RBP4), and the protein complex enters cells by targeting the STRA6 receptor. Cytoplasmic retinol binding protein 1 (CRBP1) then facilitates the conversion to retinaldehyde [32]. In vivo, oxidation of all-trans-retinal is catalyzed by retinaldehyde dehydrogenases (RALDHs) to produce all-trans-retinoic acid. RA binds to nuclear retinoic acid receptors (RARs) which is coupled with retinoid X receptors (RXRs), and the resulting complex binds to retinoic acid response elements (RAREs) on the promoter region of target genes [33, 34]. Specifically, in human, mouse and zebrafish, there are α, β and γ subunits of RARs as well as of RXRs functioning together as the ligand-activated regulators. All-trans-retinoic acid can be oxidized by CYP26 and metabolized by UDP-glucuronosyl transferases (UGTs), effectively resulting in its catabolizism [35, 36]. All-

trans-retinal can also be catalytically isomerized to 11-cis-retinal. Photo-sensitive visual pigments are produced with the coupling of photoreceptor opsins with 11-cis-retinal [37]. This conformational change consequentially initiates the phototransduction cascade. The absorption of light by these visual pigments causes photo-bleaching [38, 39] which reset the visual pigments to the ground state.

Studies with murine models have shown that *RARα* and *RXRγ* are specifically expressed in the developing retina [32]. Expression of zebrafish *rar* genes temporally coincide with expression patterns of genes involved in the synthesis, transport, and degradation of RA, including retinaldehyde dehydrogenase 2 (*raldh2*), cellular retinoic acid-binding protein 2 (*crabp2*) and *cyp26* during early body and CNS development [40]. In zebrafish retina, *rarα* is expressed at the ventral retina by 36hpf, and is globally expressed in the retina at later stage but more concentrated in the RGCs [29]. *Rxrγ* genes are widely expressed in the zebrafish retina by 48 hpf, while in embryos at 72 hpf, *rxrγ* expression in the ONL is restricted to the region near the CGZ, suggesting a continuing function for Rxrγ in the generation and differentiation of photoreceptors beyond the embryonic period [29].

The *RXRγ* gene in mouse has important roles in cone determination [1]. RXRγ and TRβ2 are required to suppress expression of the S-cone opsin in mice, while favoring the production of cones expressing M-opsin [41, 42]. There are two copies of *rxrγ* genes in zebrafish genome, namely *rxrγa* and *rxrγb*. Both are expressed in rods and non-rod retinal cells in adult fish (Sun C et al., submitted MS). RXR acts as a transcription factor that, on activation by binding of a specific ligand such as bexarotene, regulates the transcription of target genes [43, 44]. However, distinctive roles of these *rxrγ* genes in retina development remain unknown, and a role for any *rxrγ* in any vertebrate for rod development or function has not been described.

In this paper, we report the generation of zebrafish with mutations in the *rxrγa* gene. We used the clustered regularly interspaced short palindromic repeats (CRISPR)/CRISPR-associated (Cas) system, which evolved in bacteria and archaea as a defense mechanism to silence foreign nucleic acids of viruses and plasmids, as a powerful genomic-editing technique with synthetic guide RNA (gRNA) directing Cas9 nuclease-mediated alteration of endogenous genes in vivo in zebrafish [45-47]. In zebrafish, the CRISPR/Cas9 system can generate knockouts with high frequency of 75-99% [48]. Also, zebrafish reach sexual maturity by three or four months, and edited genes can be quickly passed to offspring generations from the founders. This technique was used to yield the first model of *rxrγa* knockout mutants. In addition, we provide a preliminary analysis of rod and cone opsin gene expression in these *rxrγa* loss-of-function models.

## Methods

### *Animals*

We used wild type (Tübingen or TU) zebrafish (*Danio rerio*) in this study as the background strain for the generation of mutants. Zebrafish were maintained on a 14:10 light/dark cycle in monitored, recirculating system water according to The Zebrafish Book (Westerfield). All procedures involving zebrafish were carried out in accordance with animal care protocols approved by the University of Idaho Animal Care and Use Committee. Zebrafish maintained at the University of Utah CRISPR core facility were also treated according to an approved animal care and use protocol. Potential founders, and uninjected controls of the same background strain, were shipped from the University of Utah as embryos and raised and propagated at the University of Idaho.

We used various transgenic fish lines to obtain subtypes of photoreceptors by fluorescence activated cell sorting (FACS). Rods were isolated from the line referred to as *XOPS:eGFP*, in which rods express green fluorescent protein (GFP) under control of a *Xenopus* rod opsin promoter [49]. LWS cones were isolated from *trβ2:tdTomato* transgenic zebrafish in which LWS cones express tdTomato fluorescent protein under control of the *thyroid receptor beta 2* promoter [50]. A subset of MWS cones were isolated from *rh2-2:GFP* transgenic zebrafish, in which Rh2 subtype Rh2-2 cones express GFP under control of GFP-reporter constructed adjacent to upstream regions of Rh2-2 [51]. UV cones were isolated from *sws1:GFP* transgenic zebrafish, in which UV cones express GFP under control of the UV opsin promoter [52]. SWS2 cones were isolated from *sws2:mcherry* transgenic zebrafish, in which SWS2 cones express mCherry fluorescent protein under control of the *sws2* promoter [53].

*Rxrγa knockout using the CRISPR/Cas9 system*

CRISPR target sites in the *rxrγa* gene were identified and analyzed for any possible off-target binding sites in the zebrafish genome (Zv9), using the Geneious program (Biomatters, New Zealand). The selected target site at exon 1 was GGAGATGCTGCCGTCCAGGACGG (5’ – 3’, GC: 65%), and the selected target site at exon 3 was GGACTGGGCAGTTACCCTTGCGG (5’ – 3’, GC: 60%) (Fig. 4.1).

The selected oligonucleotides were cloned into a plasmid, and the in vitro transcription was carried out to produce gRNAs. One-cell stage zebrafish embryos were injected with a solution containing 1000 ng/µl Cas9 mRNA and 400 ng/µl gRNA for both target sites. Once injected, embryos were allowed to grow for one day to assess the survival rate and collect DNA from random samples (~40 embryos) for mutant screening. High-

resolution melt analysis (HRMA) was used to detect mutations. The primers for HRMA tests are listed in Table 4.1.

Customized CRISPR/Cas9 processes (material preparation, microinjection and mutant screening) described in this research were performed by the Mutation Generation and Detection Facility, University of Utah (http://cores.utah.edu/mutation-generation-detection/). Injected and control embryos (F0) were then shipped to University of Idaho on the day following HRMA.

*Amplicon sequencing*

Amplicon sequencing was used to analyze genetic variation in the genomic region covering the two selected target sites (in exon 1 and in exon 3). DNA samples were collected from each unverified (potential founder) adult. A pair of oligonucleotide probes was designed to target and generate PCR products (amplicons), and this was followed by a second step to barcode products for sequencing.

PCR primers designed to amplify the amplicon at exon 1 were CTTTGAAAGAGCCTACTCAGAACA (forward, 5' to 3') and CCCGGAAGTATGAACGCTGT (reverse, 5' to 3'). PCR primers designed to amplify the amplicon at exon 3 were GGAAGTGCTCAGGAG (forward, 5' to 3') and TACAGGGTCTGTGGA (reverse, 5' to 3').

PCR products of regions containing two targest sites were provided to the University of Idaho's Institute for Bioinformatics and Evolutionary Studies (IBEST) Genomics Core for library preparation and deep sequencing using an Illumnia MiSeq. Sequencing data was then mapped to zebrafish genome (Zv10), and screened for mutations and possible predicted stop codons.

*FACS isolation of zebrafish rods and cones*

Adult fish were dark-adapted for at least 12 hours, and anaesthetized with MS-222. Corneas and lenses were removed with fine forceps and scissors. The retinal tissues were dissected and retinal pigment epithelium (RPE) was removed from the retina cup with fine forceps. Retinae were collected into a microcentrifuge tube containing 100µL cooled (4°C) RNAse-free phosphate-buffered saline (PBS) (pH 7.4).

With the dissociation protocol and FACS methods discussed in Chapter 3, we successfully isolated highly pure photoreceptors from different transgenic lines.

*RNA isolation and quantitative real-time PCR (qPCR)*

Eyes were dissected from mutant larvae (at 7 days post-fertilization (dfp), 10-17 larvae per sample) with fine forceps and scissors, and a retina cup was dissected from the selected adult mutant. RNA was extracted from these tissues as well as from sorted photoreceptors using the NucleoSpin® RNA kit (Macherey-Nagel) according to the manufacturer's protocol, quantified and quality-checked on a Nanodrop spectrophotometer. cDNA samples were synthesized with RNA samples using the SuperScript® kit (New England Biotech) using random hexamer primers. Gene-specific primers used for qPCR were designed using AlleleID7/84 (Premier Biosoft), and are provided in Table 4.2. qPCR was carried out with the 7900HT Fast Real-Time PCR System (Applied Biosystems, Inc.) and SYBR-Green PCRMaster Mix (Applied Biosystems, Inc.). 18S cDNA was used as the reference transcript [2]. qPCR data was then processed to evaluate their ΔΔCt values. P-values were calculated to establish the reliable range for ΔΔCt estimation.

*Propagation of mutant fish*

Adult zebrafish from the F0 (founder) generation were genotyped by amplicon sequencing as described above, and intercrossed to generate F1 compound heterozygotes. F1 adults were PCR-genotyped as described above. Selected F1 adults with the same monoallelic mutations in the germ line were intercrossed to generate homozygous mutant offspring. These offspring will be subjected to genotyping to confirm their homozygosity.

## Results

*Generation and validation of rxrγa mutant zebrafish*

The specificity of each Cas9 gRNA was scored with the likelihood of an off-target site being edited, as well as on the basis of possible mismatches [54]. For the target site at *rxrγa* exon 1, the on-target modification efficiency was 0.39 (> 0.2 as acceptable) and the off-target activity scored 91 (> 50 as acceptable). For the target sites at exon 3, the scores of on-target and off-target activities were 0.55 and 98 respectively. A diagram of target sites on the *rxrγa* locus is shown in Figure 4.1.

A total of ~270 embryos were injected. DNA samples were collected from sampled embryos for HRMA tests to identify CRISPR/Cas9 induced mutations on *rxrγa* gene. In this experiment, two-step HRMA involved PCR of a heterogeneous genomic sample to produce heteroduplexes and homoduplexes at first, followed by a subsequent melt curve analysis over a temperature gradient. Samples from injected embryos had visibly deflected melt curves (heteroduplexes) compared to wide-type melt curves (homoduplexes) (Figure 4.2). The results showed that all selected samples had possible on-target mutations at two target sites compared to the wild-type controls.

Survival rates at 1 dpf after injection and at 3 dpf upon arrival to the University of Idaho zebrafish facility were excellent as indicated in Table 4.3. A random pool of 24 embryos (F0) was allowed to develop until 7 dpf for a preliminary qPCR measurements of expressions of opsin genes and transcription factors involved in retina development. The remaining embryos continued growing to reproductive maturity.

CRISPR-mediated F0 mutants fish frequently do not display the anticipated genotype, and homozygosity at the desired target sites is hardly achieved with F0 generation [55, 56]. This mosaicism observed in the Cas9-targeted F0 fish was probably due to generation of hypomorphic clones due to in-frame indels [57]. Therefore, any anticipated phenotypic characteristics cannot be confirmed until homozygous mutants are generated.

Amplicon sequencing was successful at detecting mutations in F0 and F1 adult zebrafish carrying two different mutated alleles. Examples of indels detected at the target site of exon 3 are shown in Figure 4.3. Many mutated alleles at exon 3 were predicted to cause premature stop codons (Figure 4.3), which as a result are predicted to disrupt protein function. Mutant alleles at exon 1 were difficult to evaluate as in many cases there were rather large deletions that extended beyond the region targeted for amplicon sequencing.

*Rxrγa expression in rods and cones*

*Rxrγa* was detected as expressed in all zebrafish photoreceptor subtypes, and found to be enriched in *trβ2*+ (LWS) cones as compared to *trβ2*- cells. In contrast, *rxrγa* was found present but not enriched in all other cone subtypes, and expression of *rxrγa* was shown depleted in rods versus non-rod cells. A summary of *rxrγa* expression in in purified rods and cones of adult zebrafish is shown in Table 4.4.

*Preliminary analysis of rxrγa mutant phenotype*

Preliminary analysis of opsin expression patterns was done with two groups of larval samples, and then with a single adult compound heterozygote. Firstly, measurement of opsin expression by qPCR was done with two random samples (Group 1) of 10 larval eyes of F0 (putative founder) generation at 7 dpf with references to 7 dpf wide-type controls of the background strain. Following validation of mutant genotype, fish were bred such that F1 progeny with exon 3 alleles *rxrγa*$^{uoie325d}$*; rxrγa*$^{uoie35d}$ were crossed with F1 fish with exon 3 alleles *rxrγa*$^{uoie36d2i}$*; rxrγa*$^{uoie35d}$. Allele information is shown in Figure 4.4. The 5-bp deletion at exon 3 (e35d) was a domain of the 25 bp deletion (e325d). Moreover, the stop codons predicted to be generated by these deletions reside near each other. Therefore, these two alleles are anticipated to result in similar disruptions in protein function.

Measurement of photoreceptor opsin expression by qPCR was done with a sample of 17 larval eyes of the resulting offspring (Group 2) at 7 dpf with references to 7 dpf wild-type controls. Expression levels of several photoreceptor transcription factors in both groups were also measured. Expression of *rxrγa* was absent in all larval mutants. Expressions of *lws1, lws2, rh2-1, rh2-2, rho, rhol, sws1,* and *sws2* were significantly reduced in Group 2 larval mutants as compared to WT controls. Same expression patterning was shown in Group 1 larval mutants versus WT controls, but reduction in expressions of these opsin genes was not as severe as Group 2. Expressions of transcription factors *nr2e3*, *nrl, rxrγb,* and *thrb* were not significantly different between larval mutants and WT controls. Data suggest that *rxrγa* may have roles in regulating all opsin expressions (Table 4.5), notably in opsins of double cones (*lws* and *rh2* arrays).

The adult mutant with alleles *rxrγa*$^{uoie325d}$ *rxrγa*$^{uoie37d9i}$ was subjected to qPCR measurement of expression of selected opsin genes and transcription factors *rxrγa, rxrγb, nr2e3*. Results are shown in Table 4.6. Expression of *rxrγa* was greatly reduced in the adult

mutant as compared to that in WT control. Expressions of lws1, lws2, rh2-1, rh2-2, rho, and rhol were reduced in the mutant adult as compared to the WT control. Expressions of transcription factors *rxrγb* and *nr2e3* were also found reduced. All qPCR data of the 7 dpf and adult mutant samples suggest that CRISPR-mediated *rxrγa* knockouts likely created a model with *rxrγa* functional nulls.

Discussion and Future Studies

By the CRISPR/Cas9 technique, we successfully created a *rxrγa* mutant model in the zebrafish. Genotyping analysis has shown indels in exon 3 that are predicted to result in premature stop codons. Preliminary analysis of gene expression phenotypes suggests that these indels result in undetectable expression of the *rxrγa* transcript, and therefore mutations may result in functional nulls. Further preliminary analysis of gene expression suggests that *rxrγa* mutations may result in defects in expression of opsins. Some mutants carrying alleles *rxrγa*$^{uoie325d}$; *rxrγa*$^{uoie35d}$ were selected to generate homozygous offspring.

Hence, further experiments are needed to characterize the phenotype of zebrafish *rxrγa* homozygous mutants, and determine the role(s) of *rxrγa* in photoreceptor development, function, and/or survival. Breeding schemes are in place to generate clutches containing homozygous mutants and wildtype controls, for a more powerful experimental design. Quantitative analysis of opsin expression will be performed at 48 hpf, 72 hpf, 5 dpf, 14 dpf, and in adult of homozygous mutants vs. their heterozygous siblings, and vs. their wildtype siblings. Immunocytochemistry (ICC) experiments with LWS-specific antibody, other photoreceptor-specific antibodies (mouse monoclonal ZPR1, labeling red- and green-sensitive cones [58], and monoclonal antibody ZPR3, labeling outer segments of rods and double cones [59]), rod-specific antibody (mouse monoclonal 1D1, labeling rod opsin [49]),

and Müller glia-specific antibody (mouse monoclonal Zrf1, labeling activated Müller glia [60]) should be done to evaluate phenotypes of different retinal cells. *In situ* hybridization assays should be performed to analyze the expressions of selected retinal genes such as *lws1, lws2, rh2-1, rh2-2, rxrγb* at above-mentioned sampling ages in zebrafish embryos and larvae.

References


1. Roberts MR, Hendrickson A, McGuire CR, Reh TA: **Retinoid X receptor (gamma) is necessary to establish the S-opsin gradient in cone photoreceptors of the developing mouse retina**. *Investigative ophthalmology & visual science* 2005, **46**(8):2897-2904.
2. Mitchell DM, Stevens CB, Frey RA, Hunter SS, Ashino R, Kawamura S, Stenkamp DL: **Retinoic Acid Signaling Regulates Differential Expression of the Tandemly-Duplicated Long Wavelength-Sensitive Cone Opsin Genes in Zebrafish**. *PLoS Genet* 2015, **11**(8):e1005483.
3. Allison WT, Barthel LK, Skebo KM, Takechi M, Kawamura S, Raymond PA: **Ontogeny of cone photoreceptor mosaics in zebrafish**. *The Journal of comparative neurology* 2010, **518**(20):4182-4195.
4. Hamaoka T, Takechi M, Chinen A, Nishiwaki Y, Kawamura S: **Visualization of rod photoreceptor development using GFP-transgenic zebrafish**. *Genesis (New York, NY : 2000)* 2002, **34**(3):215-220.
5. Vihtelic TS, Doro CJ, Hyde DR: **Cloning and characterization of six zebrafish photoreceptor opsin cDNAs and immunolocalization of their corresponding proteins**. *Visual neuroscience* 1999, **16**(3):571-585.
6. Chinen A, Hamaoka T, Yamada Y, Kawamura S: **Gene duplication and spectral diversification of cone visual pigments of zebrafish**. *Genetics* 2003, **163**(2):663-675.
7. Takechi M, Kawamura S: **Temporal and spatial changes in the expression pattern of multiple red and green subtype opsin genes during zebrafish development**. *The Journal of experimental biology* 2005, **208**(Pt 7):1337-1345.
8. Marcus RC, Delaney CL, Easter SS, Jr.: **Neurogenesis in the visual system of embryonic and adult zebrafish (Danio rerio). off**. *Visual neuroscience* 1999, **16**(3):417-424.
9. Hafler BP, Surzenko N, Beier KT, Punzo C, Trimarchi JM, Kong JH, Cepko CL: **Transcription factor Olig2 defines subpopulations of retinal progenitor cells biased toward specific cell fates**. *Proc Natl Acad Sci U S A* 2012, **109**(20):7882-7887.
10. He J, Zhang G, Almeida Alexandra D, Cayouette M, Simons Benjamin D, Harris William A: **How Variable Clones Build an Invariant Retina**. *Neuron* 2012, **75**(5):786-798.
11. Schmitt EA, Dowling JE: **Early retinal development in the zebrafish, Danio rerio: Light and electron microscopic analyses**. *The Journal of comparative neurology* 1999, **404**(4):515-536.
12. Branchek T, Bremiller R: **The development of photoreceptors in the zebrafish, Brachydanio rerio. I. Structure**. *The Journal of comparative neurology* 1984, **224**(1):107-115.
13. Branchek T: **The development of photoreceptors in the zebrafish, brachydanio rerio. II. Function**. *The Journal of comparative neurology* 1984, **224**(1):116-122.
14. Durston AJ, van der Wees J, Pijnappel WW, Godsave SF: **Retinoids and related signals in early development of the vertebrate central nervous system**. *Curr Top Dev Biol* 1998, **40**:111-175.
15. Dowling JE: **NUTRITIONAL AND INHERITED BLINDNESS IN THE RAT**. *Experimental eye research* 1964, **3**:348-356.
16. Ross SA, McCaffery PJ, Drager UC, De Luca LM: **Retinoids in embryonal development**. *Physiological reviews* 2000, **80**(3):1021-1054.
17. Stull DL, Wikler KC: **Retinoid-dependent gene expression regulates early morphological events in the development of the murine retina**. *The Journal of comparative neurology* 2000, **417**(3):289-298.
18. Lupo G, Gestri G, O'Brien M, Denton RM, Chandraratna RAS, Ley SV, Harris WA, Wilson SW: **Retinoic acid receptor signaling regulates choroid fissure closure through independent mechanisms in the ventral optic cup and periocular mesenchyme**. *Proceedings of the National Academy of Sciences of the United States of America* 2011, **108**(21):8698-8703.
19. Eagleson GW, Johnson-Meeter LJ, Frideres J: **Effects of retinoic acid upon eye field morphogenesis and differentiation**. *Dev Dyn* 2001, **221**(3):350-364.

20. Hyatt GA, Schmitt EA, Marsh-Armstrong N, McCaffery P, Drager UC, Dowling JE: **Retinoic acid establishes ventral retinal characteristics**. *Development (Cambridge, England)* 1996, **122**(1):195-204.
21. Marsh-Armstrong N, McCaffery P, Gilbert W, Dowling JE, Drager UC: **Retinoic acid is necessary for development of the ventral retina in zebrafish**. *Proceedings of the National Academy of Sciences of the United States of America* 1994, **91**(15):7286-7290.
22. Kelley MW, Turner JK, Reh TA: **Retinoic acid promotes differentiation of photoreceptors in vitro**. *Development (Cambridge, England)* 1994, **120**(8):2091-2102.
23. Stenkamp DL, Gregory JK, Adler R: **Retinoid effects in purified cultures of chick embryo retina neurons and photoreceptors**. *Investigative ophthalmology & visual science* 1993, **34**(8):2425-2436.
24. Kelley MW, Turner JK, Reh TA: **Ligands of steroid/thyroid receptors induce cone photoreceptors in vertebrate retina**. *Development (Cambridge, England)* 1995, **121**(11):3777-3785.
25. Wallace VA, Jensen AM: **IBMX, taurine and 9-cis retinoic acid all act to accelerate rhodopsin expression in postmitotic cells**. *Experimental eye research* 1999, **69**(6):617-627.
26. Soderpalm AK, Fox DA, Karlsson JO, van Veen T: **Retinoic acid produces rod photoreceptor selective apoptosis in developing mammalian retina**. *Investigative ophthalmology & visual science* 2000, **41**(3):937-947.
27. Hyatt GA, Schmitt EA, Fadool JM, Dowling JE: **Retinoic acid alters photoreceptor development in vivo**. *Proceedings of the National Academy of Sciences of the United States of America* 1996, **93**(23):13298-13303.
28. Prabhudesai SN, Cameron DA, Stenkamp DL: **Targeted effects of retinoic acid signaling upon photoreceptor development in zebrafish**. *Developmental biology* 2005, **287**(1):157-167.
29. Stevens CB, Cameron DA, Stenkamp DL: **Plasticity of photoreceptor-generating retinal progenitors revealed by prolonged retinoic acid exposure**. *BMC developmental biology* 2011, **11**:51.
30. Mitchell DM, Stevens CB, Frey RA, Hunter SS, Ashino R, Kawamura S, Stenkamp DL: **Retinoic Acid Signaling Regulates Differential Expression of the Tandemly-Duplicated Long Wavelength-Sensitive Cone Opsin Genes in Zebrafish**. *PLoS Genetics* 2015, **11**(8):e1005483.
31. Paik J, Vogel S, Quadro L, Piantedosi R, Gottesman M, Lai K, Hamberger L, Vieira Mde M, Blaner WS: **Vitamin A: overlapping delivery pathways to tissues from the circulation**. *The Journal of nutrition* 2004, **134**(1):276s-280s.
32. Cvekl A, Wang W-L: **Retinoic acid signaling in mammalian eye development**. *Experimental eye research* 2009, **89**(3):280-291.
33. Chambon P: **A decade of molecular biology of retinoic acid receptors**. *FASEB journal : official publication of the Federation of American Societies for Experimental Biology* 1996, **10**(9):940-954.
34. Kumar S, Sandell LL, Trainor PA, Koentgen F, Duester G: **Alcohol and aldehyde dehydrogenases: retinoid metabolic effects in mouse knockout models**. *Biochimica et biophysica acta* 2012, **1821**(1):198-205.
35. Ross AC, Zolfaghari R: **Cytochrome P450s in the regulation of cellular retinoic acid metabolism**. *Annual review of nutrition* 2011, **31**:65-87.
36. Salyers KL, Cullum ME, Zile MH: **Glucuronidation of all-trans-retinoic acid in liposomal membranes**. *Biochimica et biophysica acta* 1993, **1152**(2):328-334.
37. Palczewski K, Kumasaka T, Hori T, Behnke CA, Motoshima H, Fox BA, Le Trong I, Teller DC, Okada T, Stenkamp RE *et al*: **Crystal structure of rhodopsin: A G protein-coupled receptor**. *Science (New York, NY* 2000, **289**(5480):739-745.
38. Palczewski K: **G Protein–Coupled Receptor Rhodopsin**. *Annual review of biochemistry* 2006, **75**:743-767.
39. Kiser PD, Palczewski K: **Retinoids and Retinal Diseases**. *Annual review of vision science* 2016, **2**:197-234.

40. Hale LA, Tallafuss A, Yan Y-L, Dudley L, Eisen JS, Postlethwait JH: **Characterization of the retinoic acid receptor genes raraa, rarab and rarg during zebrafish development**. *Gene Expression Patterns* 2006, **6**(5):546-555.
41. Ng L, Hurley JB, Dierks B, Srinivas M, Salto C, Vennstrom B, Reh TA, Forrest D: **A thyroid hormone receptor that is required for the development of green cone photoreceptors**. *Nat Genet* 2001, **27**(1):94-98.
42. Roberts MR, Srinivas M, Forrest D, Morreale de Escobar G, Reh TA: **Making the gradient: thyroid hormone regulates cone opsin expression in the developing mouse retina**. *Proc Natl Acad Sci U S A* 2006, **103**(16):6218-6223.
43. Nam KN, Mounier A, Fitz NF, Wolfe C, Schug J, Lefterov I, Koldamova R: **RXR controlled regulatory networks identified in mouse brain counteract deleterious effects of Aβ oligomers**. *Scientific Reports* 2016, **6**:24048.
44. Mounier A, Georgiev D, Nam KN, Fitz NF, Castranio EL, Wolfe CM, Cronican AA, Schug J, Lefterov I, Koldamova R: **Bexarotene-Activated Retinoid X Receptors Regulate Neuronal Differentiation and Dendritic Complexity**. *The Journal of Neuroscience* 2015, **35**(34):11862-11876.
45. Irion U, Krauss J, Nüsslein-Volhard C: **Precise and efficient genome editing in zebrafish using the CRISPR/Cas9 system**. *Development (Cambridge, England)* 2014, **141**(24):4827-4830.
46. Das BC, Thapa P, Karki R, Das S, Mahapatra S, Liu TC, Torregroza I, Wallace DP, Kambhampati S, Van Veldhuizen P *et al*: **Retinoic acid signaling pathways in development and diseases**. *Bioorganic & medicinal chemistry* 2014, **22**(2):673-683.
47. Liu J, Zhou Y, Qi X, Chen J, Chen W, Qiu G, Wu Z, Wu N: **CRISPR/Cas9 in zebrafish: an efficient combination for human genetic diseases modeling**. *Human Genetics* 2017, **136**(1):1-12.
48. Hwang WY, Fu Y, Reyon D, Maeder ML, Kaini P, Sander JD, Joung JK, Peterson RT, Yeh JR: **Heritable and precise zebrafish genome editing using a CRISPR-Cas system**. *PloS one* 2013, **8**(7):e68708.
49. Fadool JM: **Development of a rod photoreceptor mosaic revealed in transgenic zebrafish**. *Developmental biology* 2003, **258**(2):277-290.
50. Suzuki SC, Bleckert A, Williams PR, Takechi M, Kawamura S, Wong RO: **Cone photoreceptor types in zebrafish are generated by symmetric terminal divisions of dedicated precursors**. *Proc Natl Acad Sci U S A* 2013, **110**(37):15109-15114.
51. Tsujimura T, Masuda R, Ashino R, Kawamura S: **Spatially differentiated expression of quadruplicated green-sensitive RH2 opsin genes in zebrafish is determined by proximal regulatory regions and gene order to the locus control region**. *BMC genetics* 2015, **16**:130.
52. Takechi M, Hamaoka T, Kawamura S: **Fluorescence visualization of ultraviolet-sensitive cone photoreceptor development in living zebrafish**. *FEBS Letters* 2003, **553**(1-2):90-94.
53. Salbreux G, Barthel LK, Raymond PA, Lubensky DK: **Coupling Mechanical Deformations and Planar Cell Polarity to Create Regular Patterns in the Zebrafish Retina**. *PLOS Computational Biology* 2012, **8**(8):e1002618.
54. Hsu PD, Scott DA, Weinstein JA, Ran FA, Konermann S, Agarwala V, Li Y, Fine EJ, Wu X, Shalem O *et al*: **DNA targeting specificity of RNA-guided Cas9 nucleases**. *Nature biotechnology* 2013, **31**(9):827-832.
55. Hruscha A, Krawitz P, Rechenberg A, Heinrich V, Hecht J, Haass C, Schmid B: **Efficient CRISPR/Cas9 genome editing with low off-target effects in zebrafish**. *Development (Cambridge, England)* 2013, **140**(24):4982-4987.
56. Auer TO, Duroure K, De Cian A, Concordet JP, Del Bene F: **Highly efficient CRISPR/Cas9-mediated knock-in in zebrafish by homology-independent DNA repair**. *Genome research* 2014, **24**(1):142-153.
57. Jao L-E, Wente SR, Chen W: **Efficient multiplex biallelic zebrafish genome editing using a CRISPR nuclease system**. *Proceedings of the National Academy of Sciences of the United States of America* 2013, **110**(34):13904-13909.

58. Larison KD, Bremiller R: **Early onset of phenotype and cell patterning in the embryonic zebrafish retina**. *Development (Cambridge, England)* 1990, **109**(3):567-576.
59. Yin J, Brocher J, Linder B, Hirmer A, Sundaramurthi H, Fischer U, Winkler C: **The 1D4 Antibody Labels Outer Segments of Long Double Cone But Not Rod Photoreceptors in Zebrafish**. *Investigative ophthalmology & visual science* 2012, **53**(8):4943-4951.
60. Marcus RC, Easter SS, Jr.: **Expression of glial fibrillary acidic protein and its relation to tract formation in embryonic zebrafish (Danio rerio)**. *The Journal of comparative neurology* 1995, **359**(3):365-381.

## Figures and Tables

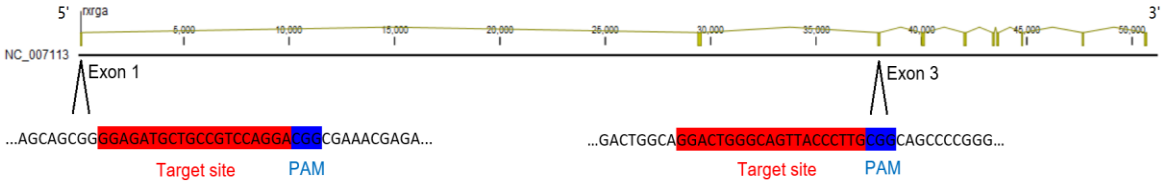


***Figure 4.1.*** Gene structure of *rxrγa* and targets sites for CRISPR/Cas9 at exon 1 and 3. Two target sites are highlighted in red, and PAM sites are highlighted in blue.

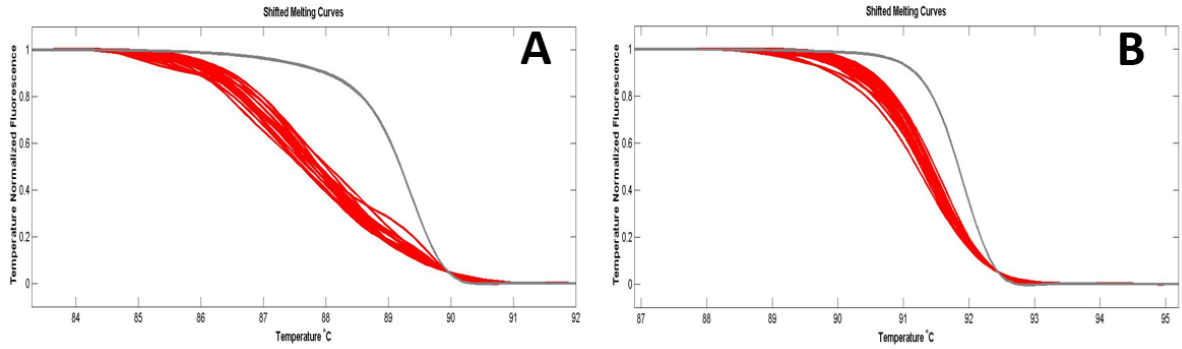


***Figure 4.2.*** HRMA at targets sites (exon 1 in A, exon 3 in B) of injected embryos are shown. In both panels, red lines represent the melting curves of injected mutants, and gray lines represents the melting curves of WT controls.

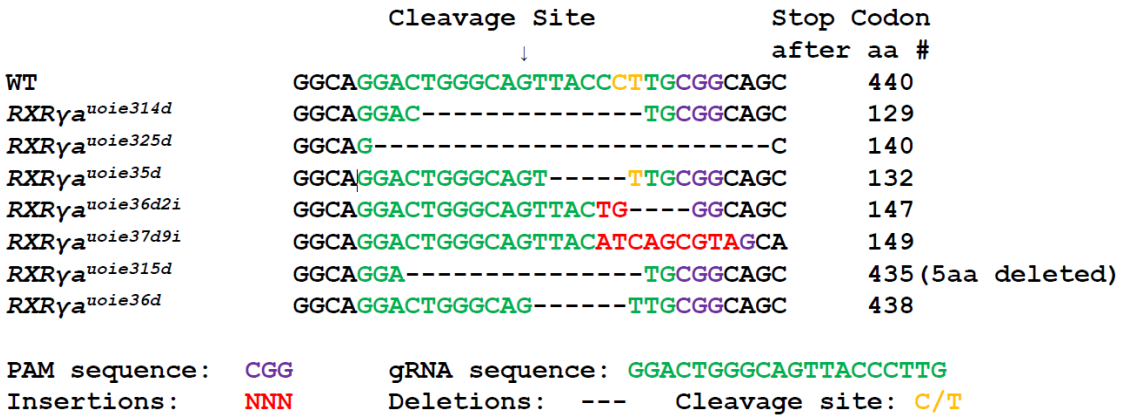


***Figure 4.3.*** Selected *rxrγa* mutant alleles in exon 3 were detected by amplicon sequencing. Cleavage patterns are shown for each allele. Positions of predicted premature stop codons mutant alleles are also shown.


***Figure 4.4.*** *Rxrγa* alleles at exon 3 selected for generating homozygous F2 generation.

**Table 4.1. Primers for HRMA.**

| Target sites | Primers | |
|---|---|---|
| | Forward | Reverse |
| Exon 1 | TAGGCTGTCGCTGTGAGAGG | CCAGTTTAGTGGCAAACTGTCTC |
| Exon 3 | CAGTGTTAGCAGCTCAGAGGACA | GGAGCTGTGTGCGGGTATTA |

**Table 4.2. Primers for qPCR experiments.**

| Gene | Sense Primer 5' -> 3' | Anti-sense Primer 5'-> 3' |
|---|---|---|
| nr2e3 | CTTGCTCAACATATTCAC | GGAAGGAGAAGTAATAGTC |
| nrl | GATGGTCAGAGGAGAATG | GGTTGTAACGAGTGCTTA |
| opn1lw1 | CCCACACTGCATCTCGACAA | AAGGTATTCCCCATCACTCCAA |
| opn1lw2 | AGAGGGAAGAACTGGACTTTCAGA | TTCAGAGGAGTTTTGCCTACATATGT |
| opn1sw1 | GAGTCACATTCAGTCTTG | GTCTATCAGCACACTTATC |
| opn1sw2 | ATCTGGGTGGTTTCCAACCG | ACAGGAGCGGAACTGTTTGTT |
| opn1mw1 | CAGCCCAGCACAAGAAACTC | AGAGCAACCTGACCTCCAAGT |
| opn1mw2 | TTTTTGGCTGGTCCCGATACA | CAGGAACGCAGAAATGACAGC |
| rho | ACTTCCGTTTCGGGGAGAAC | GAAGGACTCGTTGTTGACAC |
| rxrga | TTCACACTGGTCATTCAA | AAGGCATTATAGAGCGATT |
| rxrgb | ACATAATACAGACAGAGACT | TAATAGCACAAGACAGAATC |
| thrb | TCTGGTCTGATGAGTCTA | GTATTAGCCTGGTGATGA |
| 18S | GAACGCCACTTGTCCCTCTA | GTTGGTGGAGCGATTTGTCT |

**Table 4.3. Survival rates of injected embryos.**

| | | |
|---|---|---|
| rxrga mutants at 1 dpf | Number of embryos (Total: 212) | |
| | Survivors | Dead & Damaged |
| | 200 | 12 |
| rxrga mutants at 3 dpf | Number of embryos (Total: 190) | |
| | Survivors | Dead & Damaged |
| | 164 | 26 |

**Table 4.4. qPCR data of *rxrγa* expression in sorted photoreceptors.**

| Sorted samples from transgenic lines | Sorted photoreceptor subtypes | Rxrγa relative log2 expression of fluorescent vs. non-fluorescent samples |
|---|---|---|
| *sws1:GFP* | UV cones | -0.256 |
| *sws2:mcherry* | Sws2 cones | -0.207 |
| *rh2-2:GFP* | Rh2-2 green cones | -0.103 |
| *trβ2:tdTomato* | LWS cones | 2.804*** |
| *XOPS:eGFP* | Rods | -1.822*** |

P-values in this table were calculated with biological replicates.

Three asterisks (***) indicate a p-value ≤ 0.001, no asterisk indicates not significant.

**Table 4.5. qPCR studies of selected transcripts with *rxrya* mutants (vs. WT controls) at 7 dpf.**

| Gene ID | Relative log2 expression | |
|---|---|---|
| | Group 1 | Group 2 |
| *rxrga* | undetermined | undetermined |
| *opn1lw1* | -8.153*** | -13.072*** |
| *opn1lw2* | -4.231*** | -8.851*** |
| *opn1mw1* | -3.784** | -9.357*** |
| *opn1mw2* | -7.615*** | -13.862*** |
| *rho* | -4.829*** | -15.764*** |
| *rhol* | -4.778*** | -9.404*** |
| *opn1sw1* | -2.459* | -8.390*** |
| *opn1sw2* | -1.375* | -10.949*** |
| *nr2e3* | -0.183 | -0.906* |
| *nrl* | 0.105 | 0.466 |
| *rxrgb* | -0.229 | -0.658 |
| *thrb* | 0.147 | 0.84 |

P-values in this table were calculated with technical replicates.
Three stars (***) indicate a p-value ≤ 0.001, two stars (**) indicate a p-value ≤ 0.01, while a single star (*) indicates a p-value ≤ 0.05.

**Table 4.6. qPCR studies of selected transcripts with a *rxrya* adult mutant (vs. WT control).**

| Gene ID | Relative log2 expression |
|---|---|
| *rxrga* | *-10.754* |
| *opn1lw1* | *-13.249* |
| *opn1lw2* | *-12.485* |
| *opn1mw1* | *-5.937* |
| *opn1mw2* | *-6.449* |
| *rho* | *-4.467* |
| *rhol* | *-3.683* |
| *rxrgb* | *-2.375* |
| *nr2e3* | *-1.46* |